Universidade Estadual de Campinas
Instituto de Física Gleb Wataghin

Pedro Simoni Pasquini

Física de Neutrinos

Fenomenologia de Neutrinos e Suas Consequências

Neutrino Flavor Physics

Neutrino Phenomenology and its Consequences

Campinas
2019

Pedro Simoni Pasquini

Neutrino Flavor Physics

Neutrino Phenomenology and its Consequences

Física de Neutrinos

Fenomenologia de Neutrinos e Suas Consequências

Tese apresentada ao Instituto de Física Gleb Wataghin da Universidade Estadual de Campinas como parte dos requisitos exigidos para a obtenção do título de Doutor em Ciências

Thesis presented to the Gleb Wataghin Physics Institute of the University of Campinas in partial fulfillment of the requirements for the degree of Doctor in Science.

Orientador: Prof. Dr. Orlando Luis Goulart Peres

Este trabalho corresponde à versão final da tese defendida pelo aluno Pedro Simoni Pasquini e Orientada pelo Prof. Dr. Orlando Luis Goulart Peres.

Campinas

2019

Ficha catalográfica
Universidade Estadual de Campinas
Biblioteca do Instituto de Física Gleb Wataghin
Lucimeire de Oliveira Silva da Rocha - CRB 8/9174

Pasquini, Pedro Simoni, 1988-
P265n Neutrino flavor physics - neutrino phenomenology and its consequences / Pedro Simoni Pasquini. – Campinas, SP : [s.n.], 2019.

Orientador: Orlando Luís Goulart Peres.
Tese (doutorado) – Universidade Estadual de Campinas, Instituto de Física Gleb Wataghin.

1. Astrofísica de neutrinos. 2. Oscilações de neutrinos. 3. Física além do modelo padrão. I. Peres, Orlando Luís Goulart, 1969-. II. Universidade Estadual de Campinas. Instituto de Física Gleb Wataghin. III. Título.

Informações para Biblioteca Digital

Título em outro idioma: Física de neutrinos - fenomenologia de neutrinos e suas consequências
Palavras-chave em inglês:
Neutrino astrophysics
Neutrinos oscillations
Physics beyond the standard model
Área de concentração: Física
Titulação: Doutor em Ciências
Banca examinadora:
Orlando Luís Goulart Peres [Orientador]
Pedro Cunha de Holanda
Renata Zukanovich Funchal
Laura Paulucci Marinho
Marcelo Moraes Guzzo
Data de defesa: 08-05-2019
Programa de Pós-Graduação: Física

Identificação e informações acadêmicas do(a) aluno(a)
- ORCID do autor: https://orcid.org/0000-0002-1689-442X
- Currículo Lattes do autor: http://lattes.cnpq.br/9625378227733107

MEMBROS DA COMISSÃO JULGADORA DA TESE DE DOUTORADO DE **PEDRO SIMONI PASQUINI** RA: **074306** APRESENTADA E APROVADA AO INSTITUTO DE FÍSICA "GLEB WATAGHIN", DA UNIVERSIDADE ESTADUAL DE CAMPINAS, EM 08/05/2019.

COMISSÃO JULGADORA:

- Prof. Dr. Orlando Luís Goulart Peres - (Orientador) - IFGW/Unicamp
- Prof. Dr. Pedro Cunha de Holanda - IFGW/Unicamp
- Prof. Dr. Marcelo Moraes Guzzo - IFGW/Unicamp
- Profa. Dra. Renata Zukanovich Funchal – Instituto de Física, Universidade de São Paulo
- Profa. Dra. Laura Paulucci – Centro de Matemática, Computação e Cognição Universidade Federal do ABC

A Ata de Defesa, assinada pelos membros da Comissão Examinadora, consta no processo de vida acadêmica do aluno.

CAMPINAS
2019

In memoriam of my Uncle Valdemar “Dema” Pascoini.

To my niece Marinna Florêncio Pasquini, in the hope someday she can become a great scientist.

Acknowledgements

I would like to first thanks to the University of Campinas and its employees for the infrastructure and the opportunity to work and conduct my research in this renowned university. The fundamental support of the funding agencies FAPESP-CAPES (2014/05133-1, 2015/16809-9 and 2014/19164-6), also, This study was financed in part by the Coordenação de Aperfeiçoamento de Pessoal de Nível Superior - Brasil (CAPES) - Finance Code 001.

I would like to show my gratitude to my adviser, friend, and best men Prof. Orlando L. G. Peres who introduced me to neutrino physics and taught me along the way how to become a researcher. Also many thanks to Prof. José V. F. Valle, Prof. André de Gouvê and Vicente Pleitez for receiving me in their institution and working group. They made me become a better physicist.

The support of my family, my mother Isabela C. Simoni and my Father, Marco Antonio P. Pasquini was fundamental for me to become the person I am today. They made me curious and questioner about the world. My beloved wife Gabriela V. Stenico is also partly responsible for this thesis, she supported me in moments of difficulties and stayed by my side when needed. In many aspects, she was responsible for my growth as a human. Thanks also to my sister Julia S. Pasquini for all the years we lived together. Also, the love and support of my Grandmother Wilma Pasquini and uncle Gilberto Pasquini also made this Ph.D. possible.

I should not forget many collaborators that were fundamental in many works: Mariam Tortola, Ana C. B. Machado, Shao-Feng Ge, Sabya S. Chatterjee, César P. Ferreira, Heitor Jurkovich, Omar G. Miranda, Mahedi Masud, and Salvador C. Chullia. It was also important all my friends and colleagues that direct or indirect helped me with physics discussions of any kind and their support: Paulo V. P. Recchia, Sampsa Vihonen and Diego R. Gratieri.

Many thanks to my office mates and friends that were able to put up with my jokes during all these years: Daniel Fagundes, Rafael Norberto, David Ghirardelli, Renan Picoreti, Luis Augusto, Mariano Esteves, and Rafaela Rossi. I will miss the room 205 of the DRCC. The presence of friends in my life was of utmost importance for me to be able to keep going through any obstacles that came into my path. I wish to thanks all of them. Nevertheless, I will only mention my other best men, Lucas Contador, Rafael Parreira, Rodolfo Rodrigues and the soon to be best men Pedro C. N. de Sá. Thanks to all that made this possible, I cannot express my gratitude enough for all the help and support.

Resumo

Nesta tese discutimos vários aspectos da física de neutrinos. Começamos introduzindo o estado atual descrevendo a teoria padrão de oscillação de neutrinos. Exploramos também vários cenários de física exótica, aquela além da teoria padrão de oscilações que possam ser testadas em experiments atuais e futuros. Dividimos o trabalho em duas frentes: Fenomenologia e Teoria. Na parte de fenomenologia trabalhamos com interações não-padrão de neutrinos, não-unitariedade da matriz de mistura e efeitos de curta distancia em experimentos de oscilação. Na parte teórica nós analisamos modelos específicos como o *Warped Flavor Symmetry Model* e o *Revamped* A_4, nos quais utilizamos de correlações entre o ângulo de mistura atmosférico e a fase de CP para obter limites no espaço de parâmetro dos modelos. Além disso, mostramos que é possível utilizar uma relação simples entre o ângulo atmosférico e o ângulo de reatores para, de forma independente de modelo, restringir modelos de massa de neutrinos de alta energia.

Keywords: Neutrinos,Oscilação de Neutrinos, Física Além do Modelo Padrão

Abstract

In this thesis, we discuss several aspects of flavor neutrino physics. From the standard picture of neutrino physics, we describe the present scenario of neutrino oscillations and explore many beyond standard oscillation scenarios that could be observed or tested in current and future experiments. In the phenomenological side, we worked with Non-standard neutrino interactions and Non-unitarity of the neutrino mixing matrix in long and short baseline experiments. In the theoretical side, we also analyzed specific models such as the Warped Flavor Symmetry and the Revamped A_4, where we used the correlations among the atmospheric mixing angle and the CP-phase. We showed that it is possible to also use the correlation between the atmospheric and the reactor angle to model-independently constraint high energy neutrino mass models.

Keywords: Neutrinos, Neutrino Oscillation, Beyond Standard Model

List of Figures

Contents

Chapter 1

Introduction

> "It is no good to try to stop knowledge from going forward. Ignorance is never better than knowledge."
>
> **Enrico Fermi**

In the Standard Model of particle physics, one can group quarks and leptons in three pairs each. Those are the so-called *Fermion Families*. Each family behaves approximately in the same way as the other except that they have different masses. This is illustrated in Table 1.1 below.

Leptons		Quarks	
Family	$SU(2)$ Doublet	Family	$SU(2)$ Doublet
Electron	$\begin{pmatrix} \nu_e \\ e \end{pmatrix}_e$	Up	$\begin{pmatrix} u \\ d \end{pmatrix}_U$
Muon	$\begin{pmatrix} \nu_\mu \\ \mu \end{pmatrix}_\mu$	Charm	$\begin{pmatrix} c \\ s \end{pmatrix}_C$
Tau	$\begin{pmatrix} \nu_\tau \\ \tau \end{pmatrix}_\tau$	Top	$\begin{pmatrix} b \\ t \end{pmatrix}_T$

Table 1.1 – Fermion particles in the Standard Model and their grouping into Families.

For each family, it is given a name or 'flavor'. For the leptons, we have an

electron, muon and tau flavors. The flavor physics is the area that studies the interactions between all the fermion and quark families in order to explain why they behave the way they do and how to explain their parameters.
In this work we concentrate on the neutrinos ν because they provide a clear pathway to search for new physics: Neutrino mass is the first laboratory observation of physics beyond the Standard Model. Also, neutrino masses are strange. They are very tiny in comparison to all the other particles we observe.
During this Ph.D. we concentrated on neutrino flavor physics by the systematic study of various scenarios that go beyond the Standard Model of particle physics and how they could be tested in current and future neutrino experiments. We divided our work into two distinct approaches: (1) Phenomenology: We studied Non-standard neutrino interactions, Non-unitarity of the mixing matrix and sterile neutrinos and (2) Theory: We studied symmetry flavor models and the correlation they predict among the mixing angles. In particular, the Warped Flavor Symmetry model and the Revamped A_4 model.

In Chapter 2 we present the importance of the neutrinos in the current scenario of particle physics. In Chapter 3 we present the theory of neutrino oscillations, the experimental evidence and a detailed discussion on the correct way of derivating the neutrino oscillation probability. In Chapter 4 we present the theory behind various beyond standard model effects that are expected to be present in the neutrino oscillations, which includes Non-standard Interactions, Sterile Neutrinos, and Non-unitarity. In Chapter 5 We summarize various phenomenological analysis performed during this Ph.D., which include changes in the meson decay rate due to non-standard neutrino interactions, the interplay between θ_{13} in the measurement of θ_{23} octant and physics in short-baseline liquid argon detectors. In Chapter 6 we summarize all the theoretical analysis we performed in various models of neutrino masses. And finally in Chapter 7 we present our final remarks and conclusions. In Attachment B.1 we list all the scientific production that as published or are under review, which resulted from this work.

Chapter 2

Introduction to Neutrino Physics

> "Isn't it enough to see that a garden is beautiful without having to believe that there are fairies at the bottom of it too?"
>
> **Douglas Adams**

2.1 Importance of the Neutrino

Neutrinos are present on high energy physics and cosmology. In the former, it shines a glimpse of physics beyond the standard model, while in the later, it plays a very important role in the evolution of the universe. This is why the physics community is turning its efforts toward the understanding of all the theory that permeates the mystery that the neutrino is.

We lack knowledge on many parameters of the neutrino sector: (i) The Majorana/Dirac character of the neutrinos, (ii) The mass scale and ordering and (iii) charge conjugation-parity (CP) phase(s). Describing such parameters may be a way to unveil new and testable physics. Also, almost any extension of the standard model that can be constructed to explain neutrino masses introduces new particles. Those can produce several new interesting effects that are beyond our current knowledge of the universe: Presence of sterile neutrinos, non-unitary of the neutrino mixing matrix and non-standard interactions.

This is why the leptonic flavor physics and neutrino oscillations are a hot topic in experimental and theoretical particle physics. In special, the high energy physics community has its eyes on future neutrino experiments such as T2(H)K [17, 18], NOνA [19] and DUNE [20] that might probe for the first time the yet-to-be-measured CP phase, neutrino mass ordering and will reach a fantastic precision for the other neutrino parameters.

It is exciting that the last two parameters to be measured in the Standard Model (SM) is present in the neutrino physics: The lightest neutrino mass and the CP phase. Measuring neutrino mass is hard, but we might be able to do it with cosmology [21, 22] and, if neutrinos are in fact Majorana particles, in neutrinoless double beta decay ($0\nu\beta\beta$) [23, 24]. On the other hand, we have the CP phase, which might be related to cosmology in the Leptogenesis mechanism [25], that may help to explain the asymmetry of matter and anti-matter in the universe.

Last, but not least, all oscillation parameters and the structure of neutrino mass matrix is predicted by many neutrino mass models, and the precise measurements of all the parameters can be an important tool to probe the space parameters and even exclude such theories.

This points to open questions regarding the flavor sector of the SM which can be understood in the future, by the study of the neutrino. In particular (1) why the matter particle mass are so hierarchical (and why are neutrino mass so tiny $\lesssim$ 1eV), (2) why the value of the mixing angles of the quarks and neutrinos are the way they are and why is it different for quarks and leptons (3) Can the neutrinos be a bridge to dark matter?

Unfortunately, few practical applications of neutrino physics exist. We name them: A new era of neutrino astronomy is being born as this text is written [26]. Moreover, neutrinos are a fascinating tool to understand our Sun's interior [27] and can be used to take a very pixelated picture of it with, probably, the biggest camera ever built: the 50 kt water tank of Kamioka mine [28]. Also, they allow us to measure the earth's density profile [29] and to monitor nuclear reactor activity and construction [30, 31, 32, 33, 34].

In spite of its few practical applications, neutrinos are a door to new physics. That is why they are so broadly studied in modern high energy physics. Maybe someday,

we can use them to perceive the universe differently and do things we cannot do now.

2.2 Pocket Summary of Neutrino Physics

The standard model (SM) of particle physics predicts the existence of 3 neutrinos, all being massless neutral fermions, that interact only via weak interactions. They belong to a SU(2) multiplet, in conjunction with the left part of the charged leptons. So far, experiments found no deviation from the interaction predictions of SM,

$$\mathcal{L}_{\text{Int}} = -\frac{g}{\sqrt{2}}\overline{\nu}_{\alpha L}\not{W} l_{\alpha L} - \frac{g}{2\cos\theta_{\text{W}}}\overline{\nu}_{\alpha L}\not{Z}\nu_{\alpha L} \tag{2.1}$$

where g is the $SU(2)$ interaction constant, θ_{W} is the Weinberg angle and $\alpha = e, \mu, \tau$ *defines* the interaction basis.

Neutrino masses, on the other hand, are not expected, and they are seen as an extension to the standard model. It turns out that the basis where neutrinos have a definite mass is different from that of which they are produced via the weak interactions of Eq. 2.1. This induces the well known neutrino oscillation. This means that the key operator in the leptonic flavour physics is the mixing matrix U that relates both basis, and can be parametrized by 3 angles and a complex phase,

$$U = \begin{pmatrix} c_{12}c_{13} & s_{12}c_{13} & s_{13}e^{-i\delta} \\ -s_{12}c_{23} - c_{12}s_{23}s_{13}e^{i\delta} & c_{12}c_{23} - s_{12}s_{23}s_{13}e^{i\delta} & s_{23}c_{13} \\ s_{12}s_{23} - c_{12}c_{23}s_{13}e^{i\delta} & -c_{12}s_{23} - s_{12}c_{23}s_{13}e^{i\delta} & c_{23}c_{13} \end{pmatrix} \tag{2.2}$$

where $c_{ij} = \cos\theta_{ij}$ and $s_{ij} = \sin\theta_{ij}$.

Neutrino theory is very well understood and the interested reader finds very complete mathematical descriptions in many textbooks, in special we cite [35, 36]. Also, one can find a more focussed discussion on the nature of neutrino masses and mixing parameters in Sec 2.6

2.3 Present Status of Neutrino Parameters

In spite of its importance, we still lack knowledge of much of the neutrino parameter space. That is because neutrinos interact too weakly to allow precision measurements to be performed. Large collaborations around the world are making a huge effort to change this scenario, by building oscillation experiments that will allow us to probe the parameters to an unprecedented level of precision.

There are three groups that perform a global analysis of most of the neutrino experiments in order to provide a consistent picture of current neutrino parameter values [37]. All groups are reasonably consistent between each other, therefore here is presented only one set of parameter values in Table 2.1.

Parameter	N.H.	I.H.
$\sum_i m_i$	<0.18 eV	<0.18 eV
$\Delta m^2_{21}[10^{-5}\ \mathrm{eV}^2]$	7.55^{+20}_{-16}	7.55^{+20}_{-16}
$\lvert\Delta m^2_{31}\rvert[10^{-3}\ \mathrm{eV}^2]$	$2.50^{+0.03}_{-0.03}$	$2.42^{+0.03}_{-0.04}$
m_e [MeV]	548.57990946(22)	
m_μ [MeV]	105.6583715 (35)	
m_τ [MeV]	1776.86 (12)	

$|V_{PMNS}|$

	NH	IH
$\sin^2\theta_{12}$	0.320(20)	0.320(20)
$\sin^2\theta_{13}$	0.0216(83)	0.0222(76)
$\sin^2\theta_{23}$	0.547^{+20}_{-30}	0.551^{+18}_{-30}

$\delta_{CP}/\pi = 1.32 \pm 0.21$

Table 2.1 – Current values of lepton mass and mixing acording to [37]. N.H. Corresponds to Normal Hierarchy of neutrino masses (that is, $m_3 > m_1$) while I.H. stands for Inverted Hierarchy of neutrino masses (that is, $m_1 > m_3$).

In this text, we will always assume the central value of the parameters presented in this table, unless stated otherwise. A careful look at this table shows the current missing gaps on the leptonic sector: (1) The mass scale of neutrinos described by $\sum m_i$ (2)The sign of Δm^2_{31} which describes the mass hierarchy. (3) The correct position of θ_{23} at the trigonometric circle, that is: is it maximal ($\theta_{23} = \pi/4$) above or below $\pi/4$? and (4) although currently experiments points to $\delta_{\mathrm{CP}} \approx 3\pi/2$ what are the true value of it inside 3σ?

2.4 Neutrino Interactions in the Standard Model

There is no formal definition of which particle one should or should not call neutrino, but in the SM context, the neutrinos ν_α are the neutral left-handed spin-half particles, which interact only via weak interactions. Thus, its Lagrangian before symmetry breaking is constructed by the $SU(2)$ multiplet L_α,

$$L_\alpha = \begin{pmatrix} \nu_{\alpha L} \\ \\ l_{\alpha L} \end{pmatrix} \tag{2.3}$$

where $\alpha = e, \mu, \tau$. So, the electro-weak interaction is,

$$\mathcal{L}_{\text{Wint}} = -\frac{1}{2}\bar{L}_\alpha \left(g\vec{\tau}.\not{\vec{W}} + g'\not{B} \right) L_\alpha + \bar{E}_{\alpha R}\not{B} E_{\alpha R} \tag{2.4}$$

where $\vec{\tau}$ are the $SU(2)$ generators and $\vec{W}$ are the vector bosons of the $SU(2)$ and B is the vector boson of the $U(1)$ symmetry, E_α are the right-handed charged leptons. Notice that the $SU(2)$ interaction acts only on the left-handed particles. The $U(1)$ symmetry is not yet the usual electromagnetic symmetry and because of that is denoted as $U(1)_Y$. The Higgs mechanism gives mass to the charged fermions, therefore it couples to the Higgs field, H, resulting in an interaction of the form,

$$\mathcal{L}_{\text{Hint}} = -\frac{Y^l_{\alpha\beta}}{\sqrt{2}}\bar{L}_\alpha H E_{\beta R} + H.c. \tag{2.5}$$

Y^l is a 3×3 complex matrix. As usual, the Higgs field acquires a VEV $\langle h \rangle = v \neq 0$ and one can expand its field in a convenient gauge to $H = (0, v + h(x))$ resulting on a mass term for the charged particles. At principle the matrix $Y^l_{\alpha,\beta}$ is general. Naively one could think that it necessarily implies a mix among fermion families. That is not the case as there is a freedom in the basis choice which allows the Y^l diagonalization. Notice that it is not the case in the quark sector: There are two Higgs couplings to quarks, Y^u and Y^d in order to ensure all the quarks to be massive. The inclusion of the two Yukawa matrix increases the number of parameters to 6 quarks masses, 3 mixing angles and the CP violation phase.

2.5 General Neutrino Masses

The EW-symmetry break induces a Dirac mass for charged leptons through the interaction in the Lagrangian of Eq. 2.5. Neutrinos, on the other hand, are chargeless. This imples a different possibility, a *Majorana mass term* which allows a neutrino mass matrix that contains both Dirac and Majorana terms at the same time. In a general context we introduce the right-handed neutrinos ν_R and write the Dirac-Majorana mass matrix as a 2×2 complex matrix M, so that,

$$M = \begin{pmatrix} M^L & M^D \\ (M^D)^\dagger & M^R \end{pmatrix} \tag{2.6}$$

which are a compressed notation assuming a number n_L of L neutrinos and n_R of R fermions. The M_L is a $n_L \times n_L$ *Symmetric* matrix, M_R is a $n_R \times n_R$ *Symmetric* matrix and M_D is a $n_R \times n_L$ general complex matrix. The Lagrangian then reads,

$$\begin{aligned} \mathcal{L}_\nu =& \bar{\nu}_L i\partial\!\!\!/ \nu_L + \bar{\nu}_R i\partial\!\!\!/ \nu_R + \\ & - \frac{M^L_{\alpha\beta}}{2}\left(-\nu^T_{\alpha L} C^\dagger \nu_{\beta L} + H.C.\right) + \\ & - \frac{M^R_{\alpha\beta}}{2}\left(-\nu^T_{\alpha R} C^\dagger \nu_{\beta R} + H.C.\right) + \\ & - M^D_{\alpha\beta}\bar{\nu}_{\alpha R}\nu_{\beta L} - (M^D)^\dagger_{\alpha\beta}\bar{\nu}_{\alpha L}\nu_{\beta R} \end{aligned} \tag{2.7}$$

where α, β runs through all the possible neutrino generations properly. If right-handed neutrinos have degenerate masses to left-handed neutrinos, than the neutrinos are of the Dirac-Type, which means that Dirac neutrinos are a very special case in the context of neutrino physics.

2.6 Flavour Mixing Parameters

Unfortunately, experiments do not have enough precision yet to measure neutrino masses. Nevertheless, part of the parameter space is known to a precision degree that reachs percent level. Those parameters appear by analysis of the Lagrangian of the

SM. In Section (2.4), it was argued that the introduction of neutrino masses could result on a mixture among lepton families. This can be seen by the mass and interaction term after symmetry breaking Eq. (6.4),(2.4)

$$\begin{aligned}\mathcal{L} = -\frac{g}{2}\left(\bar{l}_{\alpha L}\not{W}^{-}\nu_{\alpha L} + \bar{\nu}_{\alpha L}\not{W}^{+}l_{\alpha L} + \nu_{\alpha L}\not{Z}^{0}\nu_{\alpha L} + l_{\alpha L}\not{Z}^{0}l_{\beta L}\right) \\ -M^{\nu}_{\alpha\beta}\left(\bar{\nu}_{\alpha L}\nu_{\beta R} + \bar{\nu}_{\alpha R}\nu_{\beta L}\right) - M^{l}_{\alpha\beta}\left(\bar{l}_{\alpha L}l_{\beta R} + \bar{l}_{\alpha R}l_{\beta L}\right)\end{aligned} \tag{2.8}$$

It is written here the most general Lagrangian, for three families of fermions in the SM plus the Dirac mass term for neutrinos (the general case should not be hard to generalize). This is written in the so called *Flavour Basis*. This basis arises naturally because the Lagrangian must be $SU(2)$ symmetric. Also, experiment suggests lepton universality [38, 39, 40, 41, 42]. On the other hand, M^{l} and M^{ν} have no definite form and are 3×3 complex matrices*.

Physics should be invariant by basis rotation. Thus, let's unitary rotate the four different leptons, l_L, ν_L, l_R, ν_R by denoting each roation by a unitary matrix: $V^{l}_{L}, V^{\nu}_{L}, V^{l}_{R}$ and V^{ν}_{R}, respectively. Now, the mass matrices become,

$$M'^{\nu}_{\alpha\beta} = M^{\nu}_{\alpha'\beta'}(V^{\nu *}_{L})_{\alpha\alpha'}(V^{\nu}_{R})_{\beta'\beta} \tag{2.9}$$

$$M'^{l}_{\alpha'\beta'} = M^{l}_{\alpha\beta}(V^{l}_{L})_{\alpha'\alpha}(V^{l*}_{R})_{\beta\beta'} \tag{2.10}$$

and

$$\begin{aligned}(V^{l*}_{L})_{\alpha\gamma}(V^{\nu}_{L})_{\gamma\beta}\left(\bar{l}_{\alpha L}\not{W}^{-}\nu_{\beta L}\right) \\ \left(\bar{\nu}_{\alpha L}\not{Z}^{0}\nu_{\alpha L}\right) \\ \left(\bar{l}_{\alpha L}\not{Z}^{0}l_{\alpha L}\right)\end{aligned} \tag{2.11}$$

Notice that the neutral current remains diagonal because the transformations are unitary. This means that flavor changing neutral currents (FCNC) are suppressed by the neutrino mass in the SM. We can now define the *mass basis* by imposing both leptons types to have diagonal matrix:

$$M^{l}_{\alpha'\beta'}(V^{l*}_{L})_{\alpha\alpha'}(V^{l}_{R})_{\beta'\beta} = \mathrm{Diag}\{\mathrm{m_e}, \mathrm{m}_\mu, \mathrm{m}_\tau\} \equiv \hat{\mathrm{M}}^{\mathrm{l}}. \tag{2.12}$$

*notice that these are the two matrix that can spoil the diagonalization of the interaction.

and

$$M'^{\nu}_{\alpha'\beta'}(V_L^{\nu *})_{\alpha\alpha'}(V_R^{\nu})_{\beta'\beta} = \mathrm{Diag}\{\mathrm{m}_1, \mathrm{m}_2, \mathrm{m}_3\} \equiv \hat{\mathrm{M}}^{\nu}. \tag{2.13}$$

Notice that if $M^{\nu} = 0$ the change of basis of Eq. (2.12) will not change any physics, since it can be absorbed by the neutrino transformation without consequences. This is not true when $M^{\nu} \neq 0$. We can now define the PMNS matrix that describes the basis in which neutrinos are *produced* by charged current interactions in comparisson with the *mass basis*:

$$U_{\mathrm{PMNS}} = (V_L^l)^{\dagger}.V_L^{\nu} \tag{2.14}$$

the Pontecorvo-Maki-Nakagawa-Sakata [43, 44], U_{PMNS} that can be parametrized by three angles and a phase in the Dirac case,

$$U_{PMNS} = \begin{pmatrix} c_{12}c_{13} & s_{12}c_{13} & s_{13}e^{-i\delta} \\ -s_{12}c_{23} - c_{12}s_{23}s_{13}e^{i\delta} & c_{12}c_{23} - s_{12}s_{23}s_{13}e^{i\delta} & s_{23}c_{13} \\ s_{12}s_{23} - c_{12}c_{23}s_{13}e^{i\delta} & -c_{12}s_{23} - s_{12}c_{23}s_{13}e^{i\delta} & c_{23}c_{13} \end{pmatrix} \tag{2.15}$$

where $c_{ij} = \cos(\theta_{ij})$ and $s_{ij} = \sin(\theta_{ij})$. For the Majorana neutrinos, we have two less degrees of freedom that cannot be phased away and the PMNS matrix is modified to,

$$U_{\mathrm{PMNS}} \rightarrow U_{\mathrm{PMNS}}.P \tag{2.16}$$

where P contains the two new phases, ϕ_1 and ϕ_2,

$$P = \begin{pmatrix} 1 & 0 & 0 \\ 0 & e^{i\phi_1} & 0 \\ 0 & 0 & e^{i\phi_2} \end{pmatrix} \tag{2.17}$$

Thus, relating the flavour basis to the mass basis requires the action of U_{PMNS} not V_L^{ν}.

Chapter 3

Neutrino Oscillation

> "It doesn't matter how beautiful your theory is, it doesn't matter how smart you are. If it doesn't agree with experiment, it's wrong."
>
> **Richard P. Feynman**

In this Chapter, we analyze carefully the concept of neutrino oscillations. We start by the experimental evidence that was compelling for physicists to accept that neutrino oscillates. Then, we present the theory of neutrino oscillations, starting in a very simple and didactic manner within a 2-neutrino framework. Later we go by the several types of theoretical formulations of neutrino oscillations, by pointing out its limitations. We briefly discuss the concept of oscillation experiments and present current and future long-baseline neutrino experiments characteristics.

3.1 Experimental Evidence

The recent Nobel Prize of 2015 was given to the discovery of neutrino oscillation, the effect of producing a neutrino of flavor ν_α and detecting a different neutrino flavor, ν_β and that the observed oscillations require neutrino mass. Two physicists, Takaaki Kajita and Arthur McDonald were awarded the prize, each representing two groundbreaking experiments, the SuperKamiokande (SK) [45] and the Sudbury Neutrino Observatory (SNO) [46, 47], respectively. The SNO experiment measured an adiabatic

(non-oscillatory) flavor conversion of solar neutrinos caused by the matter effect of our Sun. While SK measured neutrinos from different sources, including the solar. The solar neutrinos points to the existence of an oscillation scale, which we now understand as being related to the mass difference of two neutrinos, the oscillation length is $l_{\text{osc}}^{\text{solar}} = \frac{4\pi E}{|\Delta m^2_{\text{sol}}|}$. The result of KamLAND collaboration [48] remarkably shows the oscillation pattern of neutrino propagation. Their result is depicted in Fig. 3.1.

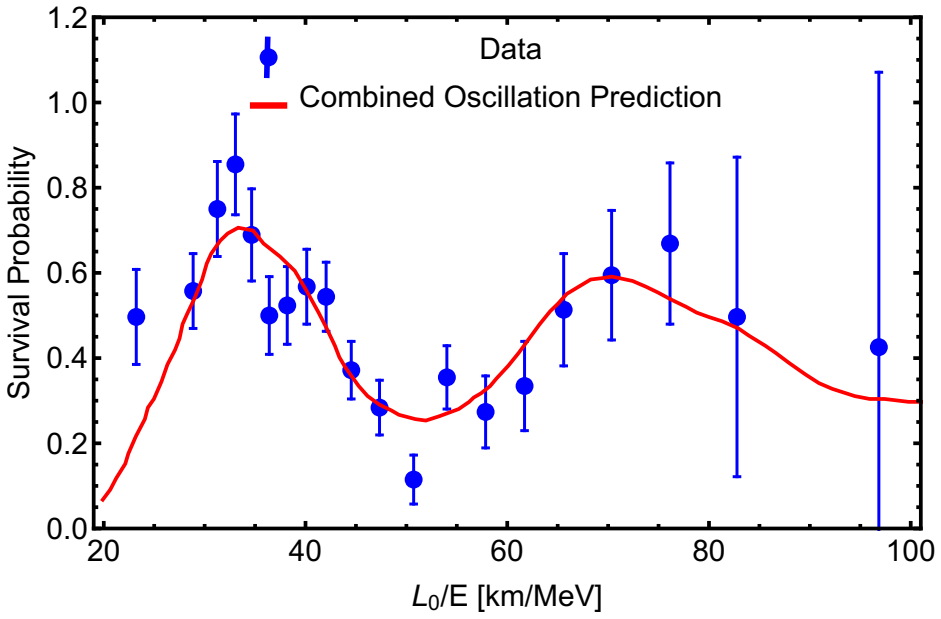

Figure 3.1 – Kamland oscillation data. The Red line represents a two neutrino fit, while the blue points the data obtained by the experiment both as a function of L_0/E_ν [km/MeV] where $L_0 = 180$ km. The mass difference measured from this result is $\Delta m^2_{\text{sol}} = (7.58 \pm 0.21) \times 10^{-5}$ eV^2.

The figure shows the ratio between the expected number of $\overline{\nu}_e$ considering oscillation and no-oscillation in Red and the data points divided by the non-oscillation Monte Carlo simulation in Blue as a function of L_0/E_ν, $L_0 = 180$ km is the effective baseline calculated by the flux-weighted distances of all the 55 nuclear power units near the detector.

The SK experiment also measured the number of atmospheric neutrinos as a function of distance. SuperKamiokande is a 50 kton water Cherenkov detector buried 1 km underground and optimized to measure muon and electron neutrinos of a wide range of energies, from 0.1 to 10 GeV. The atmospheric neutrinos are a subsequent product of pion and muon decay originated from the collision of cosmic rays in the earth's atmosphere. They travel distances ranging from 15 km up to 13000 km before interacting at the detector. Their measurement are consistent with another two flavor conversion, $\nu_\mu \to \nu_\tau$,

but with another oscillation length: $l_{\rm osc}^{\rm atm} = \frac{4\pi E}{|\Delta m^2_{\rm atm}|}$ with $|\Delta m^2_{\rm atm}| \sim 2.5 \times 10^{-3}$ eV^2.

The second oscillation length was confirmed by a conceptually different experiment, the disappearance of reactor electron anti-neutrinos at Double-Chooz [49] and RENO [50]. While Kamiokande shows that neutrinos produced in the atmosphere ν_μ are being transformed into ν_x, the reactor experiments measure the transition of $\overline{\nu}_e$ into $\overline{\nu}_x$. The amplitude of this transition is much smaller than the solar and atmospheric, which arises the need of three different mixing angles between the neutrinos: θ_{12} for the solar neutrinos, θ_{23} for the atmospheric and θ_{13} for the reactors.

3.2 The 2-Neutrino Picture

The data presented in the previous section can be fitted by the simple 2-neutrino oscillation picture. It describes the $\nu_\alpha \to \nu_\beta$ transition. The (survival) probability of detecting a ν_α changes as a function of energy (E) and distance (L) transversed by the neutrinos in the form

$$P(\nu_\alpha \to \nu_\beta) = 1 - \sin^2 2\theta_{ji} \sin^2 \left(1.267 \frac{\Delta m^2_{ij}[eV^2] L[m]}{E[MeV]} \right). \tag{3.1}$$

where θ_{ji} is called the mixing angle and $\Delta m^2_{ij} = m^2_j - m^2_i$ is the mass squared difference.

The theory of neutrino oscillation is very much similar to that of the well known spin rotation under a magnetic field [51]. Neutrinos (ν_α), $\alpha = e\mu$ are created as ortogonal combinations of propagation Eigenstates (ν_i),

$$|\nu_e\rangle = \cos\theta |\nu_1\rangle + \sin\theta |\nu_2\rangle, \tag{3.2}$$

$$|\nu_\mu\rangle = -\sin\theta |\nu_1\rangle + \cos\theta |\nu_2\rangle. \tag{3.3}$$

They can be propagated by the Hamiltonian of the system H, such that $H|\nu_i\rangle = E_i|\nu_i\rangle$, that is,

$$|\nu_\alpha(L)\rangle = \mathcal{U}(L,0)|\nu_\alpha(0)\rangle = e^{-iHL}|\nu_\alpha(L=0)\rangle = \cos\theta e^{-iE_1 L}|\nu_1\rangle + \sin\theta^{-iE_2 L}|\nu_2\rangle. \tag{3.4}$$

where $\mathcal{U}(L,0)$ is the usual quantum mechanics propagator. The probability of a state ν_α

oscillate to a state ν_β after it propagates a distance L is,

$$P_{\nu_\alpha \to \nu_\beta}(L) \equiv |\mathcal{U}(L,0)_{\beta\alpha}|\nu_\alpha(0)\rangle|^2 = \delta_{\alpha\beta} + (1 - 2\delta_{\alpha\beta}) \left[\sin^2 2\theta \sin^2 \left(\frac{\Delta E L}{2}\right)\right] \tag{3.5}$$

It turns out that, in vaccum, ν_i are the mass Eigenstates and the Hamiltonian can be written as $H = \sqrt{p^2 + M^2}$, which means $\Delta E \approx \frac{\Delta m^2}{2E}$ if $p \approx E >> m_i$. Where $\Delta m^2 = m_2^2 - m_1^2$ and E the neutrino energy. On Fig. 3.2 we plot the appearance and disappearance oscillation probability as a function of E for tipical reactor neutrinos experiments baseline $L = 1.5$ km and $\theta = \theta_{13} \approx 8.8°$. The value of $\sin^2 2\theta$ were amplified 10 times to be visible in the figure.

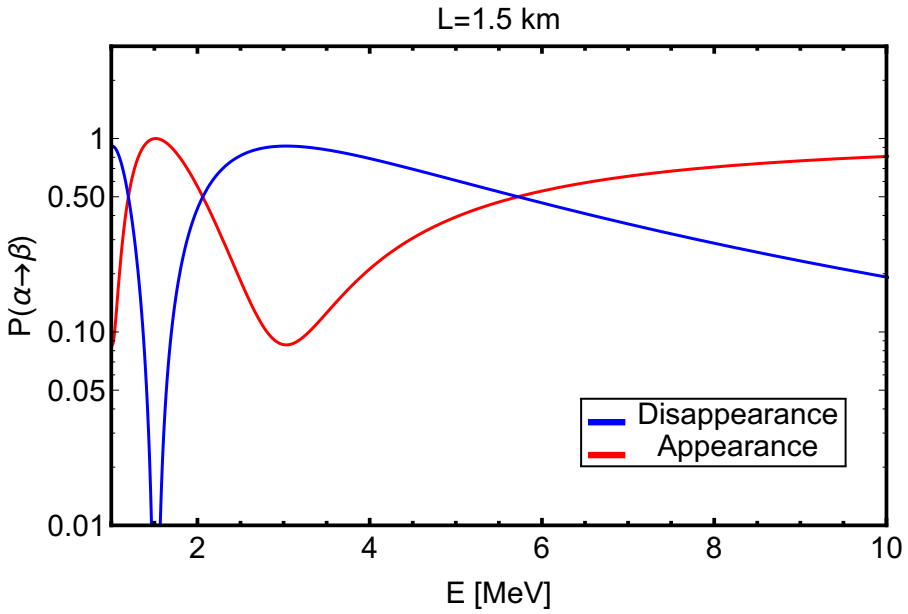

Figure 3.2 – Disappearance (blue) and Appearance (red) neutrino oscillation probability for a typical value of reactor neutrino experiments baseline $L = 1.5$ km, and $\theta = \theta_{13} \approx 8.8°$. The value of $\sin^2 2\theta$ were amplified 10 times to be visible in the plot.

We now know that there are at least 3 neutrinos with at least two mass-squared differences (Δm^2_{21} and Δm^2_{31}). Therefore, this result is an approximation, which is valid under two conditions: (1) $\frac{\Delta m_a^2}{E} << \frac{\Delta m_b^2}{E} \approx L$, in this case, the oscillation from Δm_a^2 did not start yet, or (2) $\frac{\Delta m_b^2}{E} \approx L << \frac{\Delta m_a^2}{E}$, where the oscillation due to Δm_a^2 is so fast, that it gets averaged out at the detector. In both cases $\Delta m^2 = \Delta m_b^2$ and $\sin^2\theta$ is an effective mixing angle, that depends on the actual three neutrino mixing angles θ_{ij}.

3.3 3-Neutrino Oscillation Probability

Three neutrino oscillation probability is a trivial extension of the discussion in last section. The three neutrinos ν_α, $\alpha = e, \mu, \tau$ are created as an ortogonal combination of the three massive neutrinos ν_i, $i = 1, 2, 3$,

$$|\nu_\alpha\rangle = \sum_{i=1}^{3} (U_{\text{PMNS}})^*_{\alpha i} |\nu_i\rangle. \tag{3.6}$$

where U_{PMNS} is a 3×3 unitary matrix parametrized as in Eq. 2.15. The Hamiltonian in mass basis can be approximated by

$$H_0 = \begin{pmatrix} 0 & 0 & 0 \\ 0 & \Delta_{21} & 0 \\ 0 & 0 & \Delta_{31} \end{pmatrix} \tag{3.7}$$

where $\Delta_{ij} = \Delta m^2_{ij}/2E$. Thus, the oscillation probability for three families, $P_{\alpha\beta}(L)$ is,

$$P_{\alpha\beta}(L) = |U_{\alpha j}|^2 |U_{\beta j}|^2 + 2 \sum_{j>k} |U_{\beta j} U^*_{\alpha j} U_{\alpha k} U^*_{\beta k}| \cos\left(\frac{\Delta m^2_{jk}}{2E} L - \phi_{\beta\alpha jk} \right) \tag{3.8}$$

where $\phi_{\beta\alpha jk} = \text{Arg}\left[U_{\beta j} U^*_{\alpha j} U_{\alpha k} U^*_{\beta k} \right]$. This can be extended for anti-ν by changing $\phi_{\beta\alpha jk} \to -\phi_{\beta\alpha jk}$.

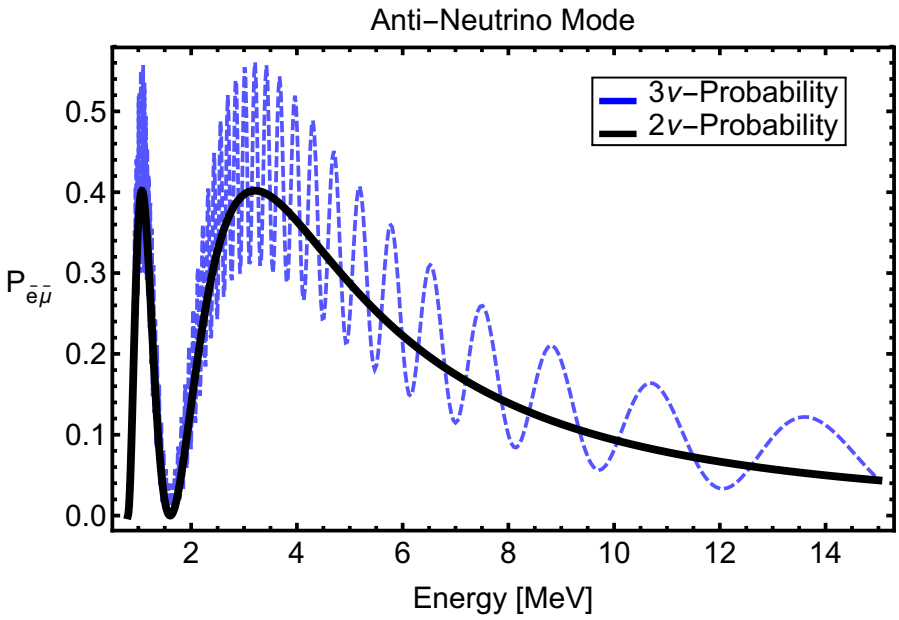

Figure 3.3 – 3-anti-Neutrino oscillation probability (blue) $P_{\overline{e\mu}}$ for baseline of $L = 53$ km as the JUNO Experiment. For comparisson, we draw also the 2-neutrino probability (black).

Two interesting new effects arise by introducing three neutrinos: (1) There are two different oscillation lengths $L_{21} = 2E/\Delta m^2_{21}$ and $L_{31} = 2E/\Delta m^2_{31}$ that can be observed. (2) A 3×3 oscillation matrix allows the introduction of a Charge-Parity phase, δ_{CP}, which changes the oscillation probability when passing from $\nu_\alpha \to \nu_\beta$ to $\overline{\nu}_\alpha \to \overline{\nu}_\beta$. On Fig. 3.3 we plot the oscillation probability as a function of energy for a medium baseline experiment, as a case study we use the JUNO experiment [52], with $L = 53$ km. This is an interesting case because matter effects are small, and we can see at the same time the oscillations due to Δm^2_{21} and Δm^2_{31}, in the figure, the 2-ν case is depicted in black while the 3ν in blue.

3.3.1 Vaccum Probability I: An Incorrect way

The oscillation probability amplitude can be calculated by usual quantum mechanics. First we take the initial state to be created as a plane wave at $t = 0$, $\psi(x,t) = Ne^{ipx}$, with momentum p and N a normalization. Since the experiment usually measure the momentum p with an uncertantie Δp such that $\Delta p >> m_i - m_j$, neutrinos are created

as a coherent combination of mass neutrinos,

$$|\text{initial}\rangle = |\nu_\alpha(x, t = 0)\rangle = \sum_i U^*_{\alpha i} N e^{ip_i.x} |\nu_i\rangle \tag{3.9}$$

and the final state is propagated as,

$$|\nu_{\text{final}}\rangle \equiv |\nu_\alpha(x, t)\rangle = e^{-iHt}|\nu_\alpha\rangle, \tag{3.10}$$

where the free Hamiltonian is,

$$H = \sqrt{P^2 + M^2}. \tag{3.11}$$

Here, P is the Momentum operator and M the mass matrix in a convenient basis. If $E, p >> m_\nu$ we can write,

$$H \approx P\left[1 + \frac{1}{2}\left(\frac{M}{P}\right)^2\right] = P + \frac{M^2}{2P} \tag{3.12}$$

and $cT \approx L$ the distance traveled by the neutrino. Hence, the final state is

$$\begin{aligned} |\nu_{\text{final}}\rangle = |\nu_\alpha(L, T = L/c)\rangle =& U_{\alpha 1} e^{-i\frac{m_1^2}{2p}L}|\nu_1\rangle + U_{\alpha 2} e^{-i\frac{m_2^2}{2p}L}|\nu_2\rangle + U_{\alpha 3} e^{-i\frac{m_3^2}{2p}L}|\nu_3\rangle \\ =& e^{-i\Phi}\left(U_{\alpha 1}|\nu_1\rangle + U_{\alpha 2} e^{-i\frac{\Delta m_{21}^2}{2p}L}|\nu_2\rangle + U_{\alpha 3} e^{-i\frac{\Delta m_{31}^2}{2p}L}|\nu_3\rangle\right) \end{aligned} \tag{3.13}$$

with $\Delta m_{ij}^2 = m_i^2 - m_j^2$.

The overall phase factor $\Phi = \frac{m_1^2}{2p}$ can be dropped out since it does not contribute to the probability amplitude. Since the neutrino mass is very small, we can take $p \approx E$, the mean energy, thus, the probability amplitude $S_{\beta\alpha}$ of detecting a $|\nu_\beta\rangle = \sum_i U_{\alpha i}|\nu_i\rangle$ neutrino is,

$$S_{\beta\alpha} = U_{\alpha 1} U^*_{1\beta} + U_{\alpha 2} U^*_{2\beta} e^{-i\Delta_{21}} + U_{\alpha 3} U^*_{3\beta} e^{-i\Delta_{31}}. \tag{3.14}$$

with, $\Delta_{ij} = \frac{L\Delta m_{ij}^2}{2E}$. Notice that this probability amplitude is different from the unity matrix only when $\Delta m_{ij}^2 \neq 0$ for some $i \neq j$. The total probability is [53],

$$P(\nu_\alpha \to \nu_\beta) = |U_{\alpha j}|^2 |U_{\beta j}|^2 + 2\sum_{j>k} |U_{\beta j} U^*_{\alpha j} U_{\alpha k} U^*_{\beta k}| \cos\left(\frac{\Delta m_{jk}^2}{2E} L - \phi_{\beta\alpha jk}\right) \tag{3.15}$$

where $\phi_{\beta\alpha jk} = \text{Arg}\left[U_{\beta j} U^*_{\alpha j} U_{\alpha k} U^*_{\beta k}\right]$ and for anti-ν one have to change only $\phi_{\beta\alpha jk} \to -\phi_{\beta\alpha jk}$.

The quantity $L_{jk} = 2\pi\frac{2E}{\Delta m^2_{jk}}$ is the oscillation length. Notice that for the existence of an oscillation pattern, it is necessary that $m^2_{jk} \neq 0$ for some combination of j, k. Neutrino oscillation is a pure quantum mechanical effect and is much similar to other processes, like spin precession or Kaon/anti-Kaon system. Neutrinos are created as a superposition of states that propagates slightly different for a given momentum p, the lightest neutrino travels faster than the heavier ones and get ahead of them. Thus, the states get out of phase and do not sum to the initial flavor state.

3.3.2 Vacuum Probability II: An Almost Correct way

Previously we saw the famous derivation of neutrino oscillation probability. Albeit being famous, *it is wrong*. Surprisingly, though, it gives the correct result. There are subtle assumptions in this derivation that are not always true nor physically acceptable.

It is easy to see the limitations of this derivation: The oscillation pattern stands up to infinity. Nevertheless, since the mass eigenstates travel with different speeds, at some point their wave-packets do not overlap anymore* and the oscillation should cease, as it is well known for supernovae netrinos [54].

Two assumptions were taken in last section:

1. Neutrino phase evolves as: $E_i T - p_i L = \frac{m_i^2}{2p} L$, as $T = L$.

2. Neutrinos are formed by plane waves.

Notice that assumption 1. does not imply that all the neutrino energies/momentum are the same, as one might think. Nevertheless, the assumption $T = L$ is an ad-hoc assumption and does not come from any calculation. Also, changing it slightly would lead to different results [55]†.

The other assumption of plane wave solutions implies the momentum p_i and energy E_i of the neutrino to be perfectly known. This should actually destroy the oscil-

*or better say, the overlapping distance becomes bigger than $1/\Delta p$.

†e.g. $T_i = L/v_i = E_i L/p_i$ imply the phase shift $\frac{m_i^2}{p} L$.

lation pattern since you would know perfectly the neutrino mass [56].

The second assumption is much easier to deal with, as it is possible to simply loose the plane wave assumption. As we shall see, by assuming a spread in the neutrino momentum, it is possible to show that the oscillation should cease to exist for distances longer than the *coherence length* of the wave functions [57]. So, let us assume that a mass eigenstate i has a momentum spread $\phi_i(q,p)$ so that the flavour neutrino α in momentum space can be written as,

$$|\nu_\alpha(x,t)\rangle = \sum_i U^*_{\alpha i} \int dq \phi_i(q,p) \frac{e^{i(q.x - E_i(q)t)}}{\left(\sqrt{2\pi}\right)^3} |\nu_i\rangle. \tag{3.16}$$

The exact form of the function ϕ_i does not need to be known, but should follow some reasonable assumptions: (1) It is centered at the momentum p and quickly vanishs to zero as $|p-q|$ becomes larger than the momentum spread σ_i. (2) It is normalized: $\int dq |\phi_i(q,p)|^2 = 1$. Thus, the amplitude for detecting a neutrino ν_β at position L is,

$$\begin{aligned} S_{\beta\alpha}(L,T) &= \int dx \langle \nu_\beta(x-L) | \nu_\alpha(x, t=T)\rangle \\ &= \sum_i U^*_{\alpha i} U_{\beta i} \int \frac{dx}{\left(\sqrt{2\pi}\right)^3} dq dq' \phi_i(q,p) \phi^*_i(q',p) e^{i[x.q - (x-L).q' - E_i(q)T]}, \end{aligned} \tag{3.17}$$

With $E_i(q) = \sqrt{q^2 + m_i^2}$. We can first integrate over x resulting in a $\delta(q-q')$ that can be used to further integrate over q' and we get,

$$S_{\beta\alpha}(L,T) = \sum_i U^*_{\alpha i} U_{\beta i} \int dq |\phi_i(q,p)|^2 e^{i(L.q - E_i(q)T)} \tag{3.18}$$

Since $|\phi_i(q,p)|^2$ is highly peaked around p, at first approximation we can assume $(L.q - E_i(q)T)$ does not vary much inside $p - \sigma_i < q < p + \sigma_i$ and write,

$$\int dq |\phi_i(q,p)|^2 e^{i(L.q - E_i(q)T)} \approx e^{i(L.p - E_i(p)T)} \int dq |\phi_i(q,p)|^2 = e^{i(L.p - E_i(p)T)} \tag{3.19}$$

and we recover the plane wave solution of Eq. 3.14 if $T = L$. But now we can go further and include the second order approximation,

$$\int dq |\phi_i(q,p)|^2 e^{i(L.q - E_i(q)T)} \approx e^{i(L.p - E_i(p)T)} \int d\delta q |\phi_i(\delta q + p, p)|^2 e^{i(L - v_i T)\delta q} \tag{3.20}$$

where $\delta q = q - p$ and $v_i = dE(q)/dq|_{q=p} = p/E_i$. The integral can be approximated by a

Gaussian-Like expansion,

$$|\phi_i(\delta q, p)|^2 = e^{2\ln|\phi_i(\delta q - p, p)|} = e^{2\ln|\phi_i(q,p)|} = Ne^{2\dot{\phi}(0)\delta q + \ddot{\phi}(0)\delta q^2 + ...} \tag{3.21}$$

where $\dot{\phi}(0) = \frac{d\ln|\phi_i(\delta q - p,p)|}{d\delta q}\Big|_{\delta q=0} = 0$ since $q = p$ is a maximum of the wave-packet and,

$$(\sigma_i^2)^{-1} \equiv \ddot{\phi}(0) = \frac{d^2\ln|\phi_i(\delta q - p, p)|}{(d\delta q)^2}\Big|_{\delta q=0}. \tag{3.22}$$

N ensures the normalization condition to the probability. At second order, Eq. 3.21 ressembles a Gaussian-packet and results in,

$$\int dq|\phi_i(q,p)|^2 e^{i(L.q - E_i(q)T)} \approx e^{i(L.p - E_i(p)T) - \frac{(L-v_iT)^2\sigma_i^2}{4}} \tag{3.23}$$

Thus, the transition matrix is,

$$S_{\beta\alpha}(L,T) \approx \sum_i U^*_{\alpha i}U_{\beta i}e^{i[L.p - E_i(p)T] - \frac{(L-v_iT)^2\sigma_i^2}{4}} \tag{3.24}$$

Here, $\frac{(L-v_iT)^2\sigma_i^2}{4}$ is a damping term that kills the probability when $L - v_iT$ are too different. We can now understand the origin of the condition $L = T$: The coherence of states can only happen to neutrino waves that propagates with velocities $v_i \approx L/T$. Since L is precisely known to the experiment and the detection is usualy performed during a time interval $T - \Delta T/2$ to $T + \Delta T/2$, where $\Delta T >> T_{ij}^{\text{osc}}$, the oscillation time. What we observe experimentaly is an avarage in time of the probability transition,

$$P_{\beta\alpha}(L) = \int dT|S_{\beta\alpha}(L,T)|^2 = \sum_{ij} U^*_{\alpha i}U_{\beta i}U^*_{\beta j}U_{\alpha j}\int dT N^2 e^{i[-(E_i(p) - E_j(p)T] - \frac{(L-v_iT)^2\sigma_i^2 + \left(L - v_jT\right)^2\sigma_j^2}{4}} \tag{3.25}$$

thus,

$$P_{\beta\alpha}(L) = \sum_{ij} U^*_{\alpha i}U_{\beta i}U^*_{\beta j}U_{\alpha j}e^{-i\Delta_{ji} - \Phi_{ij}} \tag{3.26}$$

as usual,

$$\Delta_{ji} = (E_i(p) - E_j(p))\frac{(\sigma_i^2 v_i + \sigma_j^2 v_j)}{\sigma_i^2 v_i^2 + \sigma_j^2 v_j^2}L \approx \frac{m_i^2 - m_j^2 L}{2p} = \frac{L}{L_{ij}}. \tag{3.27}$$

But we get a very interesting function Φ_{ji},

$$\begin{aligned}\Phi_{ij} =& \frac{(E_i(p) - E_j(p))^2}{\sigma_i^2 v_i^2 + \sigma_j^2 v_j^2} + \frac{L^2\sigma_1^2\sigma_2^2(v_j - v_i)^2}{\sigma_i^2 v_i^2 + \sigma_j^2 v_j^2} \\ \approx& \frac{(m_j^2 - m_i^2)^2}{4p^2(\sigma_i^2 + \sigma_j^2)} + \left(\frac{L\sigma_1\sigma_2|m_j^2 - m_i^2|}{4p^2}\right)^2 \equiv \frac{1}{L_{ij}^2(\sigma_i^2 + \sigma_j^2)} + \left(\frac{L}{L_{ij}^{\text{coh}}}\right)^2\end{aligned} \tag{3.28}$$

Notice that $\Phi_{ij} \geq 0$ where $\Phi_{ij} = 0$ means $m_i = m_j$. Moreover, the Φ_{ij} function contains a L independent part, $\frac{1}{L_{ij}^2(\sigma_i^2+\sigma_j^2)}$. It regulates how different the masses should be in order for the neutrinos to be created coherently. As $|m_i - m_j|$ grows, $L_{ij} \to 0$ and eventualy the L independent term kills the oscillation pattern.

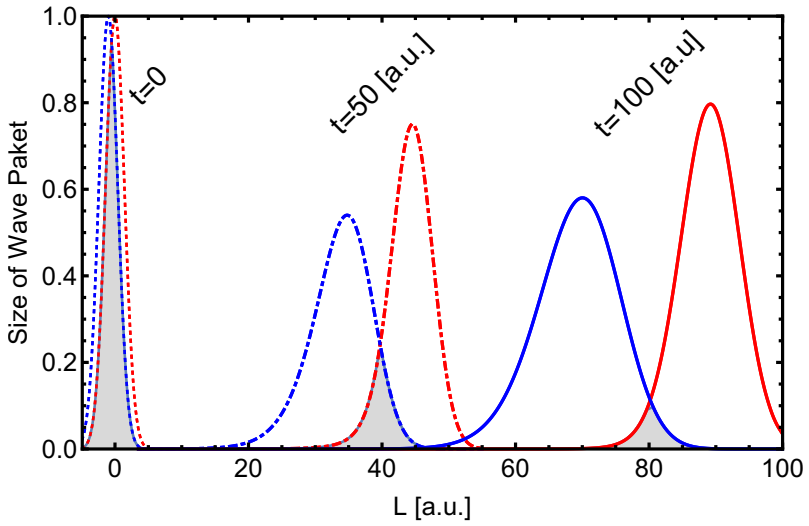

Figure 3.4 – Illustration of two wave packets with $\sigma_i = 0.3$ [a.u.] and momentum $p = 1$ [a.u.] propagation through space: Dashed-Line means $t = 0$, Dot-Dashed Lines are for $t = 50$ [a.u.] and full line $t = 100$ [a.u.]. Also, $m_1 = 0.5$ [a.u.] and $m_2 = 1.0$ [a.u.]. Plot made for this PhD thesis.

The most interesting part is L^2 dependent and is related to the coherency length $L_{ij}^{\text{coh}} = |L_{ij}|/\sigma_1\sigma_2$. Since the neutrino wave packets travel at different speeds, they separate during propagation. Thus, even if they start at with 100% overlap, at some point in space they won't overlap anymore and neutrino oscillation will cease. The wave packets propagation is illustrated in Fig. 3.4. The dashed line represents the initial wave packets and the Dot-Dashed and full lines the function after propagation. Notice that the gray area representing the overlap between both wave-functions shrinks as the time progress.

3.3.3 Vaccum Probability III: QFT approach

The intermediate wave packet model presented in the previous section provides a great improvement on the calculation of neutrino oscillations: the existence of a coherence length L_{ij}^{coh} in which neutrinos cannot oscillate anymore. Nevertheless, it doesn't completely solve all the issues on the derivation of the oscillation probability:

(1) Oscillating neutrinos cannot be directly observed. It is more relevant to create a model that accounts for the source/detection particles in the reaction

(2) An exact model for the wave packets is not possible since we are introducing them by hand. Especially the fact that we cannot measure the wave packet directly since we do not access the neutrinos. Moreover, it is not reasonable to think that all wave-packets will be the same, or that the mean momentum is the same.

(3) The subtle assumption of arriving at the detector with the same time $t = T$ is not justified.

(4) It is hard to accommodate decay of the propagating particle, using the intermediate-wave-packet model.

Those issues are solved by a Quantum Field approach to the problem. Here, we present a summarized version of the detailed calculation of [58].

In a neutrino experiment, what is really observed are the initial state production (detection) particles P_I (D_I) and final states containing a pair of tagged lepton/anti-leption, l_α, l_β, that is,

$$P_I + D_I \to P_F + D_F + \bar{l}_\alpha + l_\beta. \tag{3.29}$$

We can draw the first order diagram of this reaction as in Fig 3.5. L is a macroscopic distance. P_F (D_F) is the final state of production (detection) particles and can be interepreted as multi-particle system. The dashed-region corresponds to the unlocalization of the production/detection process.

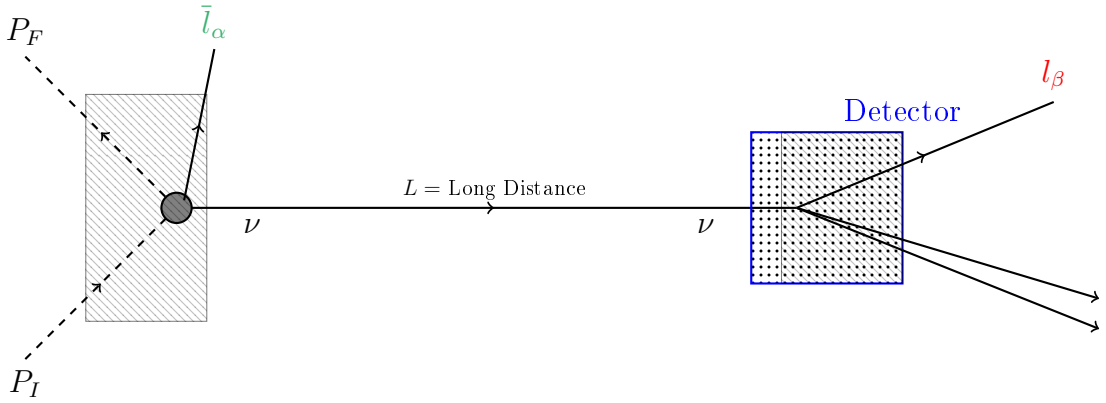

Figure 3.5 – Feynman Diagram for the process of neutrino oscillation. The whole process is described by the criation of neutrino tagged by lepton $\bar{l}_\alpha$, neutrino propagation by a macroscopic distance L and detection of the neutrino tagged by l_β. Notice that $\alpha \neq \beta$ is a possibility. In the plane wave approximation the dashed part (production/detection) is sepparated from the propagationand are substituted by neutirnos created with plane wave distribution of momentum.

The Feynman Diagram produces the transition matrix

$$A_{\alpha\beta} = \langle P_F, \bar{l}_\alpha; l_\beta, D_F | T \left\{ e^{-i\int dx^4 H_I} \right\} - 1 | P_I; D_F \rangle. \tag{3.30}$$

A state $|A\rangle$ is defined by its creation operator and a wave-packet function that describes how the localization process takes place,

$$|A\rangle = \int [dp] \psi_A a_A^\dagger(p) e^{ip.x} |0\rangle \tag{3.31}$$

x is the quadri-position vector of the particle and $[dp] = \frac{d^3p}{(2\pi)^3\sqrt{2E(p)}}$. Here, we assume a Gaussian wave function with meam momentum $\overline{p}$ and width σ_A, that is,

$$\psi_A(\vec{p}) = \left(\frac{2\pi}{\sigma}\right)^{3/4} e^{-\frac{(p-\overline{p})^2}{4\sigma^2}} \tag{3.32}$$

Notice that this assumption is much more reasonable than assuming a form for the *neutrino's wave packet* since it is possible to prepare the production/detection system.
At first order, the quantity $T\left\{e^{-i\int dx^4 H_I} - 1\right\}$ can be described by two interactions,

$$A_{\alpha\beta} = \langle P_F, \bar{l}_\alpha; l_\beta, D_F | T \left\{ \int d^4x_1 d^4x_2 \mathcal{H}_P(x_1) \mathcal{H}_D(x_2) \right\} | P_I; D_F \rangle \tag{3.33}$$

where

$$\mathcal{H}_P(x_1) = \frac{G_F}{\sqrt{2}} \sum_{\gamma i} U^*_{\omega i} \overline{\nu}_i(x_1) \Gamma^\mu l_\omega(x_1) J^P_\mu(x_1) \tag{3.34}$$

$$\mathcal{H}_D(x_2) = \frac{G_F}{\sqrt{2}} \sum_{\gamma j} U_{\theta j} \bar{l}_\theta(x_2) \Gamma^\mu \nu_j(x_2) J^D_\mu(x_2) \tag{3.35}$$

$$\tag{3.36}$$

where $\Gamma^\mu = \gamma^\mu(1-\gamma^5)$ is the usual weak-interaction vertex with G_F the Fermi constant and $U_{\alpha i}$ the neutrino mixing matrix. J^A_μ is the production (detection), $A = P$ ($A = D$), weak currents. Applying the wick-contractions it is possible to simplify the matrix element to

$$A_{\alpha\beta} = \sum_i \int d^4q U^*_{\alpha i} U_{\beta i} A^P_{\alpha i}(q) \left[G(q^2) e^{-iq.L}\right] A^D_{\beta i}(q) \tag{3.37}$$

q is the internal neutrino ν_i quadri-momentum. $G(q^2)$ is the scalar propagator, $L = x_D - x_P$ is the quadri-position difference between detection and production. $A^P_{\alpha i}$ ($A^D_{\beta i}$) is the production (detection) matrix elements which are function of the neutrino momentum q as well as the momentum of the production/detection particles,

$$A^P_{\alpha i} = \int d^4x_1 [dp_I][dp_F][dp_\alpha] \psi(p_I)\psi^*(p_F)\psi^*(p_\alpha) M_{\alpha i}(p_I, p_F, p_\alpha, q) e^{ix_1.(p_I - p_F - p_\alpha - q)} \tag{3.38}$$

$$A^D_{\alpha i} = \int d^4x_2 [dk_I][dk_F][dp_\alpha] \psi(k_I)\psi^*(k_F)\psi^*(p_\beta) M_{\beta i}(k_I, k_F, p_\beta, q) e^{ix_2.(k_I - k_F - p_\beta + q)} \tag{3.39}$$

and

$$M_{\alpha i}(p_I, p_F, p_\alpha, q) = \frac{G_F}{\sqrt{2}} J^P_\mu(p_I, p_F) \overline{u}_i(q) \Gamma^\mu v(p_\alpha), \tag{3.40}$$

$$M_{\beta i}(k_I, k_F, p_\beta, q) = \frac{G_F}{\sqrt{2}} J^D_\mu(k_I, k_F) \overline{u}(p_\beta) \Gamma^\mu u_i(q). \tag{3.41}$$

Here, we denote $J^A_\mu(q_1, q_2)$, $A = P, D$; as the fourier transform of $J^A_\mu(x)$. the variables p_I, p_F, p_α are the quadri-momentum of the production particles P_I, P_F and $\bar{l}_\alpha$ respectively, while similar for the detection particles. Notice that the integration over x_i, $i = 1, 2$ ensures the conservation of momentum in each vertex.

Assuming that $M_{\alpha i}$, $M_{\beta i}$ vary slow enough around the meam momentum of each particle, we may substitute the quantities M by their value at the mean momentum of the particles, since $\psi_A(p_A)$ is a highly peaked function. Thus,

$$A_{\alpha\beta} = \sum_{i,s_1} U^*_{\alpha i} U_{\beta i} \int d^4q M^0_{\alpha i}(q) \Psi(q) \left[G(q^2) e^{-iq.L} \right] M^0_{\beta i}(q), \tag{3.42}$$

where

$$\begin{aligned} M^0_{\alpha i}(q) =& M_{\alpha i}(\overline{p}_I, \overline{p}_F, \overline{p}_\alpha, q) \\ M^0_{\beta i}(q) =& M_{\beta i}(\overline{k}_I, \overline{k}_F, \overline{p}_\beta, q). \end{aligned} \tag{3.43}$$

As we will see, in most cases, one can also substitute q in those functions by the value of an on-shell neutrino. $\Psi(q)$ is called the overlap function and depends on the production and detection particle wave-functions,

$$\begin{aligned} \Psi(q) = & \int d^4x_2 d^4x_1 [dp_I][dp_F][dp_\alpha][dk_I][dk_F][dp_\alpha] e^{ix_1.(p_I - p_F - p_\alpha - q)} e^{ix_2.(k_I - k_F - p_\beta + q)} \times \\ & \times \psi(p_I)\psi^*(p_F)\psi^*(p_\alpha)\psi(k_I)\psi^*(k_F)\psi^*(p_\beta) \end{aligned} \tag{3.44}$$

The assumption of Gaussian function for each $\psi(P)$ as in Eq. 3.32 is usefull because it is possible to perform the integral and calculate $\Psi(q)$ analitically,

$$\Psi(q) = \frac{\pi^2}{(\sigma^3_{pP}\sigma_{eP})(\sigma^3_{pD}\sigma_{eD})} e^{-f_P(q) - f_D(q)} \tag{3.45}$$

where,

$$f_A(q) = \frac{(\vec{q} - \vec{p})^2}{4\sigma^2_{pA}} + \frac{(q_0 - p_0 - (\vec{q} - \vec{p}).\vec{v}_A)^2}{4\sigma^2_{eA}}. \tag{3.46}$$

$A = P, D$ stands for production and detection variables respectively and

$$\begin{aligned} \sigma^{-2}_{pA} =& \sigma^{-2}_{FA} + \sigma^{-2}_{IA} + \sigma^{-2}_{lA}, \\ \sigma^{-2}_{eA} =& \sigma^{-2}_{pA} \left[\frac{1}{\sigma^2_{pA}} \left(\sigma^2_{FA}\vec{v}^2_{FA} + \sigma^2_{IA}\vec{v}^2_{IA} + \sigma^2_{lA}\vec{v}^2_{lA} \right) - \vec{v}^2_A \right] \end{aligned} \tag{3.47}$$

$\vec{v}_{iA}$ are the velocities of particle i. $\vec{v}_A$ is the resulting velocity of the detection/production particles avaraged by their momentum spread,

$$\vec{v}_A = \sigma^{-2}_{pA} \left(\sigma^2_{FA}\vec{v}_{FA} + \sigma^2_{IA}\vec{v}_{IA} + \sigma^2_{lA}\vec{v}_{lA} \right) \tag{3.48}$$

and $p = (p_0, \vec{p})$ is the momentum transfer during the entire reaction,

$$p = p_I - p_F - p_\alpha = k_I - k_F - p_\beta. \tag{3.49}$$

This is as far as we can go analitically without making any extra assumption.
Let us now pause for a moment to analyze the meaning of the fundamental Eq. 3.42. It represents the coherent sum of the reactions that create neutrinos i with momentum q, those neutrinos are propagated to a distance L by the propagator $G(q^2)e^{-iq.L}$ and finally detected. The creation reaction is described by the matrix element $M^0_{\alpha i}$ and the detection by $M^0_{\beta j}$. $\Phi(q)$ represents the weight by which one should integrate all those processes and is conceptually equivalent to the intermediate neutrino wave packet, except that it allows us to model it by analyzing the production/detection process.

3.3.4 Obtaining the Standard Oscillation Probability Formula

In order to be able to obtain the neutrino oscillation formula it is necessary to make two assumptions,

(i) Neutrinos are stable, thus: $G(q) = \frac{i}{q^2 - m^2}$

(ii) Neutrino masses are small, thus: $M_{\alpha i} \approx M_{\alpha j}$ and $M_{\beta i} \approx M_{\beta j}$ even if $j \neq i$.

Returning to Eq. 3.42, the hard part is to perform the d^4q integration. We can use the Grimus-Stockinger theorem [59] and first integrate over d^3q, which gives,

$$\int d^3q \frac{\psi(q)e^{i\vec{q}.\vec{l}}}{q^2 - m^2 + i\epsilon} \xrightarrow{L\to\infty} \frac{-2\pi^2}{L}\psi\left(\sqrt{q_0^2 - m^2}\frac{\vec{l}}{L}\right)e^{i\sqrt{q_0^2-m^2}l} \tag{3.50}$$

This result imply that in the limit of large $L = |\vec{l}|$, the integral converges to the limit of real neutrinos propagating in the direction of L with momentum compatible with $q^2 = m^2$, that is, on shell. This theorem is valid as long as $q_0^2 > m^2$ and the derivatives of $\psi(q)$ and itself decreases at least with $1/\vec{q}^2$ if $\vec{q}^2 \to \infty$.
Plugging-in this result in Eq. 3.42 and calculating the squared matrix element we obtain,

$$|A_{\alpha\beta}|^2 = \sum_{ij} U^*_{\alpha i}U_{\beta i}U_{\alpha j}U^*_{\beta j}\int dq_0 dq_0' \frac{4\pi^4}{L^2} M^0_{\alpha i}(q)[M^0_{\alpha j}(q')]^* M^0_{\beta i}(q)[M^0_{\beta j}(q')]^* \Psi(q)\Psi^*(q') \times$$
$$e^{i\left[\sqrt{q_0^2-m_i^2}-\sqrt{(q_0')^2-m_j^2}\right]L} e^{i(q_0-q_0')T} \tag{3.51}$$

The detector observes the time average of neutrinos passing through a time ΔT. Thus, we will need to integrate over T with $\Delta T >> T_{\rm osc}$, which will result in an approximate delta function that sets $q_0 = q_0'$ when integrating over dq_0' and we remain with,

$$|A_{\alpha\beta}|^2 = \sum_{ij} U^*_{\alpha i} U_{\beta i} U_{\alpha j} U^*_{\beta j} \int dq_0 \frac{8\pi^5}{L^2} M^0_{\alpha i}(q)[M^0_{\alpha j}(q)]^* M^0_{\beta i}(q)[M^0_{\beta j}(q)]^* \times \\ \times \Psi_i(q)\Psi^*_j(q) e^{i\left[\sqrt{q_0^2 - m_i^2} - \sqrt{q_0^2 - m_j^2}\right]L} \tag{3.52}$$

The function $\Psi_i(q)\Psi^*_j(q)$ can be re-written as,

$$\frac{4\pi^4}{L^2}\Psi_i(q)\Psi^*_j(q) = \Phi(\vec{p}\times\vec{l}) e^{-f_i(q_0) - f_j(q_0)} \tag{3.53}$$

where

$$f_i(q_0) = \sum_{A=P,D} \left(\frac{(\sqrt{q_0^2 - m_j^2}) - \vec{p}.\frac{\vec{l}}{L}}{2\sigma_{pA}} \right)^2 + \left(\frac{q_0 - p_0 - (\sqrt{q_0^2 - m_i^2}\frac{\vec{l}}{L} - \vec{p}).\vec{v}_A}{2\sigma_{eA}} \right)^2 . \tag{3.54}$$

The function ϕ is a geometrical factor,

$$\Phi(\vec{p}\times\vec{l}) = N\frac{e^{-\frac{(\vec{p}\times\vec{l})^2}{4\sigma_P^2 l^2}}}{L^2} \tag{3.55}$$

This represents the cone around which one can send a neutrino from the source and hit the detector at a distance L given the Gaussian spread σ_P in the momentum space. And N is a normalization factor so that $N\int d\Omega\Phi = 1$. Due to the exponential nature of $f_i(q_0)$, we can use Laplace's method to perform the final integration by expand it around its maximum value and Gaussian integrate the result, we get,

$$|A_{\alpha\beta}|^2 = |M^0_\alpha(p)|^2 \Phi(\vec{p}\times\vec{l}) \left(\sum_{ij} U^*_{\alpha i} U_{\beta i} U_{\alpha j} U^*_{\beta j} e^{-i\frac{\Delta m^2_{ij} L}{4p_0} - \Phi_{ij}} \right) |M^0_\beta(p)|^2 + O\left(\frac{\Delta m^2_{ij} L}{4p_0}\right) \tag{3.56}$$

$\phi_{ij} = \phi_{ij}(L, p_0)$ is a function of the distance, energy and the detection/production parameters that regulate the energy and distance that one can observe the oscillation, it is equivalent to ϕ_{ij} in Eq. 3.28, but now it depends on how one calculate the process of neutrino production.

Eq. 3.56 is the squared matrix elements that are used in the Fermi's Golden Rule of the colision described by Fig. 3.5. If we apply the phase space integration we obtain the usual result in which there is a decoupling between production from the flux (ϕ), propagation due to oscillation and detection through cross section (σ),

$$N_{\nu_\alpha \to \nu_\beta} \sim \phi_{P_I \to P_f + \nu_\alpha + \bar{l}_\alpha}(p_0) \times P_{\alpha\beta}(p_0) \times \sigma_{D_I + \nu_\beta \to D_f + l_\beta}(p_0) \tag{3.57}$$

where

$$P_{\alpha\beta}(p_0) = \sum_{ij} U^*_{\alpha i} U_{\beta i} U_{\alpha j} U^*_{\beta j} e^{-i\frac{\Delta m^2_{ij} L}{4p_0} - \phi_{ij}} \tag{3.58}$$

3.3.4.1 The Simplest Case Study

For illustration, we can take the simplest case of a pion decaying into a charged lepton l_α and a neutrino ν ($\pi \to l_\alpha + \overline{\nu}$) propagating (and possibly oscillating) and being detected via inverse beta decay reaction ($\overline{\nu} + p^+ \to n + \bar{l}_\beta$), which can be interpreted as a neutrino oscillation from $\alpha \to \beta$ and given by the diagram of Fig. 3.6.

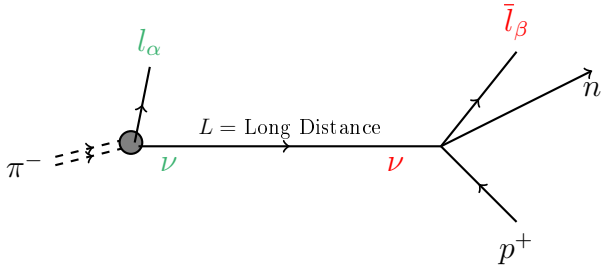

Figure 3.6 – The Feynman diagram representing the leptonic pion decay into a charged lepton l_α and a virtual neutrino ν that propagates a long distance L and is detected via inverse beta decay by transforming a proton in the detector into a neutron and a charged anti-lepton $\bar{l}_\beta$.

The cross section, $d\sigma$, for this reaction is given by,

$$d\sigma = (2\pi)^4 \frac{\langle |M|^2 \rangle}{m_p |\vec{p_\alpha}|} \delta^{(4)}(p_\pi + p_p - p_\alpha - p_\beta - p_n) \frac{d^3 p_\beta}{(2\pi)^3 2E_\beta} \frac{d^3 p_\alpha}{(2\pi)^3 2E_\alpha} \frac{d^3 p_n}{(2\pi)^3 2E_n}. \tag{3.59}$$

Where p_a corresponds to the 4-momentum of particle a. One can use the three momentum delta function to integrate over $d^3 p_n$. Now, assuming the pion and proton at rest and also assuming $p_n << M_n$, the final delta function reads $\delta(m_\pi + m_p - m_n - E_\alpha - E_\beta)$ and $\vec{p_n} = -(\vec{p_\alpha} + \vec{p_\beta})$. Thus, we can also integrate over $\frac{p_\alpha}{E_\alpha} dp_\alpha = dE_\alpha$ and obtain $E_\alpha =$

$m_\pi + m_p - m_n - E_\beta$. And we arive at

$$\frac{d\sigma}{dE_\beta d\Omega_\beta} = \frac{\langle |M|^2 \rangle \, |\vec{p}_\beta|}{2^8 \pi^5 m_p m_n} d\Omega_\alpha \tag{3.60}$$

We now recal that $\langle |M|^2 \rangle$ contains the Gaussian function $\Phi(\vec{p_\alpha} \times \vec{l})$, thus, $\sin^2\theta_\alpha \lesssim \frac{\sigma_p^2}{|\vec{p}_\alpha|} << 1$, where θ_α is the angle between $\vec{l}$ and $-\vec{p}_\alpha$. For simplicity we will set $\theta_\alpha = 0$ which results in

$$\frac{d\sigma}{dE_\beta d\Omega_\beta} = \left. \frac{\langle |M|^2 \rangle \, |\vec{p}_\beta|}{2^7 \pi^4 m_p m_n} \right|_{\theta_\alpha = 0} \tag{3.61}$$

Now $\langle |M|^2 \rangle$ depends on θ_β, ϕ_β. For this simple configuration, $\vec{v}_P = \vec{v}_\alpha$ and $\vec{v}_D = \vec{v}_\beta$, which means

$$f_i(q_0) = \frac{\left(\sqrt{q_0^2 - m_i^2} - p_\alpha\right)^2}{2\sigma^2} \tag{3.62}$$

with $\sigma^{-2} = (\sigma_\alpha^{-2} + \sigma_\beta^{-2})/2$. This means that $\Psi_i(q_0)$ is independent of the angles of $\vec{p}_\beta$ and the integration in $d\Omega_\beta$ can be done analitically. We obtain,

$$\frac{d\sigma}{dE_\beta} = \frac{4 f_\pi^2 m_\pi^2 G_f^2 E_\beta}{\pi^3 l^2} \sum_{ij} U_{\alpha i}^* U_{\beta i} U_{\alpha j} U_{\beta j}^* \int dq_0 \left[E_\alpha (q_0^2 + p_i p_j) - q_0 p_\alpha (p_i + p_j) e^{i(p_i - p_j)l - f_i(q_0) - f_j(q_0)} \right] \tag{3.63}$$

where $p_i = \sqrt{q_0^2 - m_i^2}$ with m_i the mass of neutrino i. Applying the Laplace's Method of integration we obtain,

$$\frac{d\sigma}{dE_\beta} = \frac{4 f_\pi^2 m_\pi^2 G_f^2 E_\beta}{\pi^3 l^2} \times \sum_{ij} U_{\alpha i}^* U_{\beta i} U_{\alpha j} U_{\beta j}^* |M_{ij}|^2 e^{-2\pi i \frac{l}{l_{ij}^{\text{osc}}} - \phi_{ij}^0 - \left(\frac{l}{l_{ij}^{\text{coh}}}\right)^2} \tag{3.64}$$

where

$$|M_{ij}|^2 = \left[E_\alpha (q_0^2 + p_i p_j) - q_0 p_\alpha (p_i + p_j) \right] \tag{3.65}$$

q_0 is now defined by the equation

$$\frac{2}{p_\alpha} = \frac{1}{p_i} + \frac{1}{p_j} \tag{3.66}$$

and

$$l_{ij}^{osc} = \frac{2\pi}{p_j - p_i} \tag{3.67}$$

$$l_{ij}^{coh} = \frac{\sqrt{|m_i^2 + m_j^2 - p_i p_j|}}{2\pi\sigma} l_{ij}^{osc} \tag{3.68}$$

$$\phi_{ij}^{0} = \left(\frac{2\sqrt{2}\pi\sqrt{p_i^2 + p_j^2}}{(p_i + p_j)(l_{ij}^{\rm osc})\sigma} \right)^2 \tag{3.69}$$

These quantities have the usual physical meaning. l_{ij}^{osc} is the length at which the probability oscillates by 2π. This oscillation can be observed as long as $l < l_{ij}^{coh}$ or else the neutrinos' wave-packet will have a relevant sepparation that will disentangle their oscillatory behavior. ϕ_{ij} gives the maximum mass sepparation the neutrinos may have in order for them to keep oscillating at any distance, if $\phi_{ij} << 1$ one can observe the oscillation, otherwise it is exponentially suppresed.

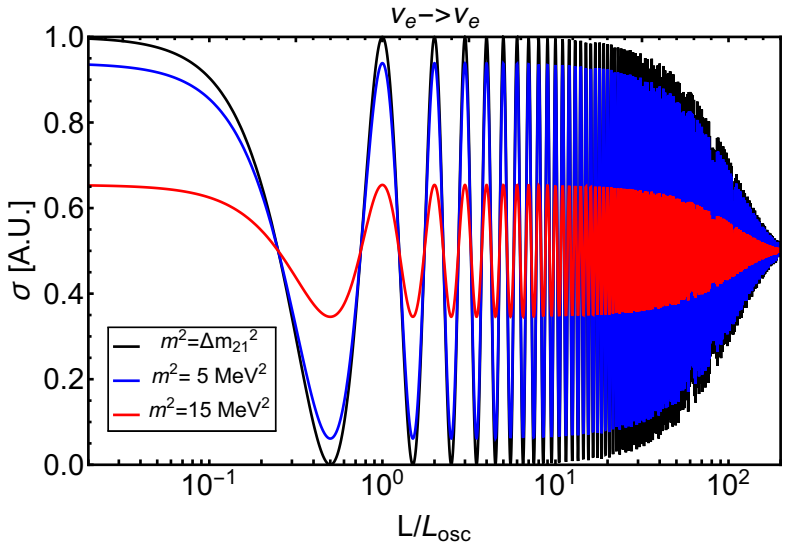

Figure 3.7 – Illustration of two wave packets with $\sigma_i = 0.3$ [a.u.] and momentum $p = 1$ [a.u.] propagation through space: Dashed-Line means $t = 0$, Dot-Dashed Lines are for $t = 50$ [a.u.] and full line $t = 100$ [a.u.]. Also, $m_1 = 0.5$ [a.u.] and $m_2 = 1.0$ [a.u.]. Plot made for this PhD thesis.

On Fig. 3.7 we show the cross-section of Eq. 3.64 for a 2-neutrino scenario and different mass squared differences, $\Delta m^2 = \Delta m_{21}^2$ (black),5 MeV^2 (blue) and 15 MeV^2 (red). Notice that as mass increases, the overall size of σ decreases due to the effect distance independent factor. Also, all oscillations cease to exists for large L. This happens for $L/L_{\rm osc} \sim 10^2$ because we took $\sigma_P, \sigma_D = 0.1$.

For a more detailed discussion of neutrino oscillations in the context of quantum field theory, see [58].

3.4 The Matter Effect

Even though neutrinos interact very little at energies around a few GeV, it is possible to probe tiny effects in their propagation when transversing a medium. That is because neutrino oscillations are sensitive to a phase difference in the Hamiltonian eigenvalues $\Delta E = E_i - E_j$, which can be as small as $\sim 10^{-13}$ eV. In fact, such effect was first predicted in [60, 61]. The coherent forward scattering of neutrinos traveling through matter gives them an effective mass. This is very similar to difraction of fotons or electrons in a not so dense medium. In the SM, such interactions can be described by the 4-fermi-interaction Lagrangian,

$$\mathcal{L} = \frac{G_F}{\sqrt{2}}(\overline{\nu}_l\gamma^\mu l)(\bar{l}\gamma_\mu\nu_l) + \frac{G_F}{s_{\theta_w}\sqrt{2}}(\bar{l}\gamma_\mu l)(\overline{\nu}_{l'}\gamma^\mu\nu_{l'}) + \text{h.c.} \tag{3.70}$$

Since on earth matter is formed by electrons, protons and neutrons, only $l = e, u, d$ are relevant. Moreover, charged currents act only upon electron neutrions and neutral current changes the propagation of all neutrinos in the same way. Under those conditions, the Hamiltonian that is responsible to the neutrino propagation in the flavor basis can be written as,

$$H = UH_0U^\dagger + V \tag{3.71}$$

where V is the matter potential matrix, in the flavor basis and can be written as

$$V_{\alpha\beta} = v_{\text{cc}}\delta_{e\alpha}\delta_{e\beta} + v_{\text{nc}}\delta_{\alpha\beta} \tag{3.72}$$

with $v_{\text{cc}} = \sqrt{2}G_{\text{F}}n_{\text{e}}$ the charged current potential and $v_{\text{nc}} = -G_{\text{F}}n_{\text{n}}/\sqrt{2}$ the neutral current potential. $n_e(n_n)$ is the electron (neutron) density of the medium. Since v_{nc} only changes a global phase, it can be subtracted from the Hamiltonian. This means that the physically relevant parameter for most cases is the potential v_{cc}.

Now, instead of diagonalizing $UH_0U^\dagger$, one should diagonalize H. The oscillation probability has the exact same form as Eq. 3.8, but now the mixing angles in vacuum

θ_{ij} should be changed to the mixing angles in matter $\theta_{ij}^{\text{mat}}(x)$ and the dispersion relation will also change due to the matter potential $E^{\text{mat}} = E^{\text{mat}}(x)$ where x defines the local position of the neutrino during propagation. Both will depend on $n_e(x)$.

3.4.1 Constant Matter Effect

For pedagogical reasons, we will simplify the calculation of the matter effect into a 2-neutrinos scenario traveling in constant matter potÃªntial. In this case, we have only one mixing angle θ and one mass squared difference Δm^2. The Hamiltonian is,

$$H_{\text{matter}} = \frac{\Delta m^2}{2E} \begin{pmatrix} \sin^2\theta & \cos\theta\sin\theta \\ \cos\theta\sin\theta & \cos^2\theta \end{pmatrix} + v_{cc} \begin{pmatrix} 1 & 0 \\ 0 & 0 \end{pmatrix} \tag{3.73}$$

Any 2×2 symmetric matrix can be brought to a convinient form,

$$H_{\text{matter}} = \begin{pmatrix} -A & B \\ B & A \end{pmatrix} + C\mathbb{1} \tag{3.74}$$

where C is a global phase irrelevant for our problem. Such matrix has eigen-values $\pm\sqrt{A^2 + B^2}$ and mixing angle $\tan 2\theta' = B/A$. In our case,

$$\begin{aligned} A =& \frac{\Delta m^2}{4E}\cos 2\theta - \frac{v_{cc}}{2} \\ B =& \frac{\Delta m^2}{4E}\sin 2\theta \end{aligned} \tag{3.75}$$

Thus, the phase difference between the matter states are

$$\begin{aligned} \Delta m^2_{\text{matter}} =& \sqrt{\Delta m^4 + (2Ev_{cc})^2 - 4\Delta m^2 E v_{cc}\cos 2\theta} \\ \tan 2\theta_{\text{matter}} =& \frac{\sin 2\theta}{\cos 2\theta - 2Ev_{cc}/\Delta m^2} \end{aligned} \tag{3.76}$$

This explicitly shows that θ_{matter} is effectively different than the vaccum angle θ. Notice the special case when $\Delta m^2 \cos 2\theta = 2Ev_{cc}$, called *ressonant transitions*, which results in

a maximal mixing of $\theta_{\text{matter}} = \pi/4$ and mass difference of

$$\Delta m^2_{\text{matter}} = \Delta m^2 \sin 2\theta. \tag{3.77}$$

The phenomenology of 3ν case is analogous, but harder to perform analitically. For illustration we plot on Fig. 3.8 the oscillation probability for the DUNE experiment ($L =$ 1300 km) as a function of energy in two cases, for an electron density of 2.957 g/cm^3 in blue and in the vacuum in red.

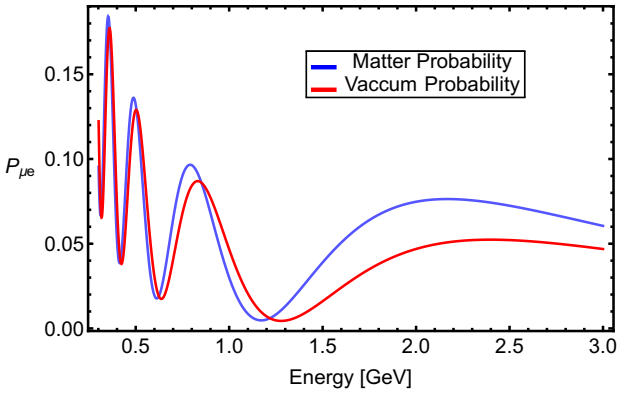

Figure 3.8 – 3-Neutrino oscillation probability $P_{\mu e}$ in matter (blue) and in Vaccum (red) for the baseline of DUNE experiment $L = 1300$ km as the Juno Experiment.

3.4.2 Matter Adiabatic Transitions

The adiabatic transitions due to the matter potential were first described in the works [62, 63, 61]. It treats the flavor adiabatic transitions of neutrinos propagating in a varying density medium. In this case, the mixing angles θ_{matter} at which the Hamiltonian is diagonal will change as neutrino propagates. Thus, for a fixed L, the matter eigenstates of the Hamiltonian are not global propagation eigenstates and different transitions may occur. If the change in the medium density is slow enough (adiabatic), the mixed neutrino states has time to adjust and evolves adiabatically. The condition for it to happen is [64],

$$\gamma = \left| \frac{2E}{\Delta m^2_{\text{matter}}} \frac{d\theta_{\text{matter}}}{dx} \right| = \left| \frac{1}{2} \frac{\sin 2\theta_{\text{matter}}}{\Delta m^2_{\text{matter}}/2E} \frac{dv_{cc}}{dx} \right| << 1. \tag{3.78}$$

γ is called the adiabaticity parameter. To see the origin of this condition and its meaning, we write the evolution equation for a 2-neutrino system explicitly,

$$i\frac{d}{dx}\nu = \frac{1}{2E}U_{\rm m}\begin{pmatrix} -m^2_{\rm matter} & 0 \\ 0 & m^2_{\rm matter} \end{pmatrix} U^\dagger_{\rm m}\nu \tag{3.79}$$

Remember that now both the $m^2_{\rm matter}$ and the mixing angle in the rotation matrix $U_{\rm m}$ depends on L, thus even if we unitary-rotate $\nu' = U_{\rm m}\nu$ we still get a non-vaninshing term $\frac{d}{dL}U_{\rm m}$. Indeed,

$$i\frac{d}{dx}\nu' = \left[\frac{1}{2E}\begin{pmatrix} -m^2_{\rm matter} & 0 \\ 0 & m^2_{\rm matter} \end{pmatrix} + i\left(U^\dagger_{\rm m}\frac{dU_{\rm m}}{dx}\right)\right]\nu' = \begin{pmatrix} -\frac{m^2_{\rm matter}}{2E} & i\frac{d\theta_{\rm matter}}{dx} \\ -i\frac{d\theta_{\rm matter}}{dx} & \frac{m^2_{\rm matter}}{2E} \end{pmatrix}\nu' \tag{3.80}$$

Notice that the off-diagonal terms in Eq. 3.80 are generated exactly by $\frac{d\theta_{\rm matter}}{dL}$. Also, if the off-diagonal terms are much smaller than the diagonal ones (that is $\gamma << 1$), there is no transition between states ν'. This means that the adiabadic condition of Eq. 3.78 imply that conversion between the local matter eigenstates can be neglected and the eigenstates propagates independently. Therefore, in such condition, the admixture of neutrino states are given by the matter mixing angle at the production of the neutrino $\theta^0_{\rm matter}$, but oscillation is still modulated by the phase difference introduced by $\Delta m^2_{\rm matter}/2E$.

This discussion imply that if say an electron neutrino is produced as ($\theta_{\rm matter}(L = 0) = \theta^0$),

$$\nu_e(L=0) = \cos\theta^0\nu_1 + \sin\theta^0\nu_2 \tag{3.81}$$

and the propagation is adiabatic, neutrinos ν_i will evolve as

$$\nu_i(L) = e^{\pm i\int_0^L \frac{\Delta m^2_{\rm matter}}{2E}dx}\nu_i(0). \tag{3.82}$$

If they are detected at a position L ($\theta_{\rm matter}(L) = \theta^1$), the oscillation probability is,

$$P^{\rm adia}_{ee} = \frac{1}{2}\left[1 + \cos 2\theta^0\cos 2\theta^1 + \sin 2\theta^0\sin 2\theta^1\cos\left(\int_0^L \frac{\Delta m^2_{\rm matter}}{2E}dx\right)\right]. \tag{3.83}$$

The most compeling example of adiabatic transitions are neutrinos from the sun. Since the distance is several times greater than the oscillation length, the oscillatory term can be avareged out, resulting in

$$P_{ee}^{\text{adia}} = \frac{1}{2}\left[1 + \cos 2\theta^0 \cos 2\theta^1\right]. \tag{3.84}$$

For $E >> 2$ MeV, $v_{cc} >> \Delta m^2/2E$ and $\cos 2\theta^0 = -1$ (that is ν_e are created as ν_2^{matter}). Outside the sun the medium density is zero, $\cos 2\theta^1 = \cos 2\theta$ and the propagation is adiabatic, thus,

$$P_{ee}^{\text{sun}}(E >> 2\text{MeV}) = \sin^2\theta \approx 0.307 \tag{3.85}$$

taking $\theta = \theta_{12}$.

Since the adiabaticity parameter, γ depends on the energy of the neutrino, even for solar neutrinos their propagation can be a bit more complicated because sun's density can be so high that it can start at densities higher than the resonant condition in Eq. 3.77 and decreases to eventually get to vacuum. In the resonant regime, the adiabaticity parameter can be relevant and transitions from matter states can occur. Under this assumptions, Eq. 3.84 is slightly changed to the so-called Parke formula [65] due to neutrinos crossing the resonance density non-adiabatically,

$$P_{ee} = \frac{1}{2}\left[1 + (1 + 2P)\cos 2\theta^0 \cos 2\theta^1\right]. \tag{3.86}$$

where P are the crossing probability between the states at resonance, if the crossing is adiabatic $P << 1$.

3.4.3 Theoretical derivation of the Matter potential

Here we will present a theoretical derivation of Eq. 3.72. When passing through a medium, the propagation of neutrinos changes sligtly because it interacts coherently with the medium. To the propagation Hamiltonian it should be added a new potential term,

$$U_{\text{PMNS}}^{\dagger} H_0 U_{\text{PMNS}} \rightarrow U_{\text{PMNS}}^{\dagger} H_0 U_{\text{PMNS}} + V_{\text{matter}} \tag{3.87}$$

where V_{matter} is called the matter potential. This can be understood by the diagram of Fig. 3.9 below,

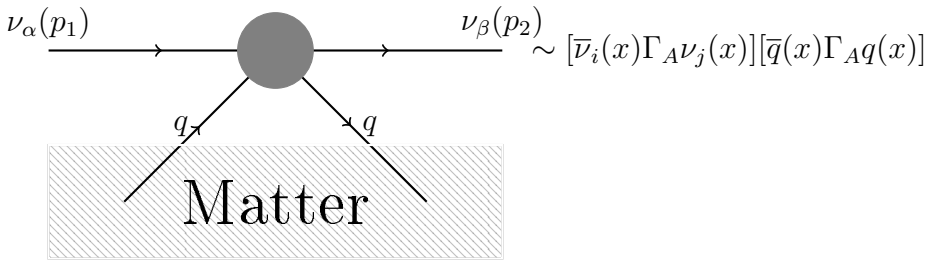

Figure 3.9 – Generic 4-point interaction for matter effect

Where q is the particles in the medium. On earth only $q = e, p, n$ are relevant. Γ_A is any combination of gamma matrix operators. This form is general, since any 4-point fermion interaction with 2 neutrinos can be written with a neutrino current of the form $\overline{\nu}_i(x)\Gamma_A\nu_j(x)$ through the Fierz Identity, see [66]. This can be seen from the neutrino lagrangian if re-written conveniently,

$$\mathcal{L} = \overline{\nu}\left(i\partial\!\!\!/ - M + \sum_q \Gamma_A J_q^A\right)\nu, \tag{3.88}$$

where $J^A = G^q\overline{q}\Gamma_A q$ is an opperator that arrises from interactions of Fig. 3.9. We will see that only the $\Gamma^A = \gamma^0$ part of J^A is relevant in most cases, thus, it will change the Einstein energy relation to $(E-V)^2 = p^2 + m^2$, which intuitively generates the correction of Eq. 3.87.

The effective Hamiltonian due to a fixed q has the form,

$$H_{int}(x) = \frac{G_{ij}^q}{\sqrt{2}}[\overline{\nu}_i(x)\Gamma_A\nu_j(x)][\overline{q}(x)\Gamma_A q(x)]. \tag{3.89}$$

The matter potential is,

$$V_{\alpha\beta} = \int dx d\vec{p_2}\frac{1}{2}\sum_{s_2}\sum_{i'j'}\frac{G_{ij}^q}{\sqrt{2}}\langle U_{\beta j}^*\nu_j(p_1,s_1)q(p_2,s_2)|f(p_2,T)$$
$$([\overline{\nu}_{i'}(x)\Gamma_A\nu_{j'}(x)][\overline{q}(x)\gamma^\mu q(x)])\,|U_{\alpha i}\nu_i(p_1,s_1)q(p_2,s_2)\rangle. \tag{3.90}$$

Notice that we assumed that the final momentum of the neutrino and the lepton won't change. That is because we are interested in the soft (coherent and foward) and elastic

scattering of neutrinos in matter. Also, we included an integration over particle q momentum and spin and added the Fermi occupation function, $f(p_2, T)$, in order to averaged over the matter states.

The coherent foward scathering hypoteses guaratees that $\langle q(p_2, s_2)|$ and $|q(p_2, s_2)\rangle$ have the same momentum, therefore,

$$\begin{aligned}\frac{1}{2}\sum_{s_2}\langle q(p_2,s_2)|\overline{q}(x)\Gamma_A q(x)|q(p_2,s_2)\rangle =& \frac{N^q(\vec{p}_2)}{2E_{p_2}}\frac{1}{2}\sum_{s_2}\overline{u}_q(p_2)\Gamma_A u_q(p_e)\\ =& \frac{N^q_{s_2}(\vec{p}_2)}{4E_{p_2}}\mathrm{Tr}[(\not{p}_2 - m_q)\Gamma_A].\end{aligned} \tag{3.91}$$

where,

$$N^q(\vec{p}_2) = \frac{1}{v}\langle q(p_2,s_2)|a^\dagger(p_2)a(p_2)|q(p_2,s_2)\rangle, \tag{3.92}$$

is the number density operator of particle q with momentum $\vec{p}_2$ and spin s_2. We can now integrate over p_2 momentum and define the function

$$j^q_A = \int d\vec{p}_2 f(p_2,T)\frac{N^q(\vec{p}_2)}{4E_{p_2}}\mathrm{Tr}[(\not{p}_2 - m_q)\Gamma_A]. \tag{3.93}$$

The neutrino part is easier. Since we do not have the $f(p_2, T)$ function,

$$\begin{aligned}&\int dx\langle\nu_j(p_1,s_1)U^*_{\beta j}|\overline{\nu}_{i'}(x)\Gamma_A\nu_{j'}(x)|U_{\alpha i}\nu_i(p_1,s_1)\rangle =\\ &\sum_{s,s'}\int dpdp'dx\frac{U^*_{\beta j}U_{\alpha i}}{2V\sqrt{E_pE'_p}}\langle a_{js_1}(p_1)a^\dagger_{i's}(p)a_{j's'}(p')a^\dagger_{is_1}(p_1)\rangle\overline{u}_\nu(p,s)\Gamma_A u_\nu(p',s')e^{ix(p-p')},\end{aligned} \tag{3.94}$$

the integration over x generates a delta function that guarantees $p = p'$ and we can now use the properties of creation and anihilation operator an write[‡],

$$\sum_{s,s'}\int dx\langle\nu_j(p_1,s_1)U^*_{\beta j}|\overline{\nu}_{i'}(x)\Gamma_A\nu_{j'}(x)|U_{\alpha i}\nu_i(p_1,s_1)\rangle = \sum_{ij}\frac{U^*_{\beta j}U_{\alpha i}}{2VE_{p_1}}\overline{u}_\nu(p_1,s_1)\Gamma_A u_\nu(p_1,s_1)\delta_{ij'}\delta_{i'j}.$$

The matter potential becomes,

$$V_{\alpha\beta}(p_1,s_1) = \frac{G_{\alpha\beta}}{\sqrt{2}E_{p_1}}j^q_A\mathrm{Tr}\left[(\not{p}_1 + m_\nu)\left(\frac{1+\gamma_5\not{s}_1}{2}\right)\Gamma_A\right] \tag{3.95}$$

[‡]Notice that for anti-neutrinos we get instead $b_{i's}b^\dagger_{j's'}$ resulting in a minus sign and $G_{\alpha\beta} \to G^*_{\alpha\beta}$.

where s_1 is the spin polarization vector of the neutrino. This is the general case matter potential. Further discussion can be foun in [67, 68, 69].

3.4.4 Matter Effect in The Standard Model

In the standard model, the matter potential takes a very simple form. In principle, one should consider Eq.3.95 for both charged and neutral current, and for particles $q = e, n, p$. Nevertheless, neutral currents act exactly the same way for all neutrino flavours, thus, it will produce a term of the form $V_{\rm nc} \propto \not{1}$ which makes no difference as it is a global phase in the oscillation amplitude. Thus, only $q = e$ via weak charged current interaction is relevant. Therefore, on Eq. 3.95, $G_{\alpha\beta} = \delta_{\alpha e}\delta_{\beta e}G_{\rm F}$. Moreover, $\Gamma_A = \gamma_\mu(1-\gamma_5)$ and we get,

$$j^q_\mu = \int d\vec{p}_2 f(p_2, T)\frac{N^e(\vec{p}_2)}{E_{p_2}}p_\mu \tag{3.96}$$

Assuming isotropic electron density, the integration becomes zero for $\mu \neq 0$ since $\int d\vec{p}_2\vec{p}M(p) = 0$, for an isotropic function $M(p)$. Thus,

$$j^q_\mu = n_e\delta_{\mu 0} \tag{3.97}$$

where n_e is the mean density of electrons in the medium. Thus,

$$V^{SM}_{\alpha\beta}(p_1) = \frac{\delta_{\alpha e}\delta_{\beta e}G_{\rm F}n_e}{\sqrt{2}E_{p_1}}{\rm Tr}\left[(\not{p}_1 + m_\nu)\left(\frac{1+\gamma_5\not{s}_1}{2}\right)\gamma_0(1-\gamma_5)\right] \tag{3.98}$$

if $s_1 = +1$, that is, neutrinos are right-handed, $\left[(\not{p}_1 + m_\nu)\left(\frac{1+\gamma_5\not{s}_1}{2}\right)\gamma_0(1-\gamma_5)\right] \sim m^2_\nu/E$. For left-handed neutrinos ($s_1 = -1$), we have,

$$V^{SM}_{\alpha\beta}(p_1) = \sqrt{2}G_{\rm F}n_e\delta_{\alpha e}\delta_{\beta e}. \tag{3.99}$$

3.5 Neutrino Oscillation Experiments

Neutrino oscillations is long proved to be a reallity. The mixing angles were measured with a precison around a few percent. Meanwhile, the physics community still lack knowledge in the leptonic sector. There are two parameters that still need to be measured: the δ_{CP} phase and the lightest neutrino mass. Also, the atmospheric angle θ_{23} contains a degeneracy in its parameter space [70], known as the octant problem. On top of that, neutrino masses are the first laboratory based phenomenon that deviates from the predictions of the SM.

Characteristics	T2K [71]	NOνA [72]	DUNE [20]	T2HK [73]
Baseline	295 km	810 km	1300 km	295 km
Detector Size	22.5 kt	14 kt	40 kt	2×190 kt
Target	Water	Liq. Scintilator	Liq. Argon	Water
Mean Energy	0.6 GeV	2.0 GeV	2.5 GeV	0.6 GeV
Exposure (POT)	7.8×10^{21}	3.6×10^{21}	1.47×10^{21}	1.56×10^{22}
Status	Running (10% POT)	Running (17% POT)	Approved Expected 2026	Approved Expected 2032

Table 3.1 – Summary of characteristics of current (T2K and NOνA) and Future (DUNE and T2HK) neutrino experiments. The exposure is in units of Protons on Target (POT).

In order to push foward the frontier in particle physics many big scientific collaborations were organized to explore the unknowns of neutrino physics. In special, the long-baseline neutrino experiments can measure the δ_{CP} [74], might be able to solve the octant problem [7] and will determine if the lightest neutrino is m_1 or m_3 [75, 76]. On Table 3.1 we summarize the main characteristics of longbaseline experiments: T2K [71], NOνA [72], DUNE [20] and T2HK [73]. In the following sections we describe how each experiments work.

In this work, we will focus only on long-baseline experiments. Nevertheless, it is worth to briefly mention that there are a lot more neutrino experiments. Accelerator-based short-baseline such as the SBN experiment [2] and MiniBoone [77] are running and searching for sterile neutrino and will be fundamental to measure neutrino cross

section for the long-baseline experiments. The future JUNO experiment [52] is a medium baseline experiment in China and might be able to measure the neutrino mass hierarchy. IceCube [78] is located in the South Pole and can measure the most energetic neutrinos from the cosmos (up to PeV scale!). The Katrin experiment [79] promise to be sensitive to neutrino masses of about ~ 0.2 eV through beta decay. And last but not least, a handfull of neutrinoless double beta decay experiments [80] that try to discover the true nature of neutrino mass.

3.5.1 Production of a Neutrino Beam

Since neutrinos do not have an electric charge, it is very challenging to produce high intensity and collimated neutrino beams. The current technology of accelerator neutrinos relies on the decay of pions to produce the necessary luminosity.

A primary accelerator collides protons of high energy[§] ($O(10-100)$ GeV) into a target, usually Graphite. About 85% of those collisions produces secondary meson particles consisting mostly of pions ($\sim 94\%$) and kaons ($\sim 6\%$). Those are collimated by a very strong magnetic field before entering into a decaying pipe. The experiments usually allow two modes, the neutrino (anti-neutrino) mode where only π^+ (π^-) are selected through the magnetic field. The mesons are unstable and decay, mostly to $\nu_\mu + \mu^+$ ($\overline{\nu}_\mu + \mu^-$). There is a small contamination of other neutrinos such as $\nu_e, \overline{\nu}_e$ and $\overline{\nu}_\mu(\nu_\mu)$, which are regarded as an intrinsic background. The remaining charged particles collide into a second target and are absorbed. Only neutrinos remain on the beam, that finally arrives at the detectors.

[§]That is why the exposure is measured as POT.

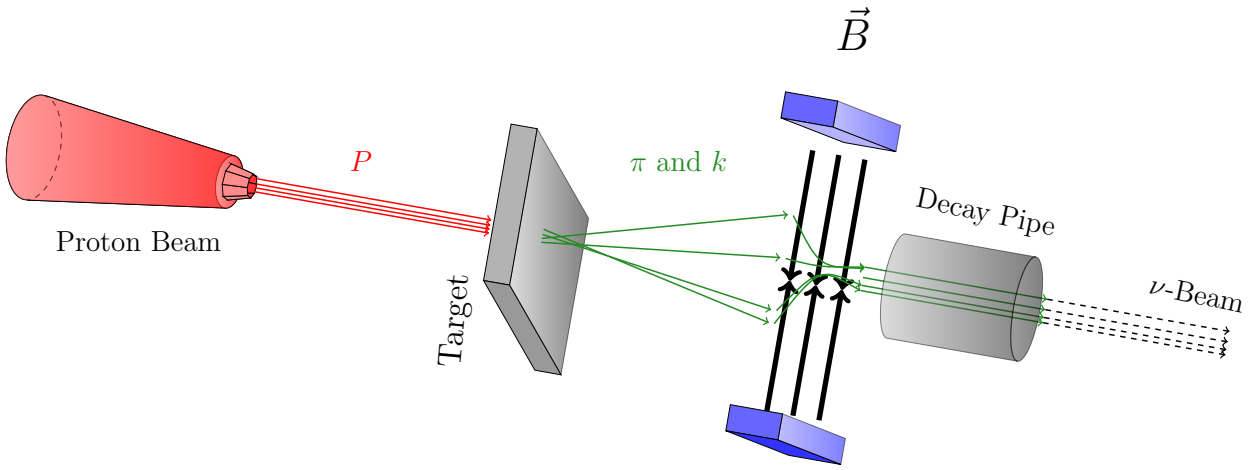

Figure 3.10 – Schematics of the neutrino beam production. A beam of protons (red) is set to collind into a target (gray) that produces a beam of secondary particles (green) consisting mostly of pions, that are focalized to later decay into neutrinos (black-Dashed) and charged leptons. Figure produced for this thesis.

A schematics of the neutrino beam production is found in Fig. 3.10. In red we depict the proton beam source, in gray the primary target of Graphite and in red the resulting meson beam, that later decay into neutrinos. A futuristic concept of accelerator-based neutrino beams aims to use the tertiary muons produced by the pion decay. Those can be stored and accelerated into another detector, and later decay into a neutrino beam, thus, providing a much more clear flux. Those are called neutrino factories [81] and a realistic experimental concept is the MOMENT experiment [82].

3.5.2 Current Long-Baseline Experiments

The two long-baseline neutrino oscillation experiments that are currently running are the T2K and NOνA experiments. Both recently performed the first measurements of the $\delta_{\rm CP}$. T2K measures: $\delta_{\rm CP}/\pi = -1.4 \pm 0.7$ [83] and NOνA: $\delta_{\rm CP}/\pi = 0.17 \pm 1$ [84]. It is interesting to note that their result is in a $\sim 2\sigma$ tension [85]. Which might be solved in the future, or reveal new physics. Below we present both experimental configurations in detail.

1. **T2K:** The Tokai to Kamiokande (T2K) experiment [86] consists of an accelerator-produced neutrino beam from the J-PARC facility. The beam is pointed off-axis (by a 2.5° angle) to the well-known Super-Kamiokande detector located 1 km inside

Mount Ikeno (Japan) 295 km from the neutrino source. The experiment has three detectors: The on-axis near detector (INGRID), the off-axis near detector (ND280), which measures the non-oscillated flux and the far detector, the Super-Kamiokande (SK) which is a 22.5 kt water Cherenkov neutrino detector. SK is also used to study solar, atmospheric neutrinos and proton decay and exists since 1983, therefore, its response is very well understood. The J-PARC Neutrino beam is produced via pion decay producing neutrinos with energy around 0.6 GeV. It can run in both neutrino and anti-neutrino mode. Its expected final exposure is 7.8×10^{21} protons on target (POT), it already runs 10% of this value. In order to simulate the experiment, we will assume an uncorrelated 5% signal normalization error and 10% background normalization error for both neutrino and antineutrino appearance and disappearance channels respectively. On Fig. 3.11 we present the expected neutrino spectrum and the sensitivity of the experiment for the parameter θ_{23} and $\delta_{\rm CP}$.

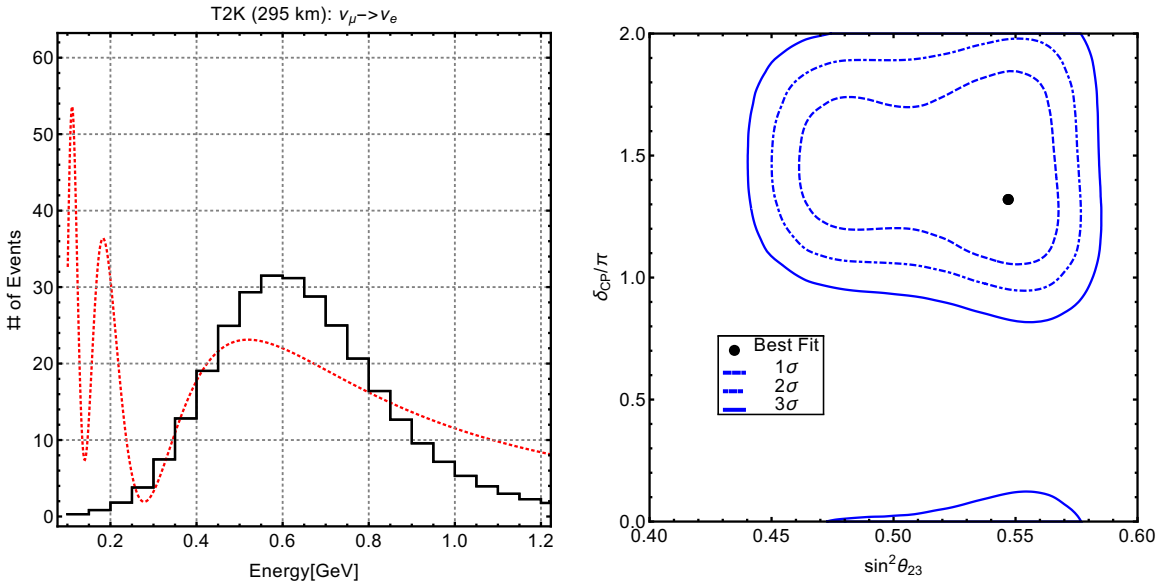

Figure 3.11 – **Left:** In Black the expected number of ν_e events as a function of measured neutrino energy with the total POT expected by end of T2K run and in Red the oscillation probability. **Right:** Expected sensitivity in the $\theta_{23} - \delta_{\rm CP}$ plane of T2K experiment for $1, 2$ and 3σ of C. L. Plot made for this PhD thesis.

3. **NOνA :** The Neutrinos at the Main Injector Off-axis ν_e Appearance (NOνA) experiment [87, 88, 72] is an off-axis (by a 0.8^0 angle) accelerator based superbeam experiment. The neutrino beam is produced by the Fermilab Main Injector, the old injection accelerator of the famous TEVATRON. The experiment consists of two detectors, the near detector is located at the Fermilab site while the far detector is a 14 kt Liquid Scintillator Detector placed in Ash River, Minnesota, 810 km

away from the neutrino source. The off-axis position is chosen in order to produce neutrinos with energy around 2 GeV. The expected POT is 3.6×10^{21} divided in 50%/50% neutrino/anti-neutrino mode. Our simulations assume uncorrelated 5% signal normalization error and 10% background normalization error for both modes. On Fig. 3.12 we present the expected neutrino spectrum and the sensitivity of the experiment for the parameter θ_{23} and $\delta_{\rm CP}$.

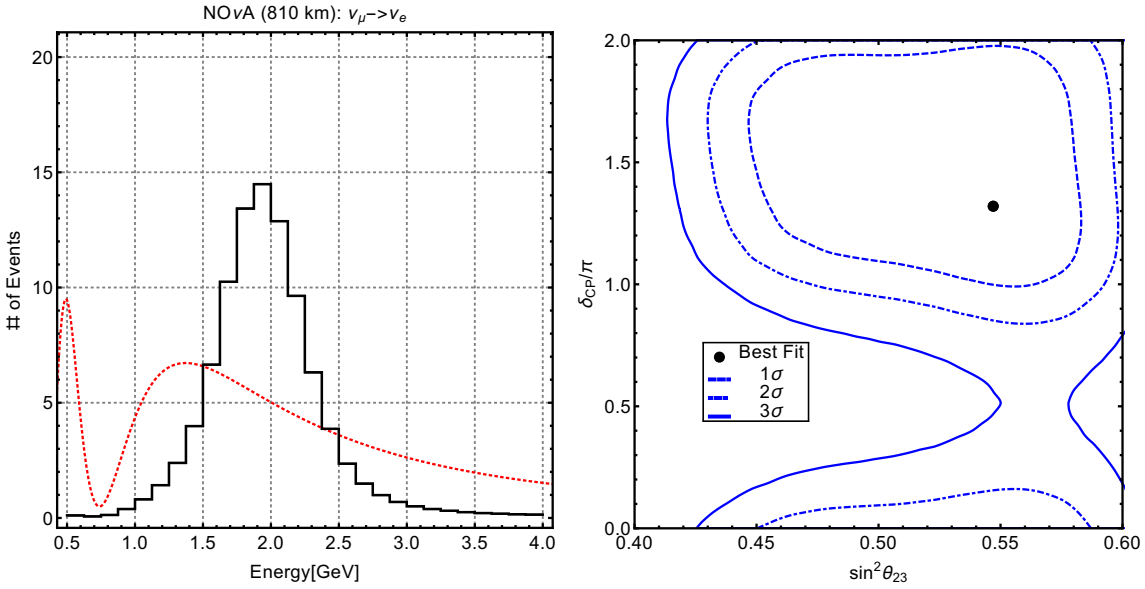

Figure 3.12 – **Left:** In Black the expected number of ν_e events as a function of measured neutrino energy with the total POT expected by end of NOνA run and in Red the oscillation probability. **Right:** Expected sensitivity in the $\theta_{23} - \delta_{\rm CP}$ plane of NOνA experiment for $1, 2$ and 3σ of C. L. Plot made for this PhD thesis.

3.5.3 Future Long-Baseline Experiments

The DUNE [20, 89, 90, 91] and T2HK [18, 73] experiments are the two largest neutrino experiments envisioned in the near future. They plan to measure neutrino parameters to unprecedented precision, they will be able to measure the neutrino mass hierarchy and might be able to solve the octant problem. Below we describe both expected experimental configurations.

4. **DUNE :** The Deep Underground Neutrino Experiment (DUNE) is a longbaseline future generation experiment. Its neutrino beam is produced by the LBNF facility and is shot on-axis to its far detector, which is a Liquid Argon Time Projection

Chambers (LArTPC). DUNE will use 4-modulus of 10 kt located at Sanford Underground Research Laboratory in Lead, South Dakota, 1300 km away from its beam source. The experiment should run for 3.5 yrs in neutrino/anti-neutrino mode each. The detailed configuration we used to simulate the experiment follows the GLB file provided by the collaboratio [92]. On Fig. 3.13 we present the expected neutrino spectrum and the sensitivity of the experiment for the parameter θ_{23} and $\delta_{\rm CP}$.

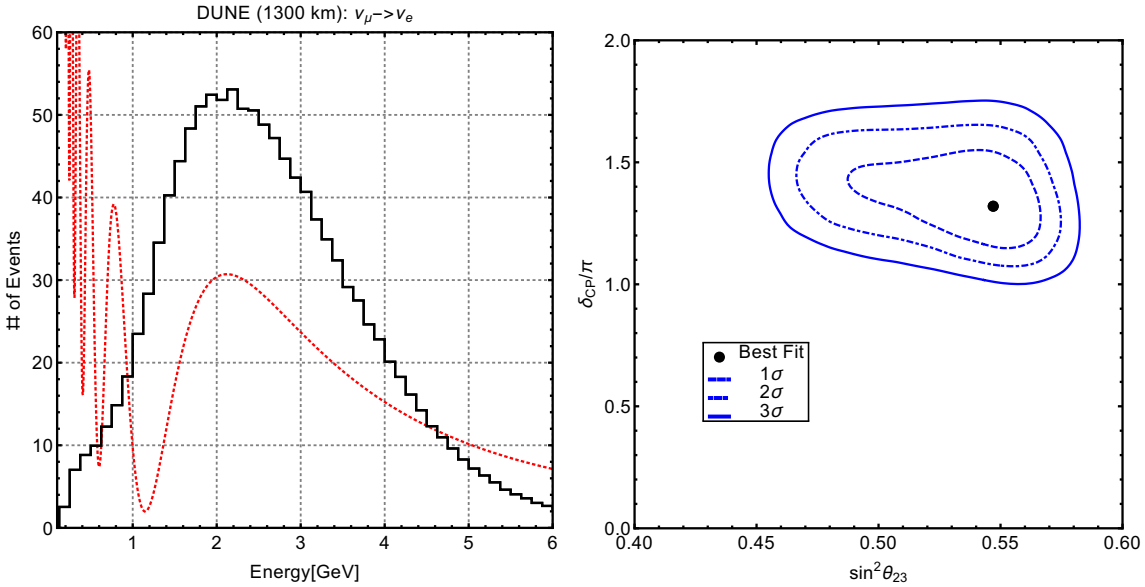

Figure 3.13 – **Left:** In Black the expected number of ν_e events as a function of measured neutrino energy with the total POT expected by end of DUNE run and in Red the oscillation probability. **Right:** Expected sensitivity in the $\theta_{23} - \delta_{\rm CP}$ plane of DUNE experiment for $1, 2$ and 3σ of C. L. Plot made for this PhD thesis.

2. **T2HK :** The Tokai to Hyper-Kamiokande (T2HK) is an upgrade of the T2K experiment by the addition of the Hyper-Kamiokande (HK) detector. The HK will consist of 2 water Cherenkov tanks with 190 kt mass. They will be located at the same site of SK, therefore its baseline is still 295 km. There will also be an upgrade on the J-PARC beamline leading to a 1.53×10^{21} POT exposure for the T2HK experiment running in a 1:3 ratio of neutrino/anti-neutrino. The T2HK is expected to be operational by 2025. In our simulations, we assume a similar neutrino energy resolution as T2K and beam normalization error. On Fig. 3.14 we present the expected neutrino spectrum and the sensitivity of the experiment for the parameter θ_{23} and $\delta_{\rm CP}$.

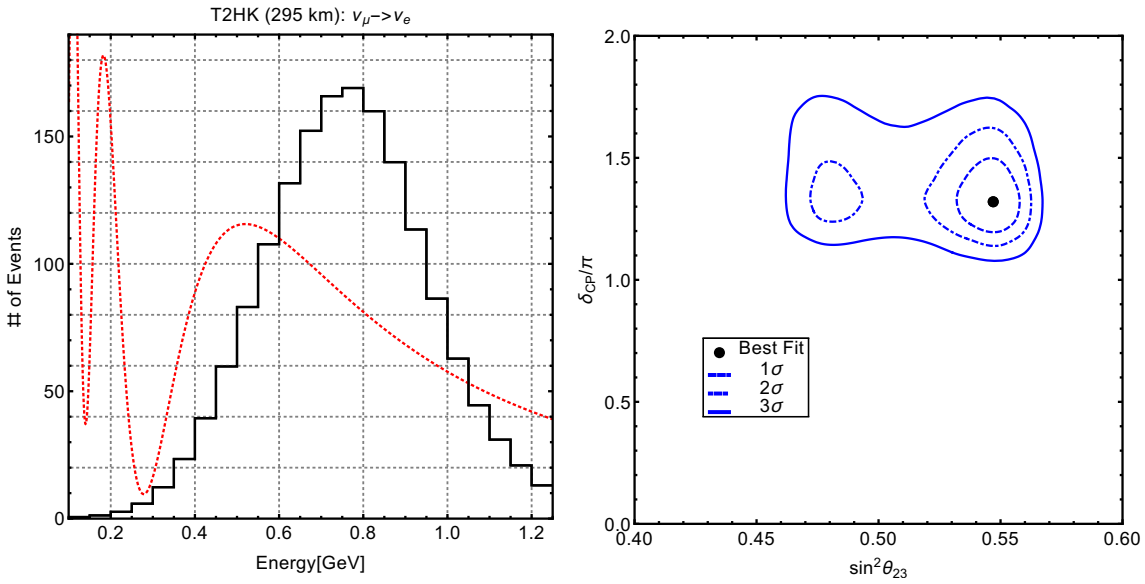

Figure 3.14 – **Left:** In Black the expected number of ν_e events as a function of measured neutrino energy with the total POT expected by end of T2HK run and in Red the oscillation probability. **Right:** Expected sensitivity in the $\theta_{23} - \delta_{\rm CP}$ plane of T2HK experiment for $1, 2$ and 3σ of C. L. Plot made for this PhD thesis.

3.6 Conclusion

In this Chapter we presented the concept of neutrino oscillation. We started by presentend a short review of the experiments that settled the ground to the understanding of neutrino oscillations. We also introduced the theoretical framework for the standard 3-neutrino oscillation in three different theoretical approaches. The quantum mechanical approach is easier to understand and more intuitive, but it is fundamentaly incorrect since it makes some assumptions that are not valid in every context. We then follow to present the Quantum field theory explanation for the standard 3-neutrino oscillation and we arive at what are the necessary conditions in order for the validity of the quantum mechanis approach. Neutrino oscillations are consistent with every neutrino experiment and is the future of the experimental neutrino physics and in the last section of this Chapter we show the future of longbaseline neutrino experiments.

Chapter 4

Beyond Standard 3-Neutrino Oscillation

"I am in a charming state of confusion"

Ada Lovelace

4.1 What is Beyond Standard Oscillation?

As discussed on Chapter 3, neutrino oscillation is an experimental fact. It can only exist if neutrinos have masses and if they are different. Thus, neutrino oscillation is a phenomenon beyond the standard model. Nevertheless, it is possible to describe the neutrino oscillations without the account of any other particle. It suffices the assumption on neutrino mass. Also, the nature of the neutrino mass does not change any of the equations: Dirac Neutrinos and Majorana Neutrinos *oscillate in the same way* [93].

It is useful to define a standard picture for neutrino oscillations that accounts for all the experimental data that was tested, we call it here the *Standard 3-Neutrino Oscillations* or S3νO for short: There exists only 3 type neutrinos ν_i, $i = 1, 2, 3$. Those have masses m_i, that are different, thus $\Delta m^2_{ij} = m^2_j - m^2_i \neq 0$ if $i \neq j$. Neutrinos are created, in vaccum, as a combination of ν_i via the weak-interaction, which we will call ν_e, ν_μ and ν_τ by their charged lepton partners, and we can relate both basis by a unitary matrix $U^\dagger_{\text{PMNS}} = U^{-1}_{\text{PMNS}}$. The neutrinos feel a matter potential when travelling through matter due to charged current and neutral current weak interactions. This can

be mathematically summarized into the propagation Hamiltonian written in flavour basis,

$$H_0 = U_{\rm PMNS}.{\rm Diag}[0, \Delta m^2_{21}/2p, \Delta m^2_{31}/2p].U^\dagger_{\rm PMNS} + {\rm Diag}[v_{\rm cc}, 0, 0] + (p + m^2_1/2p + v_{\rm nc})\mathbb{I}. \quad (4.1)$$

Where $p \approx E$ is the neutrino momentum and $v_{\rm cc} = \sqrt{2}G_F n_e$ is the charged current matter potential, with n_e the electron density in the medium. The term proportional to the identity will not be detectable by neutrino oscillation, as it is a global phase.

In next section we will present experimental and theoretical aspects of neutrino oscillation and masses that lead the physics community to explore many different models that change the assumptions in the construction of S3νO. We will call them *Beyond S3νO* (BS3νO) physics.

4.2 Non-Standard Interaction

A simple way of extending the idea of S3νO is to imagine that there might exist a new 4-fermion interaction of the form,

$$H_{int}(x) = \frac{G^q_{\alpha\beta}}{\sqrt{2}}[\overline{\nu}_i(x)\Gamma_A\nu_j(x)][\overline{q_1}(x)\Gamma_A q_2(x)], \quad (4.2)$$

that is different from the standard model interactions. This implies the existence of non-standard interactions (NSI) and can be accomplihed by the introduction of heavy bosons or scalar particles [94, 95]. In a minimal scenario, one can assume the interaction to be similar to that of the standard model, which can be parametrized as [96],

$$H_{int}(x) = \epsilon^{q_1 q_2}_{\alpha\beta}\frac{G^F}{\sqrt{2}}[\overline{\nu}_\alpha(x)\Gamma_A\nu_\beta(x)][\overline{q_1}(x)\Gamma_A q_2(x)], \quad (4.3)$$

This can generate three interesting effects on neutrino oscillations. A difference in the production (P)/detection (D), which we denote by the $\epsilon^A_{\alpha\beta}$, $A = P, D$,

$$\begin{aligned} |\nu_\alpha(t)\rangle &= (1 + \epsilon^P_{\alpha\gamma})U^*_{\gamma i}|\nu_i(t)\rangle \\ \langle\nu_\beta| &= \langle\nu_j|U_{j\gamma}(1 + \epsilon^D_{\gamma\beta}) \end{aligned} \quad (4.4)$$

And a different matter effect,

$$V_{\text{matter}} = \text{Diag}[v_{\text{cc}} + v_{\text{nc}}, v_{\text{nc}}, v_{\text{nc}}] + v_{\text{cc}}\epsilon_{\alpha\beta} \tag{4.5}$$

where,

$$\epsilon_{\alpha\beta} = \epsilon^{ee}_{\alpha\beta} + \frac{N_u}{N_e}\epsilon^{uu}_{\alpha\beta} + \frac{N_d}{N_e}\epsilon^{dd}_{\alpha\beta} \tag{4.6}$$

Where N_u (N_d) is the number of $u(d)$ type quarks in the medium. On earth, $\frac{N_u}{N_e} \approx \frac{N_d}{N_e} \approx 3$ and inside the sun $\frac{N_u}{N_e} \approx 2\frac{N_d}{N_e} \approx 1$. Constraints on all those parameters can be found in [97, 98]. Although, recent discussion argue that bounds production/detection diagonal parameters $\epsilon^A_{\alpha\alpha}$ cannot extracted from such experiments, since one can always absorb such effects in the definition of CKM matrix and the weak-constant [99].
NSI were deeply studied in the literature in various context, specially in the matter effect of long-baseline experiments [100, 101, 102, 103, 104, 105, 106].

Production/Detection NSI can produce a very interesting zero-distance effect. In the example of a neutrino beam containing only muon neutrinos (take for example neutrinos produced by pion decay), it is possible to detect electron neutrinos, if the interactions in the detector is different from that of the production,

$$P_{\mu e}(L = 0) = |(1 + \epsilon^P_{ee})\epsilon^D_{\mu e} + (1 + \epsilon^D_{\mu\mu})\epsilon^P_{e\mu}|^2. \tag{4.7}$$

Another interesting feature of NSI is the existence of regions of degeneracies in the parameter space [1, 107], which happens to cancel the visible effect of NSI even for large values of the $\epsilon_{\alpha\beta}$ parameters in the matter.

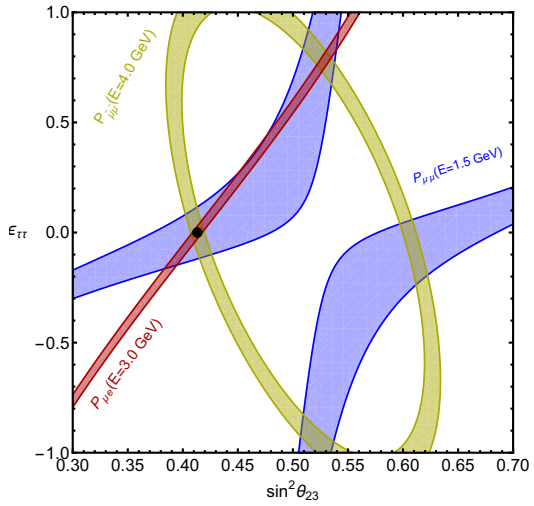

Figure 4.1 – Example of Degeneracy of NSI space parameter. The regions corresponds to the percentual difference of the $P_{\mu\alpha}$ of less than 1%. For a baseline of $L = 1300$ km, the DUNE baseline. The black dot is the S3νO point for $\sin^2\theta_{32} = 0.413$. Notice that at the point $(\sin^2\theta_{32}, \epsilon_{\tau\tau}) = (0.535, 0.7)$ all the curves intercept each other. This plot made for this PhD thesis as an updated version of similar figure of Reference [1].

This can be observed in Fig. 4.1 where we plotted the regions $|P^{\text{SM3}\nu}_{\mu\alpha} - P^{\text{NSI}}_{\mu\alpha}|/P^{\text{SM3}\nu}_{\mu\alpha} < 1\%$ for various values of $\epsilon_{\tau\tau}$ and $\sin^2\theta_{23}$. The points where all curves intercept each other are degeneracies that are difficult to observe in neutrino experiments.

4.2.1 Scalar Non-Standard Interaction

The NSI presented on Section 4.2 requires that the 4-Fermion interaction should be of the form,

$$H_{int}(x) = \frac{G^{q_1 q_2}_{\alpha\beta}}{\sqrt{2}}[\overline{\nu}_i(x)\Gamma_A\nu_j(x)][\overline{q_1}(x)\Gamma_A q_2(x)], \tag{4.8}$$

with $\Gamma^A = \gamma^\mu$ or $\gamma^\mu(1-\gamma_5)$. This is the usual interaction for spin-1 bosons. That is not always the case for scalar particles. It is not uncommon that a model prediction generates a Yukawa interaction $g_{ij}\overline{\nu}_i\nu_j\phi$. This simple case of a (pseudo-)scalar mediator gives $\Gamma_A = 1$ (or $1-\gamma_5$) and we would obtain for an isotropic dense medium, from Eq. 3.93,

$$j^e = -m_e \int d\vec{p}_2 f(p_2, T)\frac{N^e(\vec{p}_2)}{E_{p_2}} = -m_e \left\langle \frac{n_e}{E_e} \right\rangle \tag{4.9}$$

Therefore, from Eq. 3.95, the neutrino matter potential for a typical scalar interaction is

$$V^{SM}_{\alpha\beta}(p_1) = -\left\langle \frac{n_e}{E_e} \right\rangle \frac{m_e G_{\alpha\beta}}{\sqrt{2}} \mathrm{Tr}\left[(\not{p}_1 + m_\nu) \left(\frac{1+\gamma_5 \not{s}_1}{2} \right) \right] = -\sqrt{2} G_{\alpha\beta} \left\langle \frac{n_e m_e}{E_e} \right\rangle \frac{m_\nu}{E_{p_1}}$$

and similar for a pseudo-scalar. Thus, the matter potential goes as $V^{\text{scalar}} \sim O(m_\nu/E_\nu)$ and does not seem to contribute for usual matter effects. A recent paper argues that this is a very different type of NSI that changes the neutrino mass [108]. To see the difference, we re-write Eq. 3.88 by explicitly showing different opperators for scalar NSI,

$$\mathcal{L} = \overline{\nu}_\alpha \left[\gamma^\mu (i\partial^\mu + J_1^\mu) + (M_\nu + J_2) \right] \nu_\alpha.$$

J_1^μ is a vector current typical from the SM neutrino interactions and standard NSI while J_2 a scalar NSI. It is clear from this that J_1^μ changes the energy-momentum relation $p^\mu \to p^\mu + J_1^\mu$, while J_2 changes the γ^μ independent part of the Lagrangian, that is, the neutrino mass is now: $M_\nu \to M_\nu + J_2$. In fact, if the medium contain non-relativistic electrons $E_e \approx m_e$, J_2 results in an effective neutrino mass matrix: $M_\nu^{\text{eff}} = M_\nu + M_S$, where $M_S = \sqrt{2} G_{\alpha\beta} n_e$.

One must be carefull, as not all scalar interactions leads to this kind of NSI. Let's take as a case study the Type-II SeeSaw. The Yukawa interaction Lagrangian is,

$$\mathcal{L}_Y = L_\alpha^T C i\sigma_2 Y_\Delta \Delta L_\beta + \lambda_\phi \phi^T i\sigma_2 \Delta^\dagger \phi + \text{h.c.} \tag{4.10}$$

C is the charge conjugation matrix. $\Delta = \frac{1}{\sqrt{2}} \sigma_i \Delta_i$, $\Delta_i = (\Delta_1, \Delta_2, \Delta_3)$ is a tripplet scalar. L is the usual fermion doublet, ϕ a singlet scalar and σ_i the Pauli matrices. Applying Euler-Lagrange to the full lagrangian, we obtain,

$$\begin{aligned} \Delta^\alpha_{\text{classic}} &= \left[(D_\mu)^2 + \lambda_\phi \vec{T} \phi^\dagger \vec{\sigma} \phi + (M_\Delta^2 + \lambda_3 \phi^\dagger \phi) \right]^{-1}_{\alpha\beta} \left[\mu \tilde{\phi}^\dagger \sigma^\beta + \overline{L} Y_\Delta^\dagger \sigma^\beta i\sigma_2 C L \right] \\ &\approx \frac{1}{M_\Delta^2} \left[\mu \tilde{\phi}^\dagger \sigma^\alpha \phi + \overline{L} Y_\Delta^\dagger \sigma^\alpha i\sigma_2 C L \right] \end{aligned} \tag{4.11}$$

Which can be applied to Eq. 4.10 and the scalar Δ integrated out, which results in terms of 4-fermions interactions of the form

$$H_{int} = \frac{1}{M_\Delta^2} \left(L^T C i\sigma_2 Y_\Delta \vec{\sigma} L \right) \left(\overline{L} Y_\Delta^\dagger \vec{\sigma} C i\sigma_2 L \right) \tag{4.12}$$

Notice the crucial $\vec{\sigma}$. It appears because we are connecting a 3 dimensional representation of $SU(2)$, Δ, to a bi-dimensional representation of $SU(2)$, L. Eq. 4.12 can be re-arranged by a Fierz transformation, resulting in,

$$H_{int} = -\frac{(Y_\Delta)_{\sigma\gamma}(Y_\Delta)^\dagger_{\alpha\beta}}{M^2_\Delta}\left(\overline{\nu}_\alpha\gamma^\mu\nu_\gamma\right)\left(\overline{l}_\sigma\gamma_\mu l_\beta\right). \tag{4.13}$$

Which is the usual NSI interaction. Therefore, not all scalar interactions are different from the standard NSI.

4.3 Sterile Neutrinos

Another way of extending the S3νO is the addition of extra light sterile neutrinos. The idea is that they should be light enough to participate in oscillation, $m_{\text{sterile}} \lesssim 1$ eV. Notice that now the mixing matrix is not an unitary 3×3 matrix, but rather, an unitary $N\times N$, where $N = 3 + n_{\text{sterile}}$. This implies that the number of parameters rise quickly. There are $N(N-1)/2$ mixing angles. If neutrino masses are Dirac type there are also $(N-1)(N-2)/2$ phases, while for Majorana neutrinos, $N(N-1)/2$ phases.
The neutrinos are called sterile, because they cannot interact via weak-interactions. If they interact via weak-forces, they should have been observed in the famous LEP measurement of the Z decay width. It was reporter the number of neutrino N_ν as [109],

$$N_\nu = 2.9840 \pm 0.0082 \tag{4.14}$$

Notice the key assumptions on this measurement: Z-boson couplings to neutrinos are described by the Standard Model. Therefore, one could add another neutral fermion with coupling to Z, as long as the interaction coupling constant g_{new} is small enough: $(g_{\text{new}}/g_{\text{sm}})^2 \lesssim 5\times 10^{-3}$.
Cosmology also puts constraints on the effective number of neutrinos by observing anisotropy of cosmic microwave backgorund and barion acoustic oscillation. The quoted conservative value by the PDG [53] is,

$$N^{\text{eff}}_\nu = 3.13 \pm 0.32, \tag{4.15}$$

where the ΛCDM model preditcs $N^{\text{eff}}_\nu = 3.045$. This bound is harder to overcome, since they only depend on the neutrinos' states to be populated around their decouple temper-

ature.

All in all, sterile neutrinos are a hot topic in neutrino physics. This is due to three recent experimental indications in favor of short baseline oscillations:

1. The reactor anti-neutrino anomaly [110]: The number of detected $\overline{\nu}_e$ are below the expected by a few %, which indicates a 3.1σ significance of neutrino deficit. This anomaly can be explained by a mass squared difference of about 1 eV^2 and a mixing angle around $\sin^2 2\theta_{\text{new}} \sim 0.15$.

2. The Gallium neutrino anomaly [111]: Gallium based neutrino experiments rely on the reaction $\nu_e + {}^{71}Ga \rightarrow {}^{71}Ge + e^-$ as a detection of neutrinos from a radioactive source. They observe a deficit of neutrinos in two independent experiments: GALEX [112] and SAGE [113]. The significance of the deficit is 2.9σ and a mass squared difference of around 1 eV^2 and $\sin^2 2\theta_{\text{new}} \sim 0.1$ may also explain the results.

3. The LSND anomaly [114]: the LSND experiment observes an electron anti-neutrino excess from a neutrino beam created via muon-decay-at-rest. The MicroBooNE experiment was build to test such parameter space and confirmed the deficit of neutrinos [77]. The anomaly is about 3.8σ of statistical significance and the required neutrino mass should be greater than 0.1 eV^2 and $\sin^2 2\theta \sim 10^{-2}$.

A global fit analysis of all the experiments and constraints to sterile neutrinos can be found in [115].
In the near future, we might be able to observe sterile neutrinos. There exists an ongoing experiment called the Short-Baseline Neutrino Experiment (SBNE) [2]. It is a three-detector experiment, designed to finally rule out or confirm the existence of sterile neutrinos in the expected range of parameters of LSND. It relies on neutrinos from the Booster Neutrino beam at Fermilab, created from pion decay. The neutrinos energy ranges from 0.5 to 1.5 GeV and the baselines rage from 100 to 600 m. The expected sensitivity can be found in Fig. 4.2.

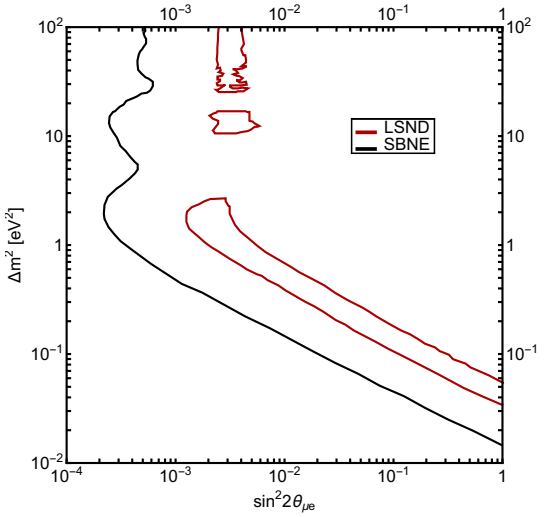

Figure 4.2 – Expected SBNE sensitivity (Black) and the allowed parameter region for LSND experiment (Red) both at 90% of C.L. for the parameters Δm^2 and $\sin^2 2\theta_{\mu e}$. The regions of this plot were obtained from a similar figure from [2].

4.4 Non-Unitarity

In the last section, we discussed the existence of light sterile neutrinos. Those that can show up in short baseline oscillations. In general, there is nothing that guarantees that the neutrino masses should be small. In fact, the bounds from Z-decay and Cosmology will not apply if the extra neutrinos are heavy enough. Moreover, almost all the neutrino mass models require the existence of heavy, or very heavy ($M_\nu > 10^{14}$ GeV), extra neutrinos. Thus, it is natural to include heavy neutrinos in the framework of neutrino oscillations.

Nevertheless, we saw on Section 3.3.3 that heavy neutrinos cannot participate on oscillation because they break coherence between the states. In fact, if the mass is higher than the experimental energy, they are kinematicaly forbidden to be created. It is very interesting to notice that, in spite of all those obstacles, the existence of heavy neutrinos might have an impact on light neutrino oscillations. Since only the $N \times N$ mixing matrix is unitary, massive neutrinos induces a non-unitarity of the 3 neutrino mixing matrix. To see that, let's assume that A is the 3×3 part of a larger unitary-

mixing $N \times N$ mixing matrix.

$$U_{N\times N} = \begin{pmatrix} A & W \\ S & T \end{pmatrix} \tag{4.16}$$

thus, A might not be unitary [116]. This can be seen by defining two matrix,

$$k = \text{Matrix}_{3\times \text{n}} = \Omega^{\dagger}(\text{A}, \text{S}) \tag{4.17}$$

$$\omega = \text{Matrix}_{\text{n}_\text{h}\times \text{n}} = (\text{W}, \text{T}) \tag{4.18}$$

Where Ω is a unitary matrix that rotates the leptons in case some model implies non-diagonal charged lepton mass. Notice that unitarity of $U^{n\times n}$ implies

$$k^{\dagger}k = \mathcal{I}_{3\times 3} \tag{4.19}$$

$$\omega^{\dagger}\omega = \mathcal{I}_{n_h\times n_h} \tag{4.20}$$

$$kk^{\dagger} + \omega\omega^{\dagger} = \mathcal{I}_{n\times n} \tag{4.21}$$

That means that only the sum $A^{\dagger}A + S^{\dagger}S$ is the unity. Moreover, the interaction lagrangian in the mass basis becames,

$$\mathcal{L} = i\frac{g}{\sqrt{2}} W_{\mu}^{-} \bar{l}\gamma_{\mu} k \nu_a + \frac{ig}{2s_{\theta_w}} Z_{\mu}\overline{\nu}(k^{\dagger}.k)\nu + \text{heavy } \nu\text{'s} \tag{4.22}$$

Which makes both interactions (charge and neutral) of light neutrinos to cease being diagonal as k and $(k^{\dagger}.k)_{n\times n}$ can mix all the neutrinos. The implementation of the matter potential is an ongoing discussion in the literature [117, 118, 119]. We will discuss both implementations in Section 4.4.1. In order to understand the concequences of a non-unitarity of the 3×3 mixing matrix, we start by writting down the relation between neutrinos in flavour/mass basis. The interesting projection $P = kk^{\dagger}$ defines the flavour (interaction) basis, as ν_α are the states ν' where,

$$P|\nu'\rangle = |\nu'\rangle. \tag{4.23}$$

which can be accomplished by,

$$|\nu'\rangle = |\nu_\alpha\rangle = k_{\alpha a}|\nu_a\rangle \tag{4.24}$$

$\alpha = e, \mu, \tau$ and $a = 1, 2, ...N$. The physical quantity measured by experiments is the probability amplitude,

$$P\left(\nu_\alpha \to \nu_\beta\right) = |S_{\beta\alpha}|^2 \tag{4.25}$$

where $S_{\beta\alpha}$ is the transition matrix element,

$$S_{\beta\alpha} = \langle \nu_\beta | \nu_\alpha(t) \rangle = \langle \nu_\beta | e^{-iHt} | \nu_\alpha \rangle \tag{4.26}$$

with Hamiltonian in the mass basis given by,

$$H = \sqrt{P^2 + M^2} \tag{4.27}$$

In vaccum, when $E < m_H$, heavy neutrinos are not kinematically possible, and can only exists as virtual particles, which can only be detected in a short period of time related to the Heisenberg principle. This can be described mathematicaly by an imaginary part of the neutrino eigen-values, $\mathrm{Im}[\sqrt{\mathrm{P^2 + M^2}}] \equiv \Gamma \neq 0$. Part of the amplitude is suppressed by an exponential factor of the order of $\Gamma \sim m_H$. This forbids the appearence of the massive neutrinos if the distance L is macroscopic. Thus, the only mixing matrix that survives is A, that is not necessary unitary. The final 3×3 (hermitian) Hamiltonian is of the form,

$$H_{\mathrm{non-uni}} = A^\dagger.\mathrm{Diag}[0, \Delta m^2_{12}/2E, \Delta m^2_{13}/2E].A \tag{4.28}$$

and

$$S^{\mathrm{non-uni}}_{\beta\alpha} = A.e^{-iLH_{\mathrm{non-uni}}}.A^\dagger \tag{4.29}$$

It was shown in [120] that it is possible to write A in a very convenient form,

$$A = A^{NP}.U_{\mathrm{PMNS}} \tag{4.30}$$

With U_{PMNS} the usual unitary mixing matrix described by the three mixing angles $\theta_{12}, \theta_{13}, \theta_{23}$ and the usual δ_{CP} phase and A^{NP} a triangular matrix that summarize the effect of non-unitary in few parameters,

$$A^{NP} = \begin{pmatrix} \alpha_{11} & 0 & 0 \\ \alpha_{21} & \alpha_{22} & 0 \\ \alpha_{31} & \alpha_{32} & \alpha_{33} \end{pmatrix}. \tag{4.31}$$

Here α_{ii} are real parameters and α_{ij}, $i \neq j$ are complex, which add only 3 new independent phases to the problem. The proof for this decomposition can be found in Appendix A.1. The S3νO can be recovered by taking $\alpha_{ii} = 1$ and $\alpha_{ij} = 0$, $i \neq j$. Current bounds on α_{ii} are also an ongoing discussion in the literature. Mostly because it is hard to extract information from meson decay without a model dependent approach. In [120], they argue to have obtained the least model dependent possible, and we present it here:

$$\begin{aligned} \alpha_{11}^2 \geq & 0.989 \\ \alpha_{22}^2 \geq & 0.999 \\ |\alpha_{21}|^2 \leq & 0.0007 \end{aligned} \tag{4.32}$$

In special we notice that the constraint on $|\alpha_{21}|^2$ comes from the NOMAD experiment [121], which is a constraint directly from oscillation. Those constraints are reasonably tight. In general it is common to imagine the neutrino sector as a poorly known region in the paramter space. But recent experiments measured the mixing angles at the few percent level. Also, under the $N \times N$ neutrino hypotesis, the unitarity of the mixing matrix is quit well stablished.

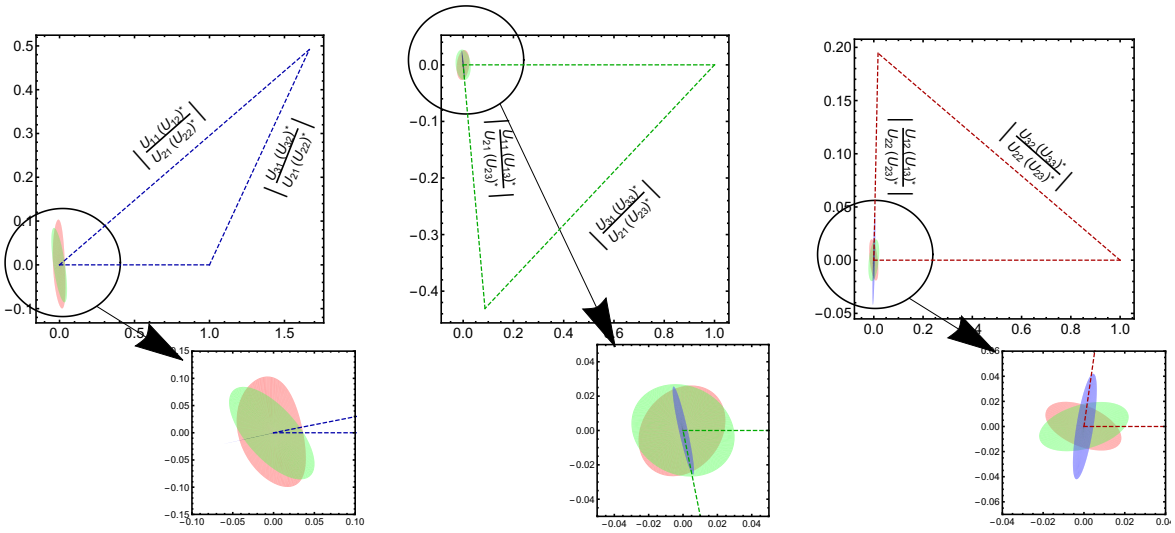

Figure 4.3 – Unitary triangles in the neutrino sector. The shaded regions represents the possible violations of non-unitary allowed by experiments in the most model independent scenario by varying α_{ij}, the colors are: α_{21}: Pink, α_{31}: Green and α_{32}: Blue. This plot was made for this PhD thesis.

We can see it visually through the unitary triangles. They are defined by the condition $A^\dagger.A$ which is equal to $\mathbb{I}$ if A is unitary. In special, the off diagonal terms

$(A^\dagger.A)_{ab}$ are interesting because in the unitary case they should sum up to zero, thus, if we draw each quantity $A^\dagger_{ia}A_{jb}$ in a complex plane, they form a triangle. Any deviation from unitary is represented by a non-closed triangle. This is shown in Fig. 4.3. We plot the normalized neutrino triangle for the unitary case in Dashed line, and vary the non-unitary parameters α_{ij} one at a time to draw the regions where the triangles won't close, the colors are: α_{21}: Pink, α_{31}: Green and α_{32}: Blue.

4.4.1 Non-Unitary Matter Effect

In order to correctly understand the matter effect in presence of non-unitary, we must start in the Lagrangian level and write down all the relevant interactions,

$$\begin{aligned}\mathcal{L} =&\overline{\nu}_j(i\partial\!\!\!/ - m_i)\nu_j + \left(A^\dagger_{i\alpha}G^{q_1q_2}_{\alpha\beta}A_{\beta j}\right)\overline{\nu}_i\gamma_\mu\nu_j J^\mu_{q_1q_2}+\\ &\overline{\nu}_a(i\partial\!\!\!/ - m_a)\nu_a + \left(W^\dagger_{a\alpha}G^{q_1q_2}_{\alpha\beta}W_{\beta b}\right)\overline{\nu}_a\gamma_\mu\nu_b J^\mu_{q_1q_2}+\\ &\left(A^\dagger_{i\alpha}G^{q_1q_2}_{\alpha\beta}W_{\beta a}\right)\overline{\nu}_i\gamma_\mu\nu_a J^\mu_{q_1q_2} + \left(W^\dagger_{a\alpha}G^{q_1q_2}_{\alpha\beta}A_{\beta j}\right)\overline{\nu}_a\gamma_\mu\nu_j J^\mu_{q_1q_2}\end{aligned} \tag{4.33}$$

$i,j = 1,2...n_l$ corresponds to n_l light neutrinos while $a,b = n_l+1, n_l+2...n_l+n_h = N$ corresponds to the heavy neutrinos. Applying Euler-Lagrange to this equation we get,

$$\nu_a^{\text{classic}} = \left[(i\partial\!\!\!/ - m_a + WG^{q_1q_2}W\gamma_\mu J^\mu_{q_1q_2})^{-1}W^\dagger G^{q_3q_4}A\gamma_\nu J^\nu_{q_3q_4}\right]_{ai}\nu_i \tag{4.34}$$

If m_a masses are large, and the matter effect is small enough, we can approximate this equation by,

$$\nu_a^{\text{classic}} \approx -\frac{1}{m_a}\left[W^\dagger G^{q_3q_4}A\gamma_\nu J^\nu_{q_3q_4}\right]_{ai}\nu_i \tag{4.35}$$

This correction is of order m_a^{-1} and goes to zero for $m_a \to \infty$. Thus, at zeroeth-order, the effective lagrangian in mass basis is,

$$\mathcal{L}_{\text{eff}} =\overline{\nu}_j(i\partial\!\!\!/ - m_i)\nu_j + \left(A^\dagger_{i\alpha}G^{q_1q_2}_{\alpha\beta}A_{\beta j}\right)\overline{\nu}_i\gamma_\mu\nu_j J^\mu_{q_1q_2} \tag{4.36}$$

Since the heavy neutrinos contribution to the vectors goes to zero, we can transform to mass basis to flavor basis by,

$$\nu_\alpha = A\nu_i \tag{4.37}$$

or,

$$\nu_i = A^{-1}\nu_\alpha \tag{4.38}$$

Thus, we can write propagation matrix as,

$$S_{\beta\alpha} = \langle\nu_\beta|e^{-iHL}|\nu_\alpha\rangle = \sum_{ij}^{N=n_l+n_h} \langle\nu_\beta|\nu_j\rangle\langle\nu_j|S|\nu_i\rangle\langle\nu_i|\nu_\alpha\rangle \xrightarrow{m_a\to\infty} A^\dagger_{\beta j}S_{ji}A_{i\alpha} \tag{4.39}$$

where S_{ij} in mass basis is,

$$S = e^{-iHL}, \tag{4.40}$$

with

$$H = \mathrm{Diag}[0, \Delta m^2_{21}/2E, \Delta m^2_{31}/2E] + A^\dagger.\mathrm{Diag}[v_{cc} - v_{nc}, -v_{nc}, -v_{nc}].A \tag{4.41}$$

4.4.2 Non-Unitarity in T2K Experiment

We showed in [3] that one can write the non-unitary neutrino oscillation probability as,

$$\begin{aligned}
P^{NP}_{ee} &= \alpha^4_{11}P_{ee}\,, && \text{(4.42a)}\\
P^{NP}_{e\mu} &= \alpha^2_{11}\alpha^2_{22}\left[P_{e\mu} + 2\mathrm{Re}\left(\frac{\alpha_{21}}{\alpha_{22}}S^*_{ee}S_{\mu e}\right) + \frac{|\alpha_{21}|^2}{\alpha^2_{22}}P_{ee}\right], && \text{(4.42b)}\\
P^{NP}_{\mu e} &= \alpha^2_{11}\alpha^2_{22}\left[P_{\mu e} + 2\mathrm{Re}\left(\frac{\alpha^*_{21}}{\alpha_{22}}S_{ee}S^*_{e\mu}\right) + \frac{|\alpha_{21}|^2}{\alpha^2_{22}}P_{ee}\right], && \text{(4.42c)}\\
P^{NP}_{\mu\mu} &= \alpha^4_{22}P_{\mu\mu} + |\alpha^2_{21}|\alpha^2_{22}(P_{\mu e} + P_{e\mu}) + |\alpha_{21}|^4P_{ee}\\
&+ \sum_{\{a_1,b_1\}\neq\{a_2,b_2\}} \mathrm{Re}[\alpha_{2a_1}\alpha^*_{2b_1}\alpha^*_{2a_2}\alpha_{2b_2}\mathrm{S}_{a_1b_1}\mathrm{S}^*_{a_2b_2}]. && \text{(4.42d)}
\end{aligned}$$

with $P_{\alpha\beta}$ the S3νO transition probabilities. This form is very suitable to experimental simulation, as it depends on well know quantities $P_{\alpha\beta}$, the new non-unitary parameters α in a simple polynomial form and the S3νO transition probability $S_{\alpha\beta}$.

Notice that e and μ probabilities depend on only three out of the 6 α's, α_{11}, α_{22} and α_{21}, moreover, α_{11} and α_{22} appear only as overall factors that change too little the equations to be noticed in current experiments. While in contrast, the channels $P_{\mu e}$ and $P_{e\mu}$ has a non-trivial dependence on α_{21} which adds a complex phase $\phi = \mathrm{Arg}[\alpha_{21}]$ with

potential to mimic the $\delta_{\rm CP}$ phase on neutrino experiments.Thus, ϕ and $\alpha = |\alpha_{21}|$ are the only two most relevant new non-unitary parameters to future long-baseline experiments.

Neutrino experiments are designed to measure standard oscillation parameters. This implies that the presence of unusual physics may spoil some of the sensitivity they can reach. Thus, it is useful to analyze the presence of non-unitary in the context of future experiments. As a case study, we took the T2(H)K experiment. We used the program NuPro [122] to perform the simulation in three scenarios: (i) Mixing Matrix Unitary, (ii) Mixing Matrix non-Unitary $\alpha \leq 2.5\%$ but no prior and (ii) Mixing Matrix non-Unitary and prior to the Non-unitary parameters.

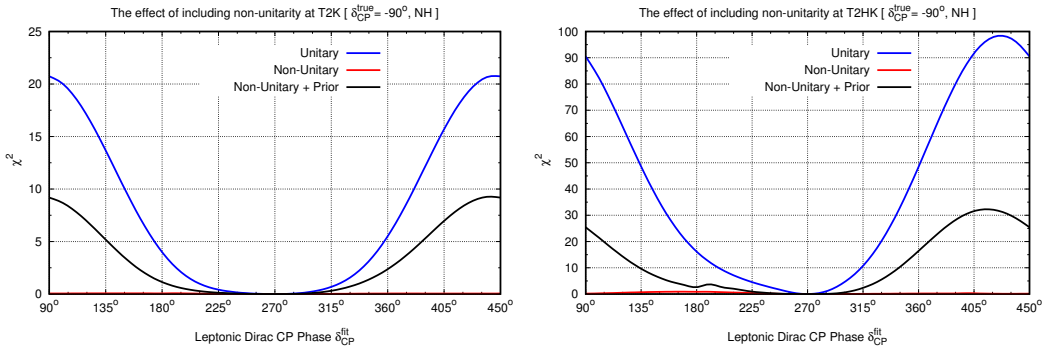

Figure 4.4 – The marginalized $\chi^2(\delta_{CP})$ function at T2K and T2HK under the assumptions of unitary mixing (blue) and non-unitary mixing with (black) or without (red) prior constraints. This figure was taken from our work [3].

The χ^2 defining the sensitivity is calculated by comparing number of neutrinos in each bin as,

$$\chi^2 \equiv \chi^2_{stat} + \chi^2_{sys} + \chi^2_{prior}\,. \tag{4.43}$$

Here, (χ^2_{stat}, χ^2_{sys}, χ^2_{prior}) stand for the statistical, systematical, and prior contributions respectively. χ^2_{stat} is defined as a Pearson distribution,

$$\chi^2_{stat} = \sum_i^{N_{\rm bin}} \left(\frac{N_i^{\rm pred} - N_i^{\rm data}}{\sqrt{N_i^{\rm data}}} \right)^2 , \tag{4.44}$$

$N^{\rm pred}$ is the number of events for test values and $N_i^{\rm data}$ is the number of events of the assumed true values, which are the central values on Table 2.1. χ^2_{sys} accounts the expected 5% flux uncertainty for the neutrino and anti-neutrino modes independently,

$$\chi^2_{sys} = \left(\frac{f_\nu - 1}{0.05} \right)^2 + \left(\frac{f_{\bar\nu} - 1}{0.05} \right)^2 . \tag{4.45}$$

and finaly χ^2_{prior} is a gaussian function of the mixing parameters around the central value and erros in table 2.1.

The resulting χ^2 of the simulations is found in Fig. 4.4 for T2(H)K in left (right). The non-unitarity extra degree of freedom allows the extra phase ϕ to mimic the spectrum of the unitary case and make the sensibility to go down.

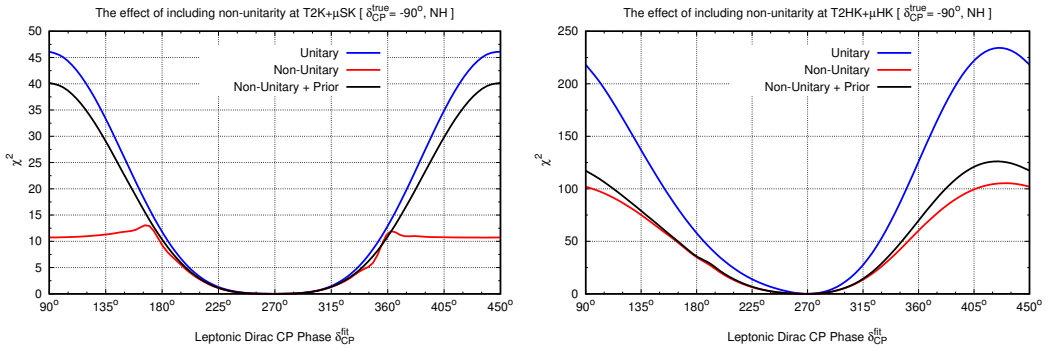

Figure 4.5 – The marginalized $\chi^2(\delta_{CP})$ function at TNT2K under the assumptions of unitarity (blue), non-unitary mixing with (black) or without (red) prior constraints. This figure was taken from our work [3].

A proposal for restoring (at least partialy) the sensitivity of T2(H)K is the adition of a muon-decay-at-rest (μDAR) source, to be detected at the Super(Hyper)-Kamiokande detector. The μDAR source is planned to operate at the J-Park laboratory. If runing in parallel with the T2K experiment, it can supplement the ν spectrum with a different energy ($\sim$ 50 MeV). In figure 4.6 we show the spectrum and background of a μDAR source. This, combined with a different baseline makes it is possible to constraint α_{21} in order to restore the sensitivity. As can be seen in the simulation of T2K+μDAR in figure 4.5 - left.

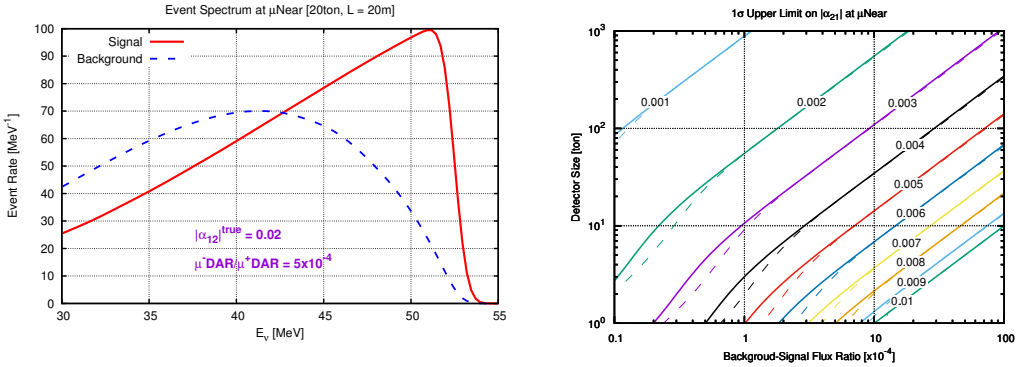

Figure 4.6 – **Left:** Spectrum of a μDAR source. The red color are muon neutrinos while the blue curve the electron neutrinos. **Right :** Sensitivity on $|\alpha_{21}|$ assuming a $L = 20$ m near detector at the μDAR source for various configurations of detector size and background ratio. This figure was taken from our work [3].

A simpler way to recover the sensibility of the T2(H)K experiment is the measurement of $|\alpha_{21}|$. We can use the zero distance effect in order to accomplish that. By setting $L = 0$ in Eq.4.42c we obtain the interesting result,

$$P_{\mu e}^{NP} = \alpha_{11}^2 |\alpha_{21}|^2. \tag{4.46}$$

Since α_{11} is close to 1, we can convert any bound on the $\mu \to e$ transition in a bound on $|\alpha_{21}|$. Now, instead of using the Super(Hyper)-Kamiokande as a detector, we need to include a near detector at the μDAR source. A $L = 20$ m is feasable. The sensitivity depends on the background and size of the detector. Possible constraints on $|\alpha_{21}|$ for different configurations of the experiment can be found in Fig. 4.5 - right.

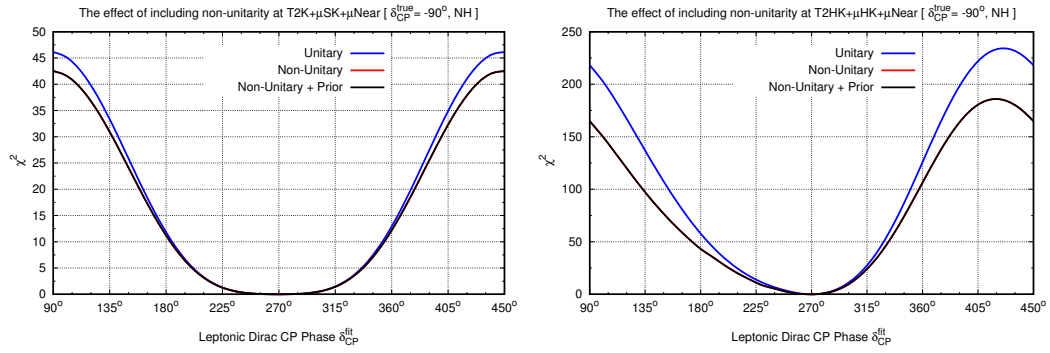

Figure 4.7 – The marginalized $\chi^2(\delta_{CP})$ function at TNT2K + μNear under the assumptions of unitarity (blue), non-unitary mixing with (black) or without (red) prior constraints. This figure was taken from our work [3].

4.5 Conclusion

The presence of anomalies in reactor and short-baseline neutrino experiments and theoretically predicted new particles required to explain the smallness of neutrino masses pushed the physics community to explore all the possibilities of expanding the picture of the standard 3-neutrino oscillation. We presented a few: Non-Standard Interactions, Non-unitary mixing matrix, and light sterile neutrinos. They are well motivated by neutrino mass models but can be realized in a phenomenological point of view that allows filtering possible scenarios. Those new phenomena modify the behavior of neutrinos in such a way that might be visible in future experiments. Moreover, in special, we showed that in some cases, they can even be mistakenly confused as standard physics, as is the case of non-unitarity in T2K.

Chapter 5

Neutrino Phenomenology

> " Your assumptions are your windows on the world. Scrub them off every once in a while, or the light won't come in."
>
> **Isaac Asimov**

In this Chapter, we explore three physical measurements that are valuable to physics that are deeply involved with neutrinos. We start by presenting the idea of using meson decay experiments, in special, the spectrum of the measured charged lepton, that is modified if neutrinos couples to scalar particles. Then we present a discussion of two different neutrino oscillation phenomenology: (1) The synergy between long and short baseline experiments necessary to obtain the correct value of θ_{23} and (2) The power of the short-baseline program of Fermilab to constraint new physics.

5.1 Meson Decay Experiments

5.1.1 Meson Total Decay

It was pointed out by Mohapatra, Chikashige and Peccei [123] that the introduction of a $SU(2)_L \times U(1)_Y$ singlet scalar particle to generate massive right-handed fermion introduces a new $U(1)$ global symmetry which can be spontaneously broken gen-

erating, analogously of what happens in the Higgs mechanism [124, 125, 126], a massive scalar particle and a massless Goldston boson, called Majoron.

At first sight one can naively say that the Majoron is not allowed experimentally, as it could not be detected so far, however it was shown [123] that due to the weakness of Majoron coupling to matter the presence of Majoron, in most cases, can be neglected.

This is not the case for the leptonic Decay of mesons: $P \to l + \nu$, where $i, l = e, \mu, \tau$ and $P = \pi, K, D, D_s$ and B. A Yukawa interaction between neutrino and a Majoron χ can induce decays of the form $P \to l\nu\chi$, such decay induces corrections on the measured total decay rate $\Gamma_{Tot} = \Gamma\left(P \to e\nu(\gamma)\right) + \Gamma\left(P \to e\nu\chi\right)$ and can be tested experimentally. This corrections are of the form roughly as [127, 128, 129]

$$\Gamma(\pi \to l\nu\chi) \sim \frac{1}{4\pi}|V_{qq'}|^2 G_f^2 m_\pi^3 \left(\frac{|g_l|^2}{32\pi^2}\right) \tag{5.1}$$

where G_f is the Fermi constant, m_π is the pion mass, $|g_l|^2 = \sum_\alpha |g_{l\alpha}|^2$, where $g_{\alpha\beta}$ is the Majoron-neutrino Yukawa coupling, $V_{qq'}$ is the CKM element, and $\alpha, \beta = e, \mu\tau$. So that any experimental confirmation (deviation) on the ratio $R_P = \frac{\Gamma(P\to e\nu(\gamma))}{\Gamma(P\to\mu\nu(\gamma))}$ compared to the theoretical prediction can be used to put limits (evaluate) on the coupling constants. The R_P ratio is known to agree experimentally [130] and theoretically [131, 132, 133] up to $\sim 10^{-3}(10^{-2})$, within the error.

An analysis of [134], probing the Majoron coupling via pion total decay and τ or μ decay spectrum, obtained the limits,

$$\begin{aligned} |g_e|^2 &< 2.2 \times 10^{-5} \\ |g_\mu|^2 &< 1.8 \times 10^{-4} \\ |g_\tau|^2 &< 1.8 \times 10^{-2}. \end{aligned} \tag{5.2}$$

This limits were reached assuming the mass, m_χ, of the Majoron as zero, using the fact that it is a Goldstone boson. Nevertheless early results in QCD by Peccei and Quinn [127, 128] and S. Weinberg [135] point out to a possibility of massive pseudo-Goldston boson, called axion, via a spontaneous break of a pseudo-symmetry. A pseudo-

symmetry happens when a physical Lagrangian L can be subdivided as

$$L = L_0 + L_B \tag{5.3}$$

where L_0 posses a true symmetry and L_B breaks the symmetry by some small parameter m so that when $m \to 0$ implies $L_B \to 0$. For the Peccei and Quinn axion, L_B is the light quark part of the Lagrangian. In the Majoron context there are two possibilities to give mass to Majorons: (i) Introducing explicitly soft break $U(1)$ terms, such as neutrino masses or a quadratic term in the pseudo-scalar potential [136] so Majorons even reach masses of order of $\sim$ 100GeV acting as Dark-matter candidate and (ii) Coupling Majorons with another Higgs doublet or new colored quarks [137, 138, 139] providing axion/Majoron mass of order of $\sim eV$.

5.1.1.1 Corrections to Meson Decay

Many models [123, 135, 137, 138, 139, 140] provide Yukawa couplings of scalar particles to neutrinos, so we focus on present limits based on a phenomenological point of view by using general Yukawa couplings,

$$-\mathcal{L} = \frac{1}{2} g_{AB} \overline{\nu}_A \nu_B \chi_1 + \frac{i}{2} h_{AB} \overline{\nu}_A \gamma_5 \nu_B \chi_2, \tag{5.4}$$

plus, we assume no restriction to the Majoron mass. Further discussion on the interactions can be found in Appendix A.2.
Such term results in a new decay channel,

$$P^{\pm} \to l^{\pm} + \nu_i + \chi \tag{5.5}$$

represented in fig.5.1.

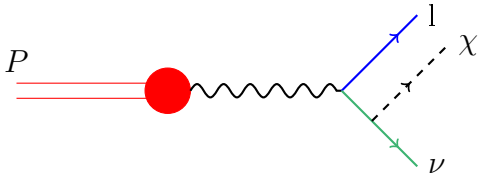

Figure 5.1 – Meson (P) decay diagram, into one lepton (l), one neutrino (ν) and the scalar (χ).

The decay rate of this reaction was calculated in [129] and is given by

$$d\Gamma(P \to l\nu\chi) = \Gamma_{l\nu}\frac{(x^2+\epsilon^2+6x\epsilon-\beta x-\beta\epsilon)\lambda^{1/2}(x,\epsilon,\beta)}{x^2(x-\epsilon)^2}\frac{|g_l|^2}{32\pi^2}dx \tag{5.6}$$

where x is the kinematic variable of the squared four momentum of the virtual neutrino and ranges from $(\sqrt{\epsilon}+\sqrt{\beta})^2$ to $(1-\sqrt{\alpha})^2$, λ is the kinematic function,

$$\lambda(x,y,z) = x^2+y^2+z^2-2xy-2xz-2zy \tag{5.7}$$

$\Gamma_{l\nu}$ is the decay constant of the meson into lepton and neutrino of invariant square mass x,

$$\Gamma_{l\nu} = \frac{G_F^2 f_P^2 |V_{qq'}|^2 m_p^3}{8\pi}[x+\alpha-(x-\alpha)^2]\lambda^{1/2}(1,x,\alpha) \tag{5.8}$$

$\epsilon = \frac{m_\nu^2}{m_\pi^2}$,$\beta = \frac{m_\chi^2}{m_\pi^2}$ and $\alpha = \frac{m_l^2}{m_\pi^2}$, note that for $x \to 0$, $\Gamma_{l\nu}$ is exactly the total decay rate at tree level for the reaction $P \to l\nu$.

Thus, using the current total decay data on different mesons, one can extract limits for neutrino-scalar coupling by comparing it with the predicted by new interactions. A detailed discussion on the calculation of important theoretical corrections to Eq. 5.1 and how to correctly include the experimental data into the analysis can be found in Appendix A.2.1 and A.2.2.

However, one should be carefull on the validity of such bounds. Here we assumed that the only modification to the decay rate comes from Eq. 5.1. Thus, any model that contain other interactions that may play any role on such reactions is not affected by it.

5.1.2 Heavy ν Analysis

Meson decay can be a probe for heavy neutrino search [141] through the analysis of the differential decay rate $\frac{d\Gamma}{dp}(P \to l\nu_H)$ of the reaction,

$$P \to l + \nu_H \tag{5.9}$$

P is a stopped meson (i.e. its momentum is zero), l is a detected lepton with momentum p and ν_H is the supposed heavy neutrino, with mass $m_H \leq m_P - m_l$. If such interaction exists, the spectrum of the leptons produced via mesonic decay would peak at specific

momentum,

$$p_{\text{peak}} = \frac{\lambda^{1/2}(m_P^2, m_l^2, m_\nu^2)}{2m_P} \tag{5.10}$$

where $\lambda(a, b, c)$ is the kinematic function. The height of the peak depends directly on the coupling of heavy neutrino and the lepton or, in terms of neutrino oscillation parameters, the heavy neutrino mixing matrix element, $|U_{lH}|^2$, that is [142],

$$d\Gamma(P \to l\nu_H) = \rho\Gamma_0 |U_{eH}|^2 \delta(p_{\text{peak}} - p_l) dp_l, \tag{5.11}$$

where ρ is a function of the ratio of the particle masses $\alpha = \frac{m_l^2}{m_P^2}$ and $\epsilon = \frac{m_H^2}{m_P^2}$,

$$\rho = \frac{\sqrt{1 + (\alpha - \beta)^2 - 2(\alpha + \beta)}(\alpha + \beta - (\alpha - \beta)^2)}{\alpha(1 - \alpha)^2} \tag{5.12}$$

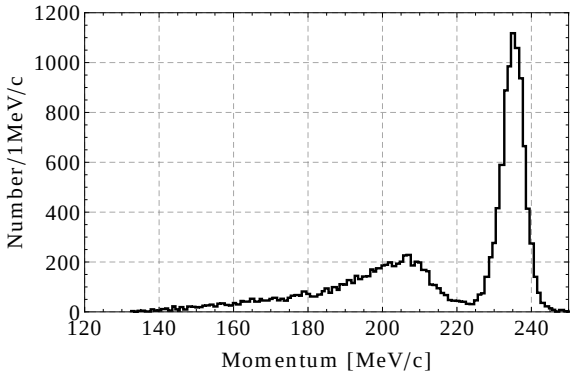

Figure 5.2 – Simulated spectrum of the leptonic Kaon decay, $K \to \mu\nu(\gamma)$ [4].

This means that by measuring the spectrum of leptons from mesonic decay* one could look up for a peak. The usual leptonic spectrum has the form presented in Fig. 5.2 the peak at $p_0 = 235.667$ MeV/c comes from the standard model neutrino with mass $m_\nu \approx 0$, the smooth curve for $p < 235.667$ MeV/c is due to the fact that the reaction $K^- \to \mu^- \overline{\nu}_\mu \gamma$ is taking place as well. The first experimental search for heavy ν in this context was done in 1980 by [143], and several others took place [144, 142, 4], they found nothing, putting some limits on m_H and $|U_{lH}|^2$ via statistical analysis of peak search.

As seen in section 5.1.1 the existence of a light scalar particle χ add a mesonic decay channel of the form $P \to l\nu\chi$. The pair $\nu\chi$ and its invariant mass can mimic a continuous spectrum of heavy neutrino (note that a three body decay has a continuous

*For example, from accelerators

kinematic region), inspection of Eq. 5.6 leads to the relation,

$$|U_{lH}|^2 = \left.\frac{\Gamma(P \to l\nu_x)}{\rho(\alpha, x, \beta)\Gamma_0}\frac{dR}{dp_l}\right|_{\beta\to x} \tag{5.13}$$

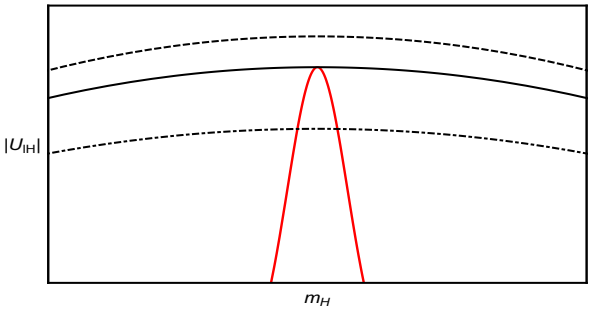

Figure 5.3 – This plot shows three hypothetical scenarios, the red line represents the peak search, the dashed line a signal and the dotted-dashed a negative signal, the solid line is the limiting case.

Previous analysis on $|U_{lH}|$ can be translated to $|g_l|^2$ as a function of m_χ. To do that, one can compare the continuous charged lepton spectrum with that of an heavy neutrino with varying mass m_H (See Fig. 5.3). In the figure the red line represents the peak search, the dashed line a signal and the dotted-dashed a negative signal, the solid line is the limiting case. Saying in other words, we can put a bound by comparing the number of events in the peak search area (below the two-body heavy neutrino search) and the three body search.

5.1.3 Combined Results

To obtain bounds on the Yukawa coupling constants $|g_\alpha^2|^2$, we used a χ_i^2 method devided into two experimental data: (1) $i = 1$ for the total decay and (2) $i = 2$ the heavy neutrino search. Then,

$$\chi_1^2 = \sum_i \frac{\left(\Gamma_{\text{Teo}}^{(i)} - \Gamma_{\text{Exp}}^{(i)}\right)^2}{\sigma_i^2} \tag{5.14}$$

where i run over the experimental total decay and,

$$\chi_2^2 = \frac{1}{n}\sum_i \left(\frac{|U_{lH}|_i^2}{\sigma_i}\right)^2 \tag{5.15}$$

where $i = 1, 2, 3...n$ runs over the experimental bounds on $|U_{lH}|^2$ is extracted from Eq. 5.13 at the experimental point i and σ_i the bound value of $|U_{lH}|^2$.

The combined result for each bound as a function of m_χ is presented in Fig. 5.4 where the green curve comes from meson total decay and the Yellow curve from heavy neutrino search. These results were published in [5].

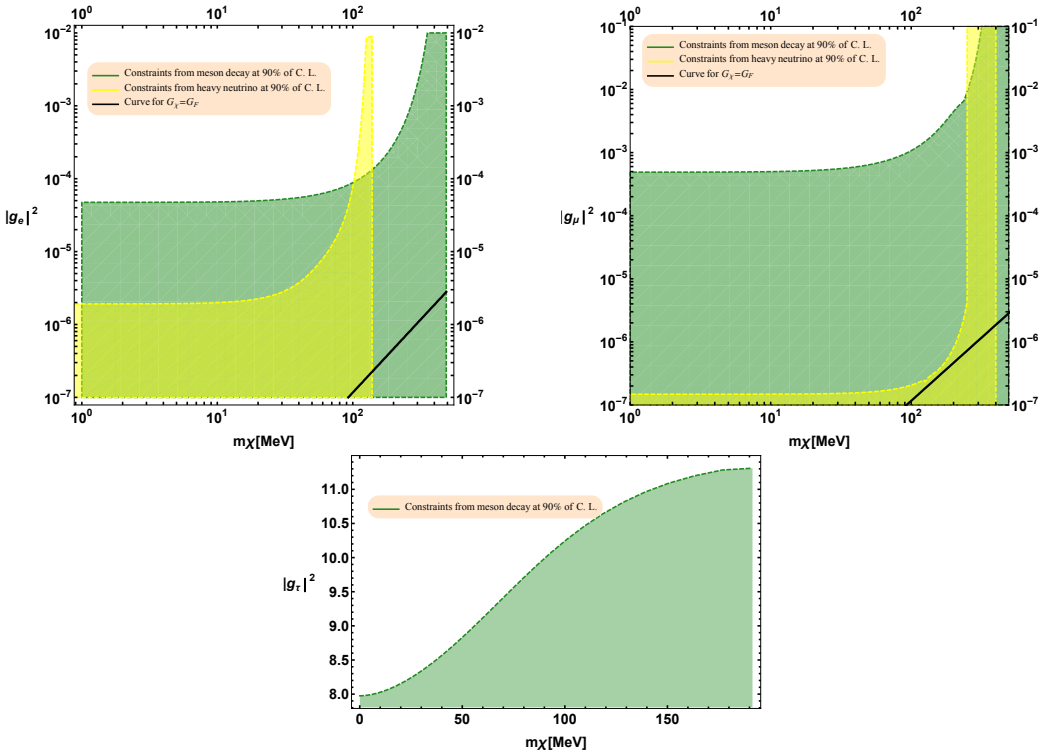

Figure 5.4 – Obtained bounds for $|g_l|^2$ for each experimental source: Green: Meson total decay and Yellow: heavy neutrino search. This plot was taken from our work [5].

In table 5.1 we summarize the previous results and the ones we obtained from such analysis for $m_\chi = 0$.

Constants	Ref. [134]	Ref. [145]	Our (Meson dec.)	Our (Heavy ν)
$\|g_e\|^2$	$< 4.4 \times 10^{-5}$	$< (0.8 - 1.6) \times 10^{-5}$	< 4.4 (4.4) $\times 10^{-5}$	1.9×10^{-6}
$\|g_\mu\|^2$	$< 3.6 \times 10^{-4}$		< 4.5 (3.6) $\times 10^{-6}$	1.9×10^{-7}
$\|g_\tau\|^2$	$< 2.2 \times 10^{-1}$		< 40 (8)	-

Table 5.1 – Comparison between previous bounds [134, 145] with our results with $m_\chi = 0$, using the rates of the meson decay at 90% C.L. and Heavy ν search. In Black the bounds marginalizing $V_{\rm CKM}$ in Red, taking the central value of uncorrelated measurements. This result is taken from our work [5].

5.2 The whole of θ_{13} on θ_{23} Octant

5.2.1 The Octant Problem

The least known mixing angle in the leptonic sector is the atmospheric angle θ_{23}, which is almost maximal: $\sin^2\theta_{23} \approx 0.5$. It was first precisely measured by Super-Kamiokande experiment [45], which measured the defict of μ-neutrinos in the atmospheric neutrino flux due to the $\nu_\mu \to \nu_\tau$ transition. This transition can be approximated by a two-neutrino oscillation,

$$P_{\mu\tau} \approx \sin^2 2\theta_{23} \sin\left(1.27\frac{\Delta m^2_{32}(eV^2)L(km)}{E(GeV)}\right), \tag{5.16}$$

that has an 'octant-blindness' to the atmospheric angle, due to the symmetric structure around the maximal mixture $\theta^{\max} = \pi/4$. Current experimental data still cannot disitnguish the octant, as it could not reach beyond the zeroth order with enough precision.

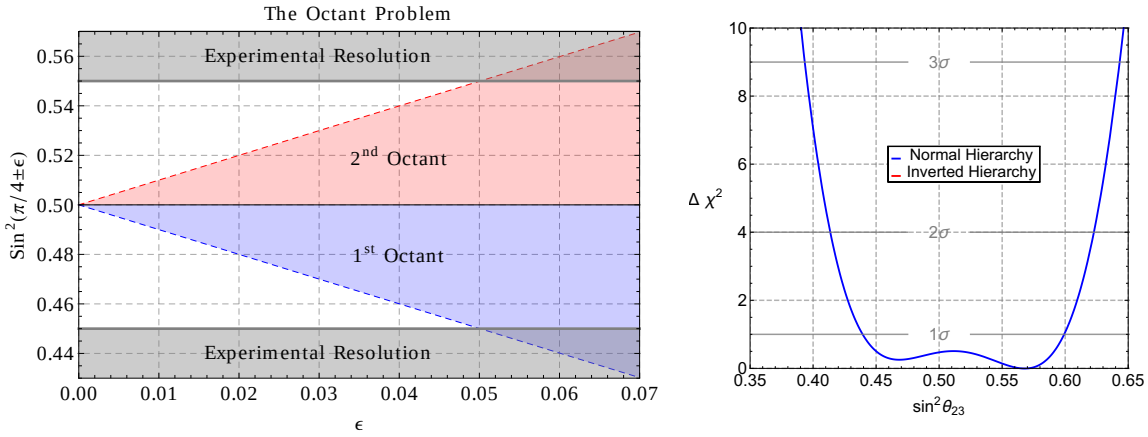

Figure 5.5 – **Left:** The octant problem illustration, the central value is given by $\theta_{23} = \pi/4$, the blue bands are the values for $\sin^2(\pi/4+\epsilon)$ and the red are for $\sin^2(\pi/4-\epsilon)$. **Right:** Global fit χ^2 as a function of $\sin^2\theta_{23}$ from the data of T2K, KamLAND and SK given by [6], Blue: NH e Red: IH. This plot was prepared for this thesis.

This leads to three possibilities (1) θ_{23} at First Octante: $\theta_{23} < \pi/4$, (2) θ_{23} at Second Octante: $\theta_{23} > \pi/4$, or (3) $\theta_{23} = \theta^{\max}$.

The global analysis from [6] slightly indicates θ_{23} in the second octant, with an indication of less than 1σ as shown in Fig. 5.5 right. Notice the two minima in the χ^2 function, which summarizes the octant problem.

5.2.2 Measuring θ_{13} Octant by measuring θ_{23}

A must-do goal to long baseline experiments would be the measurement of the correct octant of the atmospheric angle. Many papers have adressed the octant issue within the standard 3ν scenario [146, 147, 148, 149, 150, 151, 152]. Others also included the presence of new physics, such as non-standard interaction [153], non-unitarity [154, 117, 155], or a light sterile neutrino [156, 157], which could completely change the scenario.

We, on the other hand, focus on the relevancy of the reactor angle θ_{13} and on whether an improved precision in its measurement from reactors affects the experimental resolution on the measurement of θ_{23}.

We simulated both DUNE [20] and T2HK [73]. The experimental details can be found in Section 3.5. Also, the current and future resolution of θ_{13} from reactors can be found in Table 5.2.

	DC [158]	RENO [159]	Daya-Bay [160]	Global [6]
$s^2_{13}/10^{-2}$	2.85	2.09	2.09	2.34
$\delta\theta_{13}$	16.7%	13.4%	4.9%	8.5%
$\delta\theta_{13}^{\text{Expe}}$	10%	5%	3.6%	<3%

Table 5.2 – Current and expected values of the reactor mixing angle θ_{13} and its sensitivity for different experiments and current global neutrino oscillation fit.

A quick look at the appearance and survival oscillation probabilities in the presence of matter [161], shows that the θ_{13} parameter plays a big role on θ_{23} measurement. The probability is

$$P_{\mu e} \approx 4s^2_{13}s^2_{23}\sin^2\Delta_{31} + 2\alpha\Delta_{31}s_{13}\sin 2\theta_{12}\sin 2\theta_{23}\cos(\Delta_{31}\pm\delta_{CP}) = P_0 + P_I \quad (5.17)$$

$$P_{\mu\mu} \approx 1 - \sin^2 2\theta_{23}\sin^2\Delta_{31} - 4s^2_{13}s^2_{23}\frac{\sin^2(A-1)\Delta_{31}}{(A-1)^2} \quad (5.18)$$

Here V_{CC} is the charged current matter potential on earth, L and E are the propagation distance and energy of the neutrinos, respectively. $\alpha = \frac{\Delta m^2_{21}}{\Delta m^2_{31}}$, is the small parameter of the expansion, while $\Delta_{31} = \frac{\Delta m^2_{31}L}{4E}$ and $A = \frac{2EV_{CC}}{\Delta m^2_{31}}$. Only P_0 is octant sensitive.
The resolution can only be achieved if there is a finite difference between the probabilities

corresponding to the two octants. That is,

$$\Delta P \equiv P_{\mu e}^{\rm HO} - P_{\mu e}^{\rm LO} \neq 0 \tag{5.19}$$

which can be written as a function of ϵ and η defined as $\sin^2\theta_{13} = (1+\epsilon)\sin^2\theta_{13}$ and $\theta_{23} = \pi/4 \pm \eta$, we get,

$$\Delta P = \Delta P_0 + \Delta P_I \ . \tag{5.20}$$

$$\Delta P_0 \ = \ (4\eta \pm \epsilon) 4 s_{13}^2 s_{23}^2 \sin^2\Delta_{31} \tag{5.21}$$

and,

$$\Delta P_I = B\Big[\sin\theta_{13}^{\rm HO}\cos(\Delta_{31} \pm \delta_{\rm CP}^{\rm HO}) - \sin\theta_{13}^{\rm LO}\cos(\Delta_{31} \pm \delta_{\rm CP}^{\rm LO})\Big] \tag{5.22}$$

where, $\mathrm{B} = 4\sin\theta_{12}\cos\theta_{12}(\alpha\Delta)\sin\Delta_{31}$.

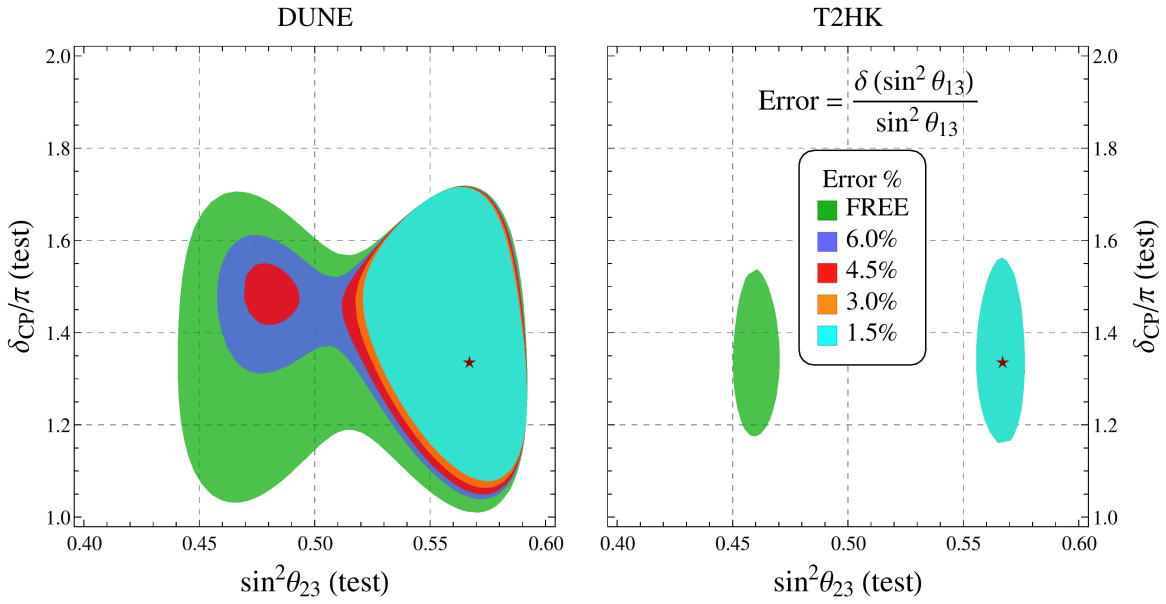

Figure 5.6 – Precision measurement of θ_{23} and δ_{CP} at 3σ ($\Delta\chi^2 = 9$) confidence. The symbol "star" denotes $\sin^2\theta_{23}^{\rm TRUE} = 0.567$ and $\delta_{\rm CP}^{\rm TRUE} = 1.34\pi$. Left (Right) panels correspond to DUNE (T2HK). Differently shaded (colored) regions correspond to various errors associated with $\sin^2\theta_{13}$. This plot was taken from our work [7].

Now, notice from Eqs. 5.21 and 5.22 that the contribution from $\epsilon \neq 0$ can partially cancel the magnitude of ΔP_0 and ΔP_I in such a way that it might fall beyond experimental sensitivity. Moreover, the larger the error, the less will be the resulting

octant sensitivity. Fig. 5.6 explicitly shows that. It plots the expected measurement from DUNE and T2HK by taking into account several assumptions on the measurement of θ_{13} and assuming $\sin^2\theta_{23}^{\rm TRUE} = 0.567$.

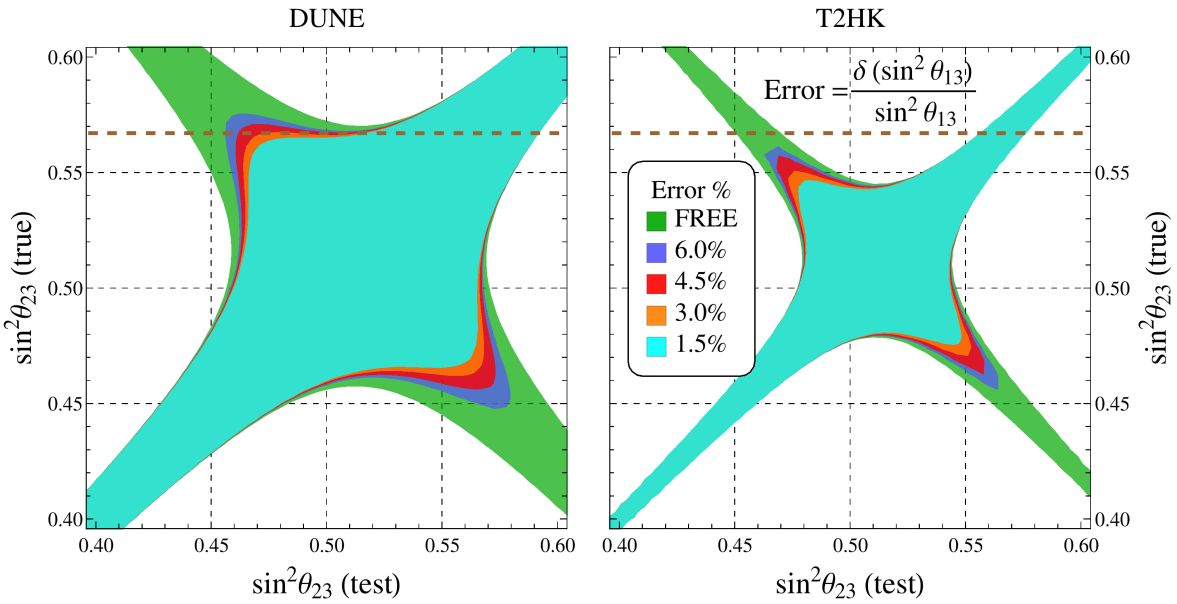

Figure 5.7 – 3σ precision measurement of θ_{23}. The left (right) panel is for DUNE (T2HK). Differently shaded regions correspond to various errors associated with $\sin^2\theta_{13}$. The thick dashed line represents the current best fit value from [6]. This plot was taken from our work [7].

The loss of sensitivity depends also on the value of θ_{23}. The closer it gets from the maximal value, the smaller is ΔP. The dependency on θ_{23} and the error on θ_{13} is illustrated in Fig. 5.7, which presents the simulated true value of θ_{23} versus its test value, there the wrong octant measurement region is bigger near the maximal mixing and that it shrinks with the error in θ_{13}. This figure also shows an astonishing result, by looking at the green region we see that if we take no prior assumption in θ_{13} we cannot use long-baseline to distinguish the octant.

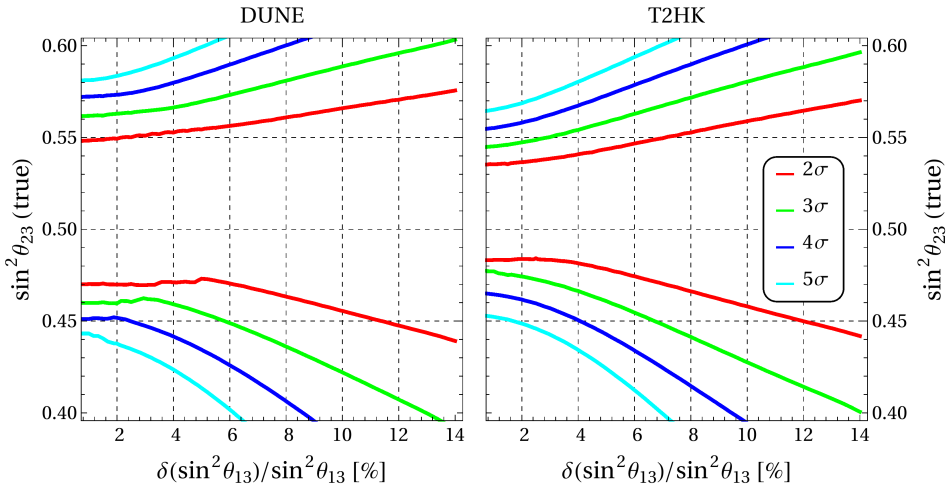

Figure 5.8 – Octant discrimination potential as a function of the relative error on $\sin^2\theta_{13}$ for the true value of $\delta_{\rm CP}^{\rm TRUE} = 1.34\pi$. The left (right) panel represents the results for DUNE (T2HK). The red, green, blue and cyan curves delimit the θ_{23} "octant-blind" region corresponding to 2, 3, 4 and 5σ confidence (1 d.o.f) for each true value of $\sin^2\theta_{23}$. This plot was taken from our work [7].

For completness we present the octant resolution power as a function of θ_{23} and error in θ_{13} in Fig 5.9 as well as its dependency on δ_{CP} in Fig 5.2. Those shows that the true value of the CP phase does not play a big role on the octant sensitivity and that the octant sensitivity is not simmetric around $\theta_{23} = \pi/4$, this is due to matter effects.

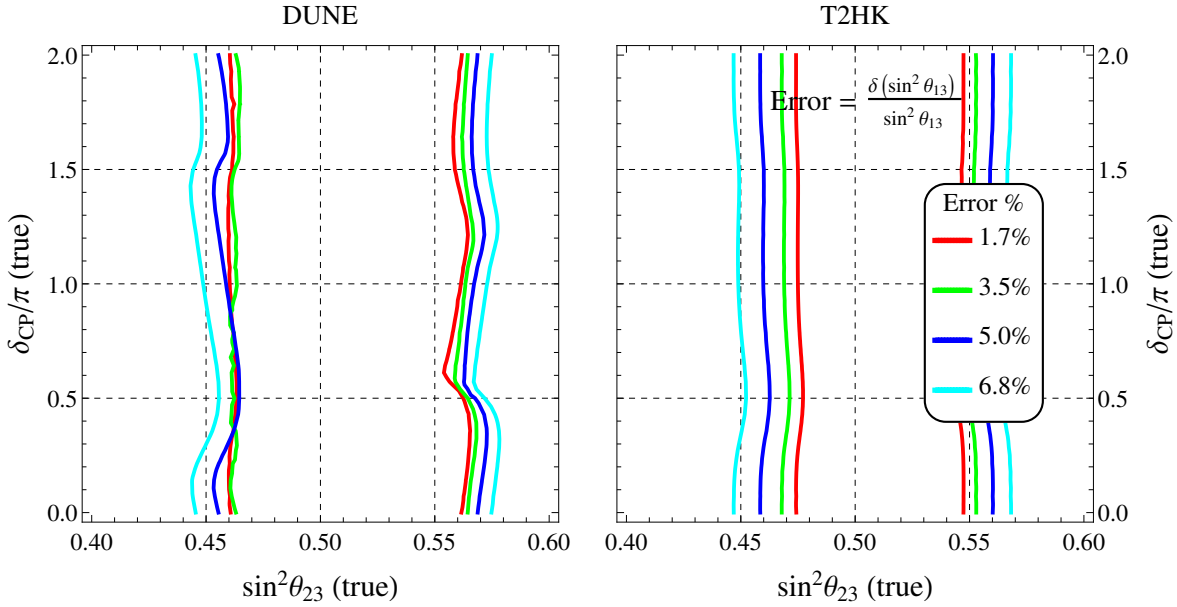

Figure 5.9 – Octant discrimination potential at 3σ confidence level in the $[\sin^2\theta_{23}, \delta_{\rm CP}]$(true) plane. The red, green, blue and cyan curves delimit the "octant-blind" regions corresponding to 1.7%, 3.5%, 5.0% and 6.8% relative errors on $\sin^2\theta_{13}$. This plot was taken from our work [7].

5.3 Short Baseline Program at Fermilab

The experimental neutrino physics agenda heavily relies on the success of execution of the DUNE program. The understanding of short distance effects is a mandatory preparation needed in order to obtain the so long expected long-baseline physics. Most of the experiments rely on the combination of near-far detector synergy in order to reach the desired precision.

The recent interest in Liquid argon detectors motivated us in the study of the physical capabilities of near detector physics. In [8] we studied what are the requirements necessary in order to be able to constraint Non-unitary, production/detection NSI and possibly sterile neutrinos in two scenarios: The SBN experiment and the yet-to-be-designed DUNE's near detector.

1. **The Short Baseline Neutrino Experiment (SBNE):** The SBNE was designed to resolve the LSND/MiniBooNE anomaly. It relies on 3 different detectors, in three different locations in order to be able to observe any oscillation pattern that might arrise in the existence of light sterile neutrinos: the SBND, MiniBooNE and ICARUS. Their characteristics are described in Table 5.3, summarizing the SBNE proposal [162]. The neutrino flux comes from the Booster Neutrino Beam (BND), containing mostly muon-neutrinos with energy not much greater than 3 GeV. The peak of the distributions is around 600 MeV.

Detector	Total Size	Active Size	Distance	Target	POT
SBND	220 t	112 t	110 m	Liq. Ar	6.6×10^{20}
MicroBooNE	170 t	89 t	470 m	Liq. Ar	1.32×10^{21}
ICARUS	760 t	476 t	600 m	Liq. Ar	6.6×10^{20}

Table 5.3 – Summary of the main features of the SBNE detectors [162].

2. **The DUNE's Near Detector:** DUNE's near detector is yet a matter of debate. While the LBNF's far detector is located at 1300 km distant from Fermilab's main injector it will require a very intense beam of neutrinos. This means that the near detector, located around 1 km, will receive an astonishing 1.7×10^6 more times the flux. Which will provide an enormous amount of neutrino events, which might lead

to the pile-up of neutrino events. Nevertheless,this amount of data might be usefull to search for new physics besides the ones proposed by the DUNE project. We analised three configurations for possible near detectors at the DUNE's beamline. We used an ICARUS version of SBNE and an improved version, which we called ICARUS+ and also the protoDUNE detector, which is the prototype of the future DUNE's far detector. Our assumptions can be found in Table 5.4.

Detector	Active Size	Distance	E range (GeV)	Target
ICARUS	476 t	600 m	0 to 3	Liq. Argon
ICARUS+	476 t	600 m	0 to 5	Liq. Argon
protoDUNE-SP	450 t	600 m	0 to 5	Liq. Argon

Table 5.4 – Suggestions for near detectors in DUNE.

As discussed in Chapter 4, the presence of non-unitary or NSI contains a zero-distance effect of the form,

$$P_{\mu e}(L=0) = B_{\mu e}\,. \tag{5.23}$$

where $B_{\mu e} \approx |\alpha_{21}|^2$ or $|\epsilon^D_{e\mu}+\epsilon^P_{\mu e}|^2$ for non-unitary and NSI respectively. Thus, measurement of short-baseline neutrinos can be used to constrain new physics. On Fig. 5.10 we show the expected sensitivity of each configuration. Notice that SBNE can reach $|B_{\mu e}|^2 < 3\times10^{-4}$, which is a little bit better than current constraint on $|\alpha_{21}|^2$. But DUNE's near detector can reach an order of magnitude less.

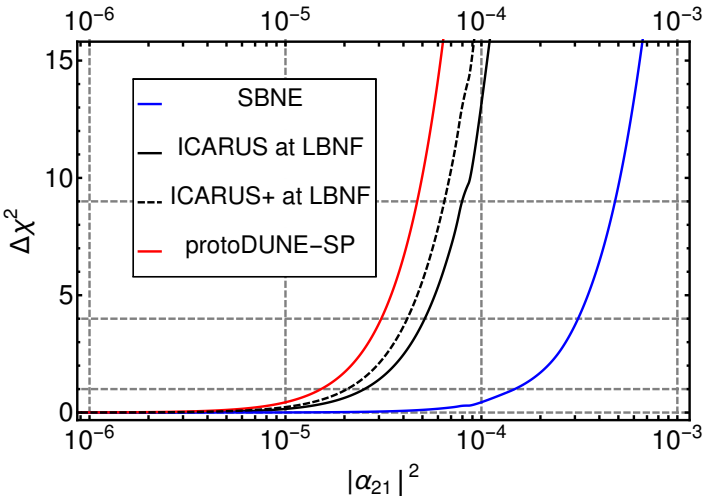

Figure 5.10 – Sensitivity of each configuration assumed: SBN experiment (blue), ICARUS at LBNF (black-solid), ICARUS+ at LBNF (black-dashed) and protoDUNE-SP (red). All of them are assumed to be located at 600 m from the neutrino source and running for 3.5 years in the neutrino and 3.5 in the anti-neutrino mode. This plot was taken from our work [8].

An important issue on these measurements is the lack of a near detector. Since they are zero distance effects, you cannot calibrate your knowledge of the flux by the presence of a detector closer to the beam source. On the contrary, one should rely on the measurement and prediction of the flux by external measurements. This gives rise to systematics that can change not only the overall normalization but also the shape of the neutrino flux. The DUNE collaboration might be able to predict the flux by measurements of the muons from pion decay and hadrons responsible for the creation of the beam [91]. Unfortunately, such predictions tend to be much less precise than the use of a near detector, which can reach the 0.1% level. The results on Fig. 5.10 assumes a shape uncertainty of around 1%. In Fig. 5.11 we show the requirement in order to reach several values of $B_{\mu e}$ at 90% C.L. as a function of the detector distance.

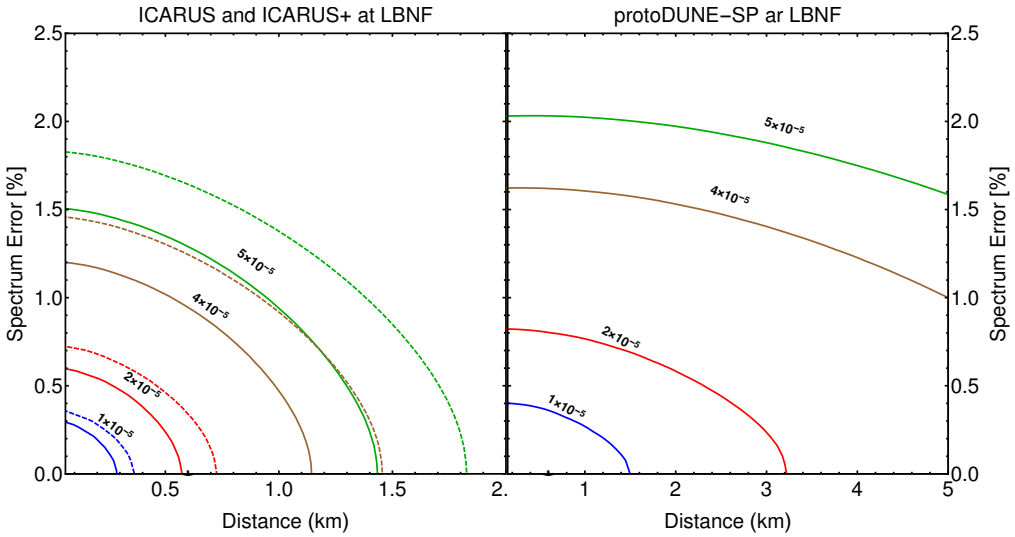

Figure 5.11 – **Left:** 90% C.L. sensitivity to $|\alpha_{21}|$ for ICARUS (solid line) and ICARUS+ (dashed line) for various combinations of the baseline and the spectrum error. **Right:** 90% C.L. protoDUNE-SP sensitivity for various combinations of baseline and spectrum error. Lines correspond to $B_{\mu e} < 10^{-5}$ (blue), $B_{\mu e} < 2 \times 10^{-5}$ (red), $B_{\mu e} < 4 \times 10^{-5}$ (brown) and $B_{\mu e} < 5 \times 10^{-5}$ (green). This plot was taken from our work [8].

For completeness, we also analyzed the possibilities of study the presence of sterile neutrinos under the assumption that no nearer detector exists and when there are two detectors, one near and the other not so far. An optimal baseline for the DUNE beam and an sterile neutrino of mass around 1 eV is 2.4 km. The sensitivity curves can be found in Fig. 5.12.

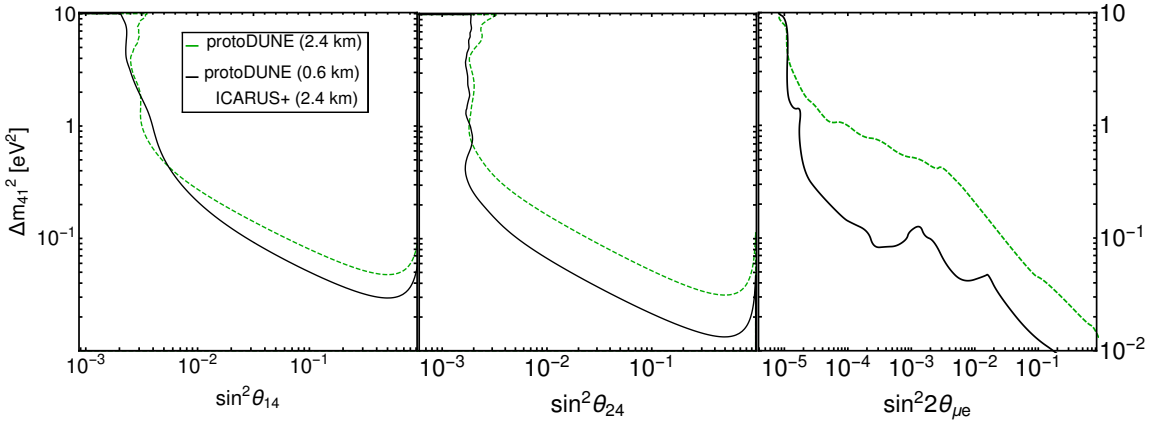

Figure 5.12 – The LBNF near detectors at 90% C.L. sensitivity to the 3+1 neutrino scheme is given in black for the combination of protoDUNE-SP at 0.6 km and ICARUS+ at 2.4 km. The Dashed-Green curve shows the result for the protoDUNE-only case at 2.4 km from the LBNF. **Left:** $\sin^2\theta_{14}$ versus Δm^2_{41} **Center:** $\sin^2\theta_{24}$ versus Δm^2_{41} and **Right:** $\sin^2 2\theta_{\mu e}$ versus Δm^2_{41}. A 1% spectrum error is assumed in all cases. This plot was taken from our work [8].

Accelerator neutrinos are interesting for sterile neutrino studies, because it is possible to desantangle the θ_{14} and θ_{24} parameter, since you can measure the ν_μ and ν_e flux at the same time.

5.4 Conclusion

In this Chapter we presented three different analysis of neutrino effects related to the phenomenology of neutrinos.

In Section 5.1 We performed a model-independent analysis on neutrino-scalar Yukawa interactions using recent data on meson decay em search for the heavy neutrino. We included in the calculation, for the first time the mass of the scalar particle. We also found that heavy neutrino search improves the bounds on those Yukawa interactions significantly to $|g_e|^2 < 1.9 \times 10^{-6}$ and $|g_\mu|^2 < 1.9 \times 10^{-7}$, for $m_\chi = 0$, the dependency on the scalar mass can be found in Fig. 5.4.

Knowing if θ_{23} value is indeed $< \pi/4$ or $> \pi/4$ is an interesting result for model builders. That is why future experiment's main goal is to measure this parameter with high precision. In Section 5.2 we showed that long baseline experiments have limited precision which is directly related to how you would account the knowledge of the value of θ_{13} which is precisely measured by reactor experiments. In special, the expected 3% precision in the θ_{13} angle might not be sufficient if $0.42 < \sin^2 2\theta_{23} < 0.56$.

The DUNE neutrino beam will contain the highest flux of neutrinos made by man so far. This is an incredible achievement that can be explored in several ways. Its far detector is established and its capabilities are well understood in the literature, nevertheless, the DUNE near detector is currently under discussion and does not have fixed characteristics. In Section 5.3 We aim to heat the discussion by showing the physical potential of the near detector and what are the requirements it must achieve in order to be used independently of the far detector. since the number of events is expected to be extremely high, we showed that the near detector can search for new physics in NSI, Non-unitary, and Sterile neutrinos, provided that the uncertainties in the energy dependency of neutrino flux and cross section are known up to a few percents.

Chapter 6

Neutrino Mass Models

"In math, you're either right or you're wrong."

Katherine Johnson

Up until now, we treated various aspects of neutrinos oscillation in a phenomenological point of view. Moreover, the existence of neutrino masses and mixing angles were the only fundamental assumptions needed to explain the experimental data. Nonetheless, a few particularities of neutrinos suggests that the mechanisms behind neutrino masses are different than for other fermions.

Firstly, neutrino masses are not a prediction of the Standard Model: besides neutrino oscillations, it is possible to explain all the physics without it. Secondly, neutrinos are the only neutral fermions. This opens up a very interesting possibility of *Majorana Masses* [163] which can also lead to *Lepton number violation* processes. Third, neutrino mixing parameters are a source of CP asymmetry, which can hint on the explanation of the proportion of matter/anti-matter in the universe. Fourth, neutrino masses are inconveniently small.

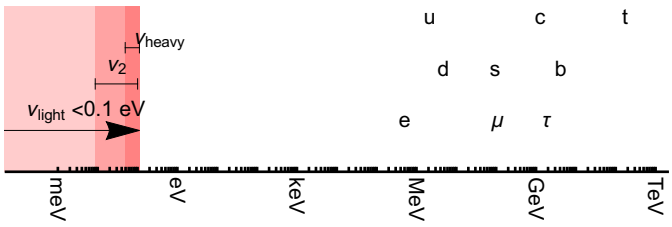

Figure 6.1 – Mass scales of known fermion particles. This picture was made for this thesis based on a similar image in [9].

The smallness of neutrino masses is illustrated in Fig. 6.1. Particles in the Standard Model have masses between $\sim$ MeV to hundreds of GeV, while the sum of neutrino masses lie below the eV scale. Even if there is nothing forbidden such hierarchical mass distribution. It is at least odd that the same mechanism could explain 12 orders of magnitude of masses. Hence, it is fundamentally important to formulate a complete theory that can explain why neutrinos are not massless. In this Chapter we present the two realizations of neutrino mass matrix: Dirac or Majorana. We show two complete neutrino mass models that can explain the smallness of neutrino masses and are very predictive and show how we can use future, low energy, neutrino experiments to contraint the space parameter of those models.

6.1 The Simple Dirac Mass Model

It is possible to give mass to the neutrinos by the same Higgs mechanism that acts on all the other fermions. In order to do that, it is only necessary to add three fermion singlets $(\nu_R)_i$, $i = 1, 2, 3$ and the Higgs interaction the same way the up-type quarks gain mass,

$$\mathcal{L} = -\frac{Y^{\nu}_{\alpha\beta}}{\sqrt{2}} \bar{L}_{\alpha} \tilde{H} \nu_{\beta R} + h.c. \tag{6.1}$$

Where

$$\tilde{H} = i\sigma_2 H^*, \tag{6.2}$$

is the self-adjoint representation of the Higgs field allowed in $SU(2)$ and σ_2 is the second Pauli Matrix. Now, when the Higgs acquires a VEV, $h \to v$, and $(M_{\nu})_{\alpha\beta} = vY^{\nu}_{\alpha\beta}$ and neutrinos are of the *Dirac Type*. Although simple and symmetric, this mechanism does not explain why the neutrino masses are so different from the other fermions.

It is also interesting to notice that Dirac Neutrinos Conserve (Total) Lepton Number. In the Standard Model, it is usual to introduce three family lepton numbers L_{α}, $\alpha = e, \mu, \tau$ that are conserved because the whole Lagrangian is invariant under each of the three transformations,

$$\nu_{\alpha L} = e^{i\theta_{\alpha}} \nu_{\alpha L}, \qquad l_{\alpha} = e^{i\theta_{\alpha}} l_{\alpha} \tag{6.3}$$

where l_α is the charged lepton. When neutrinos have mass, the free Dirac neutrino Lagrangian becomes,

$$\mathcal{L}_D = i\bar{\nu}_{\alpha L}\partial\!\!\!/\nu_{\alpha L} + i\bar{\nu}_{\alpha R}\partial\!\!\!/\nu_{\alpha R} - m_{\alpha\beta}\left(\bar{\nu}_{\alpha L}\nu_{\beta R} + \bar{\nu}_{\alpha R}\nu_{\beta L}\right) \tag{6.4}$$

and it is not possible to diagonalize the charged fermion and neutrino mass matrix at the same time. It is easy to see that in the first case Eq. (6.4) is not invariant by this three transformations individually (if $m_{\alpha\beta} \neq$ diagonal), but is by a single transformation,

$$\nu_{\alpha L} = e^{i\theta}\nu_{\alpha L}, \qquad l_\alpha = e^{i\theta}l_\alpha \tag{6.5}$$

this means that instead of the three lepton numbers conserved, Dirac-Massive neutrinos conserves total lepton number, L.

6.2 Majorana Neutrinos

The Dirac mass term is not the only one available to construct a theory of neutral fermions. The other possibility is try to write a non-vanishing quadratic term with only the L (or R) part of the fermion field. This is possible because one don't need to use the full four component spinor to describe fermions. It is possible to construct a right-handed term starting from ν_L, let's denote it ψ_R,

$$\psi_R = \zeta C\bar{\nu}_L^T \tag{6.6}$$

where ζ is a phase and C is the charged conjugation operator. To see that it is indeed a right neutrino, note first that the operator $P_L = \frac{1-\gamma_5}{2}$ selects the left part of the fermion, so if $P_L\psi = 0$, then, $\psi = \psi_R$ (is only right-handed). Indeed,

$$P_L C\bar{\nu}_L^T = CP_L^T\bar{\nu}_L^T = C\left(\bar{\nu}_L P_L\right)^T = C\left(\left[P_R\nu_L\right]^\dagger\gamma_0\right)^T \tag{6.7}$$

Where $P_R = \frac{1+\gamma_5}{2} = P_L^\dagger$. Since, $P_R\nu_L = \frac{1+\gamma_5}{2}\frac{1-\gamma_5}{2}\nu = 0$, and

$$P_L\psi_R = 0 \tag{6.8}$$

and the subscribed R on ψ is justified. If a spinor obeys

$$\psi = C\bar{\psi}^T \tag{6.9}$$

or equivalently,

$$\psi_R = \zeta C\bar{\psi_L}^T \tag{6.10}$$

which is just imposing in Eq. (6.6), $\nu_R = \psi_R$, then $\psi = \psi_L + C\bar{\psi}_L^T$ and,

$$\bar{\psi}\psi = -\psi_L^T C^\dagger \psi_L + h.c \neq 0 \tag{6.11}$$

And the Majorana Lagrangian can be written as,

$$\mathcal{L} = \bar{\psi}_L i\partial\!\!\!/ \psi_L - \frac{m}{2}\left(-\psi_L^T C^\dagger \psi_L + \bar{\psi}_L C\bar{\psi}_L^T\right). \tag{6.12}$$

Note from Eq. (6.12) that, unlike the Dirac case, the Majorana neutrino does not conserves lepton number: the transformation $\nu' = e^{i\theta}\nu$ does not make the Lagrangian invariant. This also implies that no $U(1)$ charge can be assigned to the massive Majorana Fermions. Another way to see this is by looking at a possible fermion current, $j_\mu = \bar{\psi}\gamma_\mu\psi$. If $\psi = \psi^C$, then,

$$\bar{\psi}\gamma_\mu\psi = \bar{\psi^C}\gamma_\mu\psi^C = -\psi^T C^\dagger \gamma_\mu C\bar{\psi}^T = \bar{\psi}C\gamma_\mu^T C^\dagger\psi = -\bar{\psi}\gamma_\mu\psi \tag{6.13}$$

So, $j_\mu = -j_\mu = 0$ and no $U(1)$ gauge symmetry is possible. This discussion also implies that Majorana Fermions cannot absorb phases. While in the Dirac case in a 3×3 Dirac Matrix scenario there is only one physical CP-violation phase δ, the Majorana Neutrinos has three, δ, δ_2 and δ_3. Also, every model that generates Majorana masses has to have a *total* lepton number violating term.

6.2.1 The See-Saw Model

The idea behind the seesaw mechanism consists on a high energy mass scale M that is hidden for low energy physics except by an effective Lagrangian term suppressed by M^{-1}, so that for large M, M^{-1} is small, just like the playground toy see-saw. The simplest conception of this mechanism is taking only one extra particle, a right-handed

fermion, $N_R \sim (1,1,0)_{+1}$ and a Lagrangian of the form (omitting kinetic terms),

$$\mathcal{L} = -\frac{Y_\nu}{\sqrt{2}}\overline{L}\tilde{H}N_R - \frac{M}{2}\overline{N^c}_R N_R + h.c. \tag{6.14}$$

where only one flavor was considered for simplicity. In this model, one have corrections to the neutrino propagator of the form,

$$L^T C\tilde{H}\left(\int dq \frac{-(Y_\nu)^2(\not{q}+M)}{2(q^2-M^2)}\right)\tilde{H}^\dagger L = \tag{6.15}$$

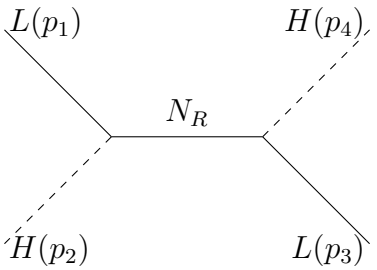

with $q = p_1 + p_2 - (p_3 + p_4)$. For low q ($q^2 << M^2$), the term inside parenthesis can be approximate by $-\frac{(y^\nu)^2}{2M}$ and the interaction becomes the usual Weinberg operator [164]. This approximation is better understood observing the full Lagrangian,

$$\mathcal{L} = \overline{L}\not{\partial}L + \overline{N}_R\not{\partial}N_R - \frac{y_\nu}{\sqrt{2}}\overline{L}\tilde{H}N_R - \frac{M}{2}\overline{N^c}_R N_R + H.C \tag{6.16}$$

the classical equation of motion reads,

$$(\not{\partial} - M)N_R^{\text{clas}} + \frac{Y_\nu}{\sqrt{2}}\tilde{H}^\dagger L = 0 \tag{6.17}$$

so the classical solution N_R^{clas} is,

$$N_R^{\text{clas}} = (\not{\partial} - M)^{-1}\frac{y^\nu}{\sqrt{2}}\tilde{H}^\dagger L \tag{6.18}$$

By expanding the action around the classical solution, $N_R = N_R^{\text{clas}} + N_R^{(1)}$,

$$S = \int dx\overline{L}\not{\partial}L + \frac{Y_\nu^2}{2}\int dy\overline{L^c}(x)\tilde{H}(x)(\not{\partial} - M)^{-1}\tilde{H}^\dagger(y)L(y) + \\ \text{Things not dependent on H, L} + O(N_R^{(1)}). \tag{6.19}$$

Therefore, if M is much bigger them the usual energy scale of the reaction, $(\not{\partial} - M)^{-1} \approx -M^{-1}\delta(x-y)$ and $O(N_R^{(1)}) \sim M^{-2}$ and one can integrate out all the N_R dependency obtaining the Weinberg dimension five operator,

$$\mathcal{L}_{\text{mass}} = -\frac{(y^\nu)^2}{2M}L^T C\tilde{H}\tilde{H}^\dagger L = -\frac{(y^\nu)^2}{2M}\left(L^T Ci\sigma_2\vec{\sigma}L\right)\left(H^T Ci\sigma_2\vec{\sigma}H\right) \tag{6.20}$$

finally, when the Higgs acquires a VEV, v, the following neutrino mass term appears,

$$\mathcal{L} = -\frac{(y^\nu)^2 v^2}{2M}\left(\overline{\nu}_L C\overline{\nu}_L^T + H.C.\right) \tag{6.21}$$

and one can see that it generates Majorana masses. For the usual Higgs VEV, $v \approx 246$ GeV and usual couplings $Y_\nu \sim 0.1$, masses M of the order of $M \sim 10^{13}$ GeV are necessary to reproduce the sub-eV scale of neutrino masses, these energies are much higher than any particle accelerator dreams of reaching.

6.3 Neutrino Oscillations Constraints on HEP

The experimental physics has relied on particle colliders for decades in order to search and test High Energy Physics (HEP). On the other side, many of the high energy models try to explain not only the smallness of neutrino masses but also predict the value of the mixing angles. This is possible because a given model A may contain a set of n_A free parameters $\{x_i\}$ in the leptonic section, which might be smaller than the number of parameters in the S3νO, $n_{\text{SM3}\nu} = 3$ masses+3 angles+1 (or 3) phases=7 (or 9). Thus, if $n_a < n_{\text{SM3}\nu}$, when one tries to write the mixing angles as a function of the n_A parameters, that is,

$$\begin{aligned}\theta_{ij} \equiv& \theta_{ij}(\{x_k\})\\ \Delta m^2_{ij} \equiv& \Delta m^2_{ij}(\{x_k\})\\ \delta_{\text{CP}} \equiv& \delta_{\text{CP}}(\{x_k\}),\end{aligned}$$

correlations are naturally introduced among them. This is very common for models that introduce discrete flavor symmetries in order to accommodate the lepton families. As we argued in [10], any model containing sharp correlations between θ_{23} and δ_{CP} can be probed using future long-baseline experiments, since their main goals are to measure both parameters with amazing precision. In the next sections, we will show two case studies of this situation for UV complete models that generates Dirac or Majorana masses for neutrinos.

6.3.1 Warped Flavor Symmetry Model

Our first example is the Warped Flavor Symmetry Model (WFSM) presented in [165]. It is constructed in a five-dimensional AdS_5 space, whose metric is described by,

$$ds^2 = e^{-2ky}\eta_{\mu\nu}dx^\mu dx^\nu - dy^2, \tag{6.22}$$

k is the curvature scale of the space. The fifth simension should be compactified since it was not detected. The minimal version uses a $S_1/\mathbb{Z}_1$ symmetry attaching the orbtifold to $y = 0$ (UV brane) and $y = L$ (IR brane). The SM Charged Lepton masses are generated by interactions in UV brane of the form $\sim (\phi\overline{\Psi}_l)H\psi_{l_i}$, with Ψ_l a $\Delta(27)$ tripplet formed by the ψ_{l_i} SM fermions, while *Dirac* neutrino masses are generated by interactions in the IR brane of the form $\sim (\xi\sigma_a\overline{\Psi}_l)\tilde{H}\Psi_{\nu_i}$, $a = 1, 2$. ξ, σ_a and ϕ are all localized scalars that acquire a Vaccum expectation Value (VeV). Since $\xi\sigma_a$ lives in the IR brae, the smallness of neutrino masses are naturally explained as the neutrino-mass term is exponentially suppresed by a function of the curvature k. Notice that this does not happen for the charged leptons, since ϕ is localized in the UV brane.

An interesting feature of this model is that the flavour symmetry constraints the form of the Lepton and Neutrino mass matrix which imposes correlations between all the 4 neutrino oscillation. They are predicted by only two angles: θ_ν and ϕ_ν,

$$\sin^2\theta_{12} = \frac{1}{2 - \sin 2\theta_\nu \cos\phi_\nu} \tag{6.23}$$

$$\sin^2\theta_{13} = \frac{1}{3}(1 + \sin 2\theta_\nu \cos\phi_\nu) \tag{6.24}$$

$$\sin^2\theta_{12} = \frac{1 - \sin 2\theta_\nu \sin(\pi/6 - \phi_\nu)}{2 - \sin^2\theta_\nu \cos\phi_\nu} \tag{6.25}$$

$$J_{\rm CP} = -\frac{1}{6\sqrt{3}}\cos 2\theta_\nu, \tag{6.26}$$

where $J_{\rm CP}$ is the Jarlskog invariant, $J_{\rm CP} = {\rm Im}[U^*_{e1}U^*_{\mu 3}U_{\mu 1}U_{e3}]$ [166]. This means that, by comparing the predicted relation given by the two free parameters and the measured mixing angles, one can probe the model using low energy neutrino oscillation experiments.

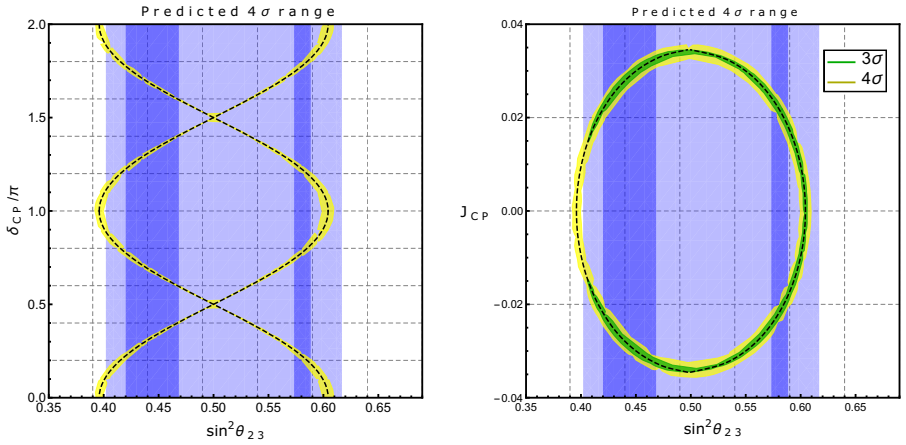

Figure 6.2 – Illustration of the correlation between θ_{23} and $\delta_{\rm CP}$ (left) or $J_{\rm CP}$ (right) in the WFSM. The bands correspond to 3 (green) and 4 (yellow) σ of the parameter space available. The blue region is the current constraint on the mixing parameter without correlation. In the left plot, we choose to present only the 4σ contour for better visualization. This figure was taken from our work [10].

This can be seen in Fig.6.2. There we illustrate the correlation between θ_{23} and $\delta_{\rm CP}$ (left) or $J_{\rm CP}$ (right). The bands correspond to 3 (green) and 4 (yellow) σ of the parameter space available using current constraints on the mixing parameter. If nature chooses $\delta_{\rm CP} = \pi$ and $\sin^2\theta_{23} = 0.5$ the model should be excluded as it cannot produce such a solution. Notice the model has a 2σ tension, however, the central values of the mixing angles are generated by minimization of all the mixing parameters at the same time, while the model has only 2 parameters. The most stringent limit comes from the solar angle of θ_{12}.

6.3.2 Longbaseline Constraints on WFSM

To quantify the future long baseline sensitivity of testing our benchmark oscillation model, in [11] we used GLoBES software [167] to simulate current and future longbaseline experiments, T2(H)K, NOνA and DUNE. The sensitivity is obtained by a χ^2 analyzis in which we minimized over the free oscillation parameters: θ_ν and ϕ_ν.

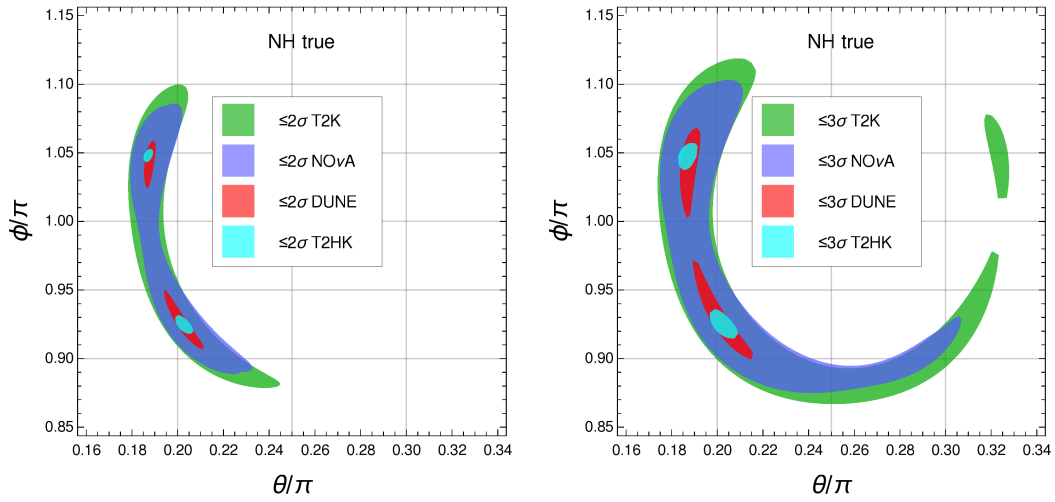

Figure 6.3 – Expected future allowed regions of the two model parameters θ_ν and ϕ_ν for $\Delta\chi^2 < 4$ (left) and 9 (right) in four cases: T2K (dark green), NOνA (blue), DUNE(Red) and T2HK (cyan). The plots assume Normal Hierachy (NH) as true. This figure was taken from our work [11].

The regions are calculated by defining the equation,

$$\Delta\chi^2 \equiv \chi^2(\theta_\nu, \phi_\nu) - \chi^2_{\text{min}}(\theta_{ij}, \delta_{\text{CP}}) \tag{6.27}$$

The resulting region is plotted in Fig. 6.3 for $\Delta\chi^2 < 4$ (left) and 9 (right). Notice that in special, DUNE and T2HK greatly reduces the allowed region of Fig. 6.2.

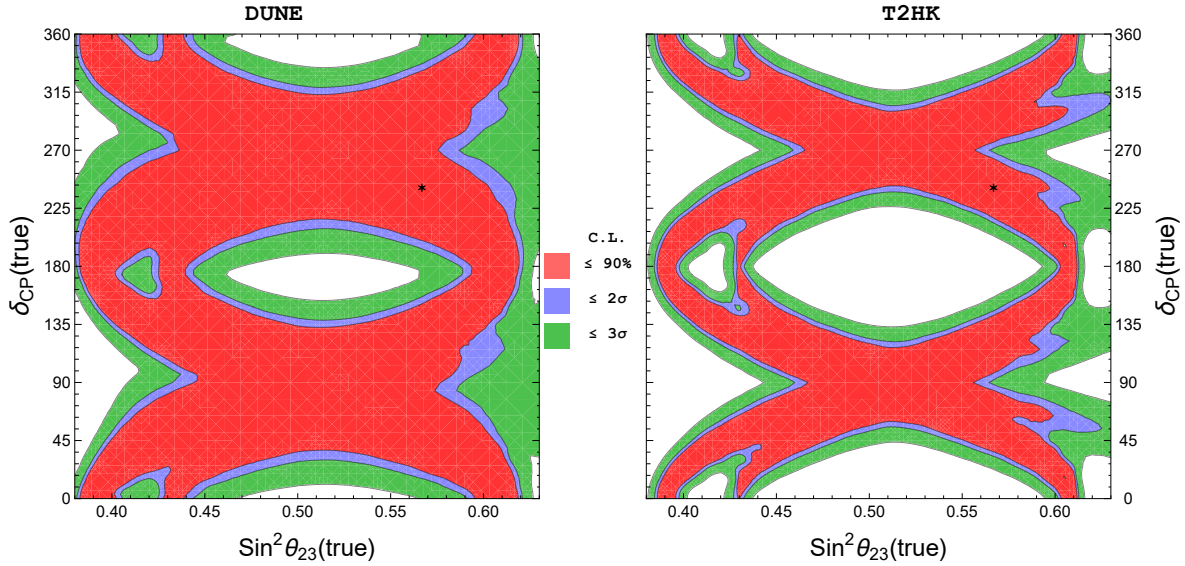

Figure 6.4 – Exclusion capabilities of future long-baseline experiments DUNE (left) and T2HK (right) to exclude the WFSM as a function of the true values of the neutrino mixing angles, $\sin^2\theta_{23}^{\text{true}}$ and $\delta_{CP}^{\text{true}}$ for normal neutrino mass ordering (NH). The shaded regions denote $\Delta\chi^2 < 2.71$ (red), 4 (blue) and 9 (darker green), The star denotes the current unconstrained minimum value. This figure was taken from our work [11].

An interesting analysis to perform is the capability of future experiments to be able to exclude the model. To do that, we performed the the same calculation for each possible value of the values $\theta_{23}^{\text{true}}$ and $\delta_{\text{CP}}^{\text{true}}$. The regions are plotted in Fig. 6.4. The bands correspond the points in parameter space where the model cannot be excluded at 90% C.L., 2σ and 3σ. Thus, although future measurements might tightly constraint the parameter space, only a small region of the parameter space can effectively be used to fully exclude the model.

6.3.3 Babu-Ma-Valle Model

A Majorana-mass type model that presents such correlation is the famous Babu-Ma-Valle A_4 model (BMV) [168]. The model is a specific version of the Minimal Supersymmetric Standard Model (MSSM) that postulate a A_4 flavor symmetry that correlates the families of leptons and quarks. The main idea is to break A_4 on a high scale (much higher than the electroweak breaking). The charged lepton mass is generated by the combination of symmetry breaking from the extra scalars of the model and a Higgs like scalar ϕ_1. In the neutrino sector, the mass matrix is generated by another Higgs-like scalar ϕ_2 that relates two Majorana fields (ν_i, N_i^c). Which results in a traditional See-saw mechanism. Unfortunately, the neutrino mass matrix produces *degenerate* neutrino masses. Non-degenerate masses are created by loop corrections and lead to a specific form for the PMNS matrix* that depends on only one parameter, θ,

$$U_\nu(\theta) = \begin{pmatrix} \cos\theta & -\sin\theta & 0 \\ \sin\theta\sqrt{2} & \cos\theta\sqrt{2} & -1/\sqrt{2} \\ \sin\theta\sqrt{2} & \cos\theta\sqrt{2} & 1/\sqrt{2} \end{pmatrix}. \tag{6.28}$$

This clearly does not fit the current neutrino parameters, as it predicts $\sin^2\theta_{13} = 0$. But the model is not dead. In [169] it was shown that it is possible to revamp the A_4 model in order to accommodate the neutrino masses and mixing. It is done by the introduction of a A_4 singlet scalar that couples to the charged leptons and changes their mass matrix.

*see [168] for the discussion.

This implies that the new mixing matrix is now of the form

$$U_{\rm PMNS} = U_l(\beta)^\dagger . U_\nu(\theta). \tag{6.29}$$

Now, the two parameters β (β is complex) and θ can explain current neutrino parameters. But correlations between $\delta_{\rm CP}$ and θ_{23} are introduced, as can be seen in Fig. 6.5.

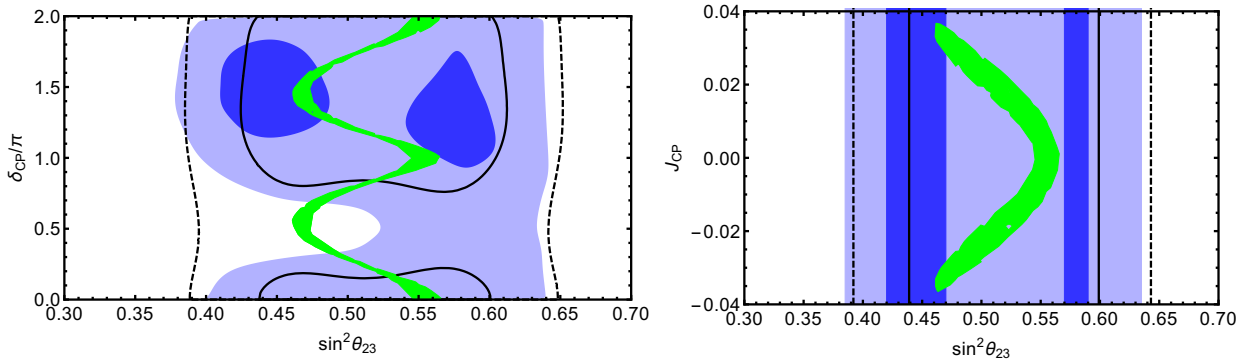

Figure 6.5 – Illustration of the correlation between θ_{23} and $\delta_{\rm CP}$ (left) or $J_{\rm CP}$ (right) in the BMV model. The band corresponds to 90% (green) C.L. of the parameter space available. The blue region is the current constraint on the mixing parameter without correlation. In the $\delta_{\rm CP}$ phase we choose to present only the 4σ contour for better visualization. This figure was taken from our work [12].

Notice that this model has a different pattern correlation between the mixing parameters, in special, large deviations from the maximality of θ_{23} cannot be fitted. A similar procedure to the previous section can be done in order to obtain future DUNE and T2HK sensitivity. The result is presented in Fig. 6.6. The bands correspond to $1, 2, 3$ and 4 and σ intervals while the black curve is currently allowed 90% C.L. interval assuming non-correlated parameters.

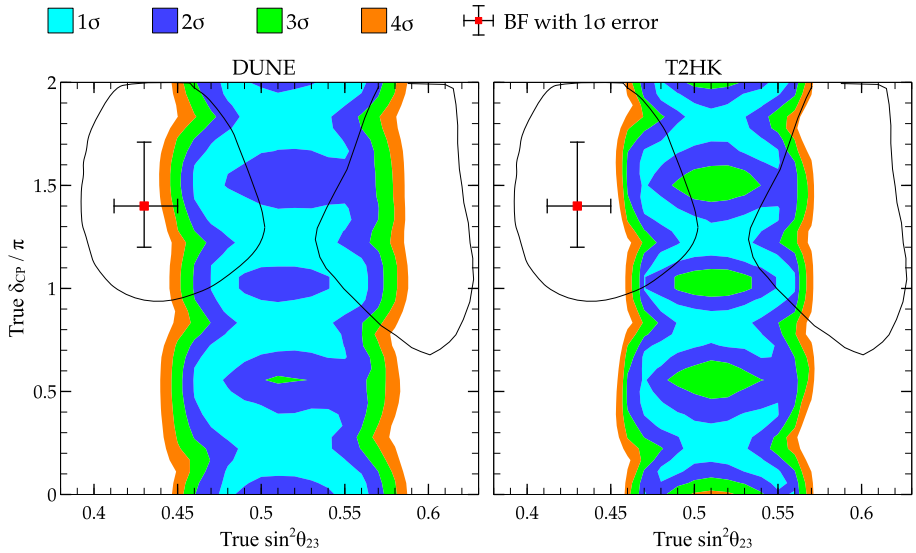

Figure 6.6 – Exclusion capabilities of future long-baseline experiments DUNE (left) and T2HK (right) to exclude the BMV model as a function of the true values of the neutrino mixing angles, $\sin^2\theta_{23}^{\text{true}}$ and $\delta_{CP}^{\text{true}}$ for normal neutrino mass ordering (NH). The shaded regions denote $\Delta\chi^2 < 2.71$ (cyan), 4 (blue) and 9 (green) and 16 (Orange), The red dot denotes the current unconstrained minimum value and the black curve the current allowed 90% C.L. interval assuming non-correlated parameters. This figure was taken from our work [12].

6.4 Flavour Symmetry Models in Long-Baseline Experiments

Last sections described how it is possible to use long-baseline experiments to probe the models that correlate θ_{23} and δ_{CP}. However, this is not the only type of relation between mixing parameters that can be exploited to probe Hight Energy Physics. The current value of the neutrino parameters shows that there are two 'small' quantities: the value of the reactor angle, θ_{13}, and the deviation of the atmospheric angle, θ_{23}, from its maximal value $\pi/4$. It is suggestive to think that maybe both deviations are reminiscent consequences of a symmetry breaking, which can relate both values by a generic function described by,

$$\theta_{13} = f(\pi/4) + f'(\pi/4)\left|\frac{\pi}{4} - \theta_{23}\right| + ... \approx \theta_{13}^0 + f\left|\frac{\pi}{4} - \theta_{23}\right|. \tag{6.30}$$

Hence, it is not uncommon for a model to start with an antaz matrix U'_ν that predicts $\sin^2\theta_{13} = 0$ and $\sin^2\theta_{23} = 1/2$ and make small deviations in order to explain the observed value of such parameters, thus $U'_\nu \to U_{\text{PMNS}}$. In fact, there are a lot of models that rely

on this methodology. A compendium of such models and references to their construction are presented in Table 6.1.

Model	f	θ_{13}^0[rad]	Model	f	θ_{13}^0[rad]
[13]	$\sqrt{2}$	0	$U_{BM}.U_{23}U_{13}$	1/2	0
[170, 171]	0.35	[0,0.35]	$U_{TBM}.U_{23}U_{12}$	2	0.157
[172]	0.1 or 10	0.62	$U_{TBM}.U_{23}U_{13}$	$1/\sqrt{2}$	0
[173]	$1/\theta_0$	[-1,1]	$U_{TBM}.U_{13}U_{12}$	$2/\sqrt{2}$	0
$U_{13}.U_{TBM}$	6.3	0	$U_{BM}.U_{13}U_{12}$	$\sqrt{3/2}$	0
$U_{12}.U_{TBM}$	6.3	0	$U_{BM}.U_{23}U_{12}$	$\sqrt{3/2}$	0
$U_{TBM}.U_{23}$	$1/\sqrt{3}$	0	$U_{BM}.U_{23}U_{13}$	1/2	0

Table 6.1 – Compendium of models that starts with an ansatz matrix that predicts $\sin^2\theta_{13} = 0$ and $\sin^2\theta_{23} = 1/2$ that results in correlations among such parameters. All the possible combinations of corrections from Tri-Bi-MAximal (TBM), Bi-Maximal (BM) were considered in [174].

In [14] we showed that it is possible to probe a model independent, but phenomenolocaly motivated correlation between the atmospheric mixing and the reactor angle. As an example, we used the DUNE experiment as a case study. However, it is important to point out that the octant degeneracy may interfere in the sensitivity of such relation, as was shown in [70]. This can be bypassed by a combination of long-baseline and reactor measurements.

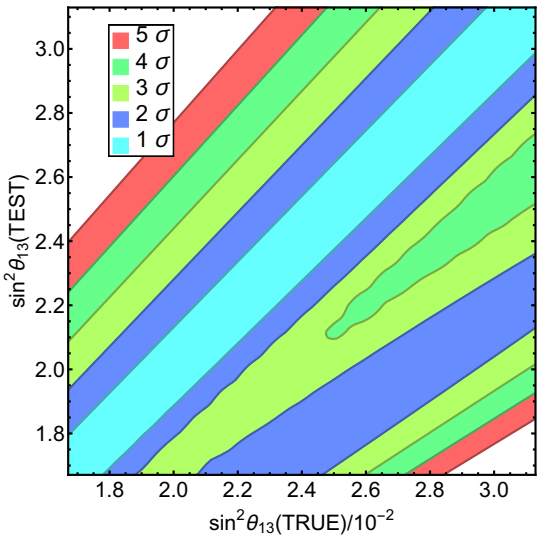

Figure 6.7 – DUNE expected sensitivity to the θ_{13} mixing parameer assuming a correlation of Eq. 6.30 taking $\theta_{13}^0 = 0$ and $f = \sqrt{2}$ (Tetrahedral Symmetry model [13]). The shaded regions describe 1 to 5 sigma confidence intervals. This figure was taken from our work [14]

We showed in [7] that a synergy between both types of experiment can partly lift the octant problem. If we take the expected sensitivity of Daya-Bay to reach 3% of the value of $\sin^2\theta_{13}$ [175], it is possible to constraint the values of θ_{13}^0 and f using the relation in Eq. 6.30. In Fig. 6.7 we show the special case of $\theta_{13}^0 = 0$ and $f = \sqrt{2}$ from the Tetrahedral Symmetry model [13]. We plotted the correlation between $\sin^2\theta_{13}$ (test) and $\sin^2\theta_{13}$ (true). We see that for true values of θ_{13} there is a small band that the model can explain the result inside the 1σ.

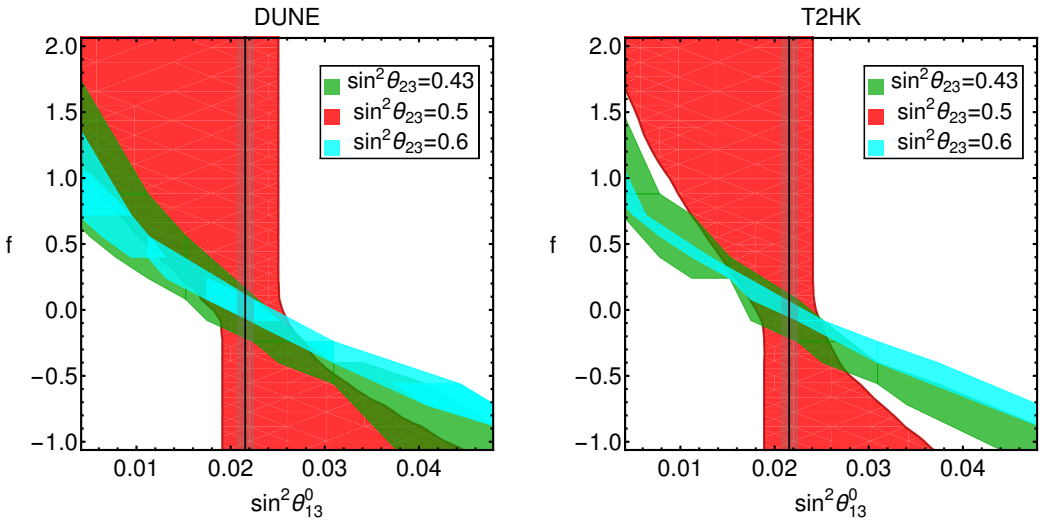

Figure 6.8 – Allowed regions of θ_{13}^0 and f for three different values of $\sin^2\theta_{23}$: 0.42 (green), 0.5 (red) and 0.6 (cyan). The gray region represents the 1σ allowed parameter region of θ_{13}This figure was taken from our work [15]

Notice that most of the parameter space will be probed by the DUNE experiment in conjunction with reactor measurements. For completeness, in Fig. 6.8, we present the allowed regions of θ_{13}^0 and f for three different values of $\sin^2\theta_{23}$: 0.42 (green), 0.5 (red) and 0.6 (cyan). The gray region represents the 1σ allowed parameter region of θ_{13}.

6.5 Conclusion

simulation of the capability of future baseline experiments to constraint or even exclude the warped flavor model and the BMV model. We showed that those experiments can shrink down the parameter space and that parts of the parameter space can be used to exclude them with more than 3 σ of confidence. Moreover, a careful analysis should be performed by the upcoming experiment in order to disentangle the physics, as the

assumption of which model is true can significantly change the minimum value of the parameters.

The achievements of future neutrino experiments lie beyond being able to precisely measure neutrino oscillation parameters. It can also teste predictive high energy models. In Section 6.3 We showed that it is possible to perform such tests without the need of simulating each model at a time. We took a very general correlation that exists in several models, Eq. 6.30, and were able to perform a model-independent analysis that embraces many types of neutrino mass theoretical frameworks.

Chapter 7

Conclusions

Recent advances in experimental high energy physics have settled one of the most interesting scenarios in the history of physics. The standard model (SM) has passed with flying colors most of its tests after the latest LHC run. On the other hand, some non-trivial theoretical issues indicate that the SM is not the final answer.

The search for beyond standard model effects expands every year due to a joint effort of the community. In the neutrino sector, the long-baseline experiments ($L/E \sim 500$ km/ GeV) such as T2(H)K, NOνA and DUNE will reach an incredible precision in measuring neutrino-oscillation parameters. There are also short-baseline neutrino experiments such as SBN, miniBooNE, LSND, and others, that try to look for a sign of a slippery sterile neutrino with a mass around 1 eV. This is a prolific era for high energy physics indeed.

This plethora of new and interesting phenomena that can be observed using neutrinos and the push of the academy towards the understanding of neutrinos is the main motivation for the subject of this thesis.

The theoretical aspects of neutrino oscillation are well known in the literature, but since it is a vast new field, there are just a few texts that present the general overview of the community. This is why in Chapter 1 and 3 we presented the currents status of the standard 3-neutrino oscillation theory, by taking a deep and careful look into the nuances of obtaining the standard formulas. In Chapter 4 we presented relevant phenomenological

extensions of the standard 3-neutrino oscillation theory, the Non-Standard Interactions, the Non-unitarity of neutrino mixing matrix and sterile neutrinos.

In the rest of the thesis, we took two theoretical directions that can be used to assist the search for new physics: Bottom-up and Top-down.

The Bottom-up approach consists of the analysis of all possible effective scenarios that may arise inside the context of the SM that was presented in Chapter 4. While the Top-down approach is based on the realization of UV complete high energy models that reproduces the SM in low energy but contains some non-trivial residual effects. Our research was focussed on studying the neutrino oscillation and neutrino mass models, and it has been done in both directions.

In Section 5.1 We studied how the presence of Yukawa interactions between neutrinos and massive scalar particles, $\mathcal{L} \sim g_{ij}\overline{\nu}_i\nu_j\phi$, could change the total decay rate and the decay spectrum of mesons into leptons. We improved the exclusion limits on the coupling constants between neutrinos and scalars by two orders of magnitude for the muon neutrino coupling $|g_\mu|^2 < 1.9\times10^{-7}$ at 90% of C. L. This was possible by using data from very precise measurements of the Kaon decay spectrum rather than the usual total decay rate, this resulted in the publication in [5]. We also worked with the consequences of non-unitary of the neutrino mixing matrix due to the existence of extra heavy neutrinos that might not be produced in oscillation experiments. In Section 4.4.2 We analyzed it in the context of T2K and showed how it could jeopardize the measurement of $\delta_{\rm CP}$. Nevertheless, as we showed, the possibility of using the μ-Decay-at-Rest experiment in J-park can restore T2K sensitivity. The muon decay-at-rest has a well-known decay spectrum and a different baseline/energy (15 km/ 50 MeV $\sim$ 300) that, when combined with accelerator neutrinos, disentangle degeneracies in the oscillation probability induced by the non-unitary CP phases. This resulted in the publication in [3].

Also, we explored the physical possibilities of a near detector at the DUNE experiment in Section 5.3. We analyzed the physics potential of the near detector in constraining non-unitary, non-standard interactions and sterile neutrinos at the eV scale. And what the impact of systematics into those measurements would be. Such analysis resulted in the work published in [8].

It is important to notice that separating tiny effects coming from new physics is hard. It is necessary to have a very well understanding of the standard 3 neutrino paradigm and its parameter degeneracies. Our contribution to this topic is the analysis in Section 5.2. We showed how well a precise measurement of the reactor angle θ_{13} can contribute to the measurement of the θ_{23} octant and what are the limitations. In special, the 3% expected precision in the measurement of $\sin^2\theta_{13}$ allow the octant measurement if the atmospheric mixing angle, θ_{23} is not in the range $0.42 < \sin^2\theta_{23} < 0.56$. This result was published in [7].

The phenomenological approach described above is very useful to model-independent constraint new physics. But this comes with a price. Generally, model-independent constraints are looser when compared to ones coming from more specific scenarios. That is why it is worth to study particular predictive models and their consequences. This can be done by analyzing the predicted correlations between masses and mixing or by the new particles and interactions that may arise from a particular symmetry.

As a case study, in Section 6.3, we took two models, the Warped Flavor Symmetry model, which predicts a sharp correlation between the atmospheric angle, θ_{23}, and the Dirac CP phase and presented the possible phase-space in which one could probe such model for the long-baseline experiments. And we performed a similar analysis for the Revamped Babu-Ma-Valle model. We presented the parameter space that can be constrained at 3σ by future neutrino experiments such as T2HK and DUNE. This analysis resulted in 3 publications [10, 11, 12].

In Section 6.4 we showed that it is possible to extend this analysis by considering possible correlations between θ_{23} and the reactor angle. This correlation is particularly interesting because it can be generated by small changes to symmetric mixing matrix such as the Bi-maximal, Tri-Bimaximal and Golden Ratio. Thus, one can create a general parametrization that can be used to easily translate bonds from the experimental data to a particular model. Such idea resulted in the publication in [14] and all those analyses were summarized in the invited review we wrote in [15].

In summary, we took a closer look at the theory of neutrino oscillations and its theoretical subtleties. Also, we aimed to study a diversity of phenomena that can provide observables in neutrino experiments and how one can use them to constraint new physics.

Chapter 8

Bibliography

1. de Gouvêa, A. & Kelly, K. J. Non-standard Neutrino Interactions at DUNE. *Nucl. Phys.* **B908**, 318–335 (2016). 1511.05562.

2. Antonello, M. *et al.* A Proposal for a Three Detector Short-Baseline Neutrino Oscillation Program in the Fermilab Booster Neutrino Beam (2015). 1503.01520.

3. Ge, S.-F., Pasquini, P., Tortola, M. & Valle, J. W. F. Measuring the leptonic CP phase in neutrino oscillations with nonunitary mixing. *Phys. Rev.* **D95**, 033005 (2017). 1605.01670.

4. Artamonov, A. V. *et al.* Search for heavy neutrinos in $K^+ \to \mu^+ \nu_H$ decays. *Phys. Rev.* **D91**, 052001 (2015). [Erratum: Phys. Rev.D91,no.5,059903(2015)], 1411.3963.

5. Pasquini, P. S. & Peres, O. L. G. Bounds on Neutrino-Scalar Yukawa Coupling. *Phys. Rev.* **D93**, 053007 (2016). [Erratum: Phys. Rev.D93,no.7,079902(2016)], 1511.01811.

6. Forero, D. V., Tortola, M. & Valle, J. W. F. Neutrino oscillations refitted. *Phys. Rev.* **D90**, 093006 (2014). 1405.7540.

7. Chatterjee, S. S., Pasquini, P. & Valle, J. W. F. Resolving the atmospheric octant by an improved measurement of the reactor angle. *Phys. Rev.* **D96**, 011303 (2017).

1703.03435.

8. Miranda, O. G., Pasquini, P., Tórtola, M. & Valle, J. W. F. Exploring the Potential of Short-Baseline Physics at Fermilab. *Phys. Rev.* **D97**, 095026 (2018). 1802.02133.

9. de Gouvea, A. *et al.* Working Group Report: Neutrinos. In *Proceedings, 2013 Community Summer Study on the Future of U.S. Particle Physics: Snowmass on the Mississippi (CSS2013): Minneapolis, MN, USA, July 29-August 6, 2013* (2013). URL http://www.slac.stanford.edu/econf/C1307292/docs/IntensityFrontier/Neutrinos-12.pdf. 1310.4340.

10. Pasquini, P., Chuliá, S. C. & Valle, J. W. F. Neutrino oscillations from warped flavor symmetry: predictions for long baseline experiments T2K, NOvA and DUNE. *Phys. Rev.* **D95**, 095030 (2017). 1610.05962.

11. Chatterjee, S. S., Pasquini, P. & Valle, J. W. F. Probing atmospheric mixing and leptonic CP violation in current and future long baseline oscillation experiments. *Phys. Lett.* **B771**, 524–531 (2017). 1702.03160.

12. Chatterjee, S. S., Masud, M., Pasquini, P. & Valle, J. W. F. Cornering the revamped BMV model with neutrino oscillation data. *Phys. Lett.* **B774**, 179–182 (2017). 1708.03290.

13. Frampton, P. H., Kephart, T. W. & Matsuzaki, S. Simplified Renormalizable T-prime Model for Tribimaximal Mixing and Cabibbo Angle. *Phys. Rev.* **D78**, 073004 (2008). 0807.4713.

14. Pasquini, P. Reactor and atmospheric neutrino mixing angles' correlation as a probe for new physics. *Phys. Rev.* **D96**, 095021 (2017). 1708.04294.

15. Pasquini, P. Long-Baseline Oscillation Experiments as a Tool to Probe High Energy Flavor Symmetry Models. *Adv. High Energy Phys.* **2018**, 1825874 (2018). 1802.00821.

16. Ablikim, M. *et al.* Precision measurements of $B(D^+ \to \mu^+\nu_\mu)$, the pseudoscalar decay constant f_{D^+}, and the quark mixing matrix element $|V_{\rm cd}|$. *Phys. Rev.* **D89**,

051104 (2014). 1312.0374.

17. Abe, K. *et al.* Measurements of neutrino oscillation in appearance and disappearance channels by the T2K experiment with 6.6×10^{20} protons on target. *Phys. Rev.* **D91**, 072010 (2015). 1502.01550.

18. Abe, K. *et al.* Letter of Intent: The Hyper-Kamiokande Experiment — Detector Design and Physics Potential —. *arXiv* (2011). 1109.3262.

19. Ayres, D. S. *et al.* NOvA: Proposal to Build a 30 Kiloton Off-Axis Detector to Study $\nu_\mu \to \nu_e$ Oscillations in the NuMI Beamline (2004). hep-ex/0503053.

20. Acciarri, R. *et al.* Long-Baseline Neutrino Facility (LBNF) and Deep Underground Neutrino Experiment (DUNE) (2015). 1512.06148.

21. Lesgourgues, J. & Pastor, S. Massive neutrinos and cosmology. *Phys. Rept.* **429**, 307–379 (2006). astro-ph/0603494.

22. Roy Choudhury, S. & Choubey, S. Updated Bounds on Sum of Neutrino Masses in Various Cosmological Scenarios. *JCAP* **1809**, 017 (2018). 1806.10832.

23. Furry, W. H. On transition probabilities in double beta-disintegration. *Phys. Rev.* **56**, 1184–1193 (1939).

24. Cardani, L. Neutrinoless Double Beta Decay Overview (2018). 1810.12828.

25. Davidson, S., Nardi, E. & Nir, Y. Leptogenesis. *Phys. Rept.* **466**, 105–177 (2008). 0802.2962.

26. Gallo Rosso, A., Mascaretti, C., Palladino, A. & Vissani, F. Introduction to neutrino astronomy. *Eur. Phys. J. Plus* **133**, 267 (2018). 1806.06339.

27. Gonzalez, G. The Sun's Interior Metallicity Constrained by Neutrinos. *Mon. Not. Roy. Astron. Soc.* **370**, L90–L93 (2006). astro-ph/0605647.

28. Collaboration, S.-K. Latest visit: 26/02/2019. http://www-sk.icrr.u-tokyo.ac.

jp/sk/physics/solarnu-intro-e.html.

29. Donini, A., Palomares-Ruiz, S. & Salvado, J. Neutrino tomography of Earth. *Nature Phys.* **15**, 37–40 (2019). 1803.05901.

30. Lasserre, T. *et al.* SNIF: A Futuristic Neutrino Probe for Undeclared Nuclear Fission Reactors (2010). 1011.3850.

31. Christensen, E., Huber, P. & Jaffke, P. Antineutrino reactor safeguards - a case study (2013). 1312.1959.

32. Cribier, M. Neutrinos for Peace. *J. Phys. Conf. Ser.* **593**, 012004 (2015).

33. Anjos, J. C. *et al.* Using Neutrinos to Monitor Nuclear Reactors: the Angra Neutrino Experiment, Simulation and Detector Status. *Nucl. Part. Phys. Proc.* **267-269**, 108–115 (2015).

34. Alfonzo, J. A. M. *et al.* Neutrinos Angra experiment: commissioning and first operational measurements (2018). 1812.11604.

35. Kayser, B., Gibrat-Debu, F. & Perrier, F. The Physics of massive neutrinos. *World Sci. Lect. Notes Phys.* **25**, 1–117 (1989).

36. Giunti, C. & Kim, C. W. *Fundamentals of Neutrino Physics and Astrophysics* (Oxford, UK: Univ. Pr. (2007) 710 y 2007).

37. De Salas, P. F., Gariazzo, S., Mena, O., Ternes, C. A. & Tórtola, M. Neutrino Mass Ordering from Oscillations and Beyond: 2018 Status and Future Prospects. *Front. Astron. Space Sci.* **5**, 36 (2018). 1806.11051.

38. Aguilar-Arevalo, A. *et al.* Improved Measurement of the $\pi \to e\nu$ Branching Ratio. *Phys. Rev. Lett.* **115**, 071801 (2015). 1506.05845.

39. Cirigliano, V. & Rosell, I. Two-loop effective theory analysis of pi (K) —> e anti-nu/e [gamma] branching ratios. *Phys. Rev. Lett.* **99**, 231801 (2007). 0707.3439.

40. Aaboud, M. *et al.* Precision measurement and interpretation of inclusive W^+ , W^- and Z/γ^* production cross sections with the ATLAS detector. *Eur. Phys. J.* **C77**, 367 (2017). 1612.03016.

41. Pich, A. Precision Tau Physics. *Prog. Part. Nucl. Phys.* **75**, 41–85 (2014). 1310.7922.

42. Abulencia, A. *et al.* Measurements of inclusive W and Z cross sections in p anti-p collisions at s**(1/2) = 1.96-TeV. *J. Phys.* **G34**, 2457–2544 (2007). hep-ex/0508029.

43. Pontecorvo, B. Inverse beta processes and nonconservation of lepton charge. *Sov. Phys. JETP* **7**, 172–173 (1958). [Zh. Eksp. Teor. Fiz.34,247(1957)].

44. Maki, Z., Nakagawa, M. & Sakata, S. Remarks on the unified model of elementary particles. *Prog. Theor. Phys.* **28**, 870–880 (1962). [,34(1962)].

45. Fukuda, Y. *et al.* Evidence for oscillation of atmospheric neutrinos. *Phys. Rev. Lett.* **81**, 1562–1567 (1998). hep-ex/9807003.

46. Ahmad, Q. R. *et al.* Measurement of the rate of $\nu_e + d \rightarrow p + p + e^-$ interactions produced by ^8B solar neutrinos at the Sudbury Neutrino Observatory. *Phys. Rev. Lett.* **87**, 071301 (2001). nucl-ex/0106015.

47. Ahmad, Q. R. *et al.* Direct evidence for neutrino flavor transformation from neutral current interactions in the Sudbury Neutrino Observatory. *Phys. Rev. Lett.* **89**, 011301 (2002). nucl-ex/0204008.

48. Abe, S. *et al.* Precision Measurement of Neutrino Oscillation Parameters with KamLAND. *Phys. Rev. Lett.* **100**, 221803 (2008). 0801.4589.

49. Abe, Y. *et al.* Reactor electron antineutrino disappearance in the Double Chooz experiment. *Phys. Rev.* **D86**, 052008 (2012). 1207.6632.

50. Ahn, J. K. *et al.* Observation of Reactor Electron Antineutrino Disappearance in the RENO Experiment. *Phys. Rev. Lett.* **108**, 191802 (2012). 1204.0626.

51. Cohen-Tannoudji, B., C. Diu & F., L. *Quantum mechanics* (New York, Wiley 1991).

52. Jollet, C. The JUNO experiment. *Nuovo Cim.* **C39**, 318 (2017).

53. Particle data group, review of particle physics. *Phys. Rev. D* **98**, 030001 (2018). URL https://link.aps.org/doi/10.1103/PhysRevD.98.030001.

54. Kersten, J. & Smirnov, A. Yu. Decoherence and oscillations of supernova neutrinos. *Eur. Phys. J.* **C76**, 339 (2016). 1512.09068.

55. Kobach, A., Manohar, A. V. & McGreevy, J. Neutrino Oscillation Measurements Computed in Quantum Field Theory. *Phys. Lett.* **B783**, 59–75 (2018). 1711.07491.

56. Kayser, B. On the Quantum Mechanics of Neutrino Oscillation. *Phys. Rev.* **D24**, 110 (1981).

57. Nussinov, S. Solar Neutrinos and Neutrino Mixing. *Phys. Lett.* **63B**, 201–203 (1976).

58. Beuthe, M. Oscillations of neutrinos and mesons in quantum field theory. *Phys. Rept.* **375**, 105–218 (2003). hep-ph/0109119.

59. Grimus, W. & Stockinger, P. Real oscillations of virtual neutrinos. *Phys. Rev.* **D54**, 3414–3419 (1996). hep-ph/9603430.

60. Wolfenstein, L. Neutrino Oscillations in Matter. *Phys. Rev.* **D17**, 2369–2374 (1978). [,294(1977)].

61. Mikheyev, S. P. & Smirnov, A. Yu. Resonance Amplification of Oscillations in Matter and Spectroscopy of Solar Neutrinos. *Sov. J. Nucl. Phys.* **42**, 913–917 (1985). [,305(1986)].

62. Wolfenstein, L. Neutrino Oscillations and Stellar Collapse. *Phys. Rev.* **D20**, 2634–2635 (1979).

63. Mikheev, S. P. & Smirnov, A. Yu. Neutrino Oscillations in a Variable Density Medium and Neutrino Bursts Due to the Gravitational Collapse of Stars. *Sov. Phys.*

JETP **64**, 4–7 (1986). [,311(1986)], 0706.0454.

64. Langacker, P., Leveille, J. P. & Sheiman, J. On the Detection of Cosmological Neutrinos by Coherent Scattering. *Phys. Rev.* **D27**, 1228 (1983).

65. Parke, S. J. Nonadiabatic Level Crossing in Resonant Neutrino Oscillations. *Phys. Rev. Lett.* **57**, 1275–1278 (1986). [,328(1986)].

66. Nishi, C. C. Simple derivation of general Fierz-like identities. *Am. J. Phys.* **73**, 1160–1163 (2005). hep-ph/0412245.

67. Broncano, A., Gavela, M. B. & Jenkins, E. E. The Effective Lagrangian for the seesaw model of neutrino mass and leptogenesis. *Phys. Lett.* **B552**, 177–184 (2003). [Erratum: Phys. Lett.B636,332(2006)], hep-ph/0210271.

68. Linder, J. Derivation of neutrino matter potentials induced by earth. *Submitted to: Am. J. Phys.* (2005). hep-ph/0504264.

69. Gavela, M. B., Hernandez, D., Ota, T. & Winter, W. Large gauge invariant non-standard neutrino interactions. *Phys. Rev.* **D79**, 013007 (2009). 0809.3451.

70. Minakata, H., Sugiyama, H., Yasuda, O., Inoue, K. & Suekane, F. Reactor measurement of theta(13) and its complementarity to long baseline experiments. *Phys. Rev.* **D68**, 033017 (2003). [Erratum: Phys. Rev.D70,059901(2004)], hep-ph/0211111.

71. Duffy, K. Current Status and Future Plans of T2K. In *Proceedings, Prospects in Neutrino Physics (NuPhys2016): London, UK, December 12-14, 2016* (2017). URL https://inspirehep.net/record/1598133/files/arXiv:1705.01764.pdf. 1705.01764.

72. Childress, S. & Strait, J. Long baseline neutrino beams at Fermilab. *J. Phys. Conf. Ser.* **408**, 012007 (2013). 1304.4899.

73. Abe, K. *et al.* Physics potential of a long-baseline neutrino oscillation experiment using a J-PARC neutrino beam and Hyper-Kamiokande. *PTEP* **2015**, 053C02 (2015). 1502.05199.

74. Aoki, M., Hagiwara, K. & Okamura, N. Measuring the CP violating phase by a long baseline neutrino experiment with hyper-Kamiokande. *Phys. Lett.* **B554**, 121–132 (2003). hep-ph/0208223.

75. Gandhi, R., Ghoshal, P., Goswami, S., Mehta, P. & Sankar, S. U. Earth matter effects at very long baselines and the neutrino mass hierarchy. *Phys. Rev.* **D73**, 053001 (2006). hep-ph/0411252.

76. Nunokawa, H., Parke, S. J. & Zukanovich Funchal, R. Another possible way to determine the neutrino mass hierarchy. *Phys. Rev.* **D72**, 013009 (2005). hep-ph/0503283.

77. Aguilar-Arevalo, A. A. *et al.* A Search for electron neutrino appearance at the $\Delta m^2 \sim 1\text{eV}^2$ scale. *Phys. Rev. Lett.* **98**, 231801 (2007). 0704.1500.

78. Aartsen, M. G. *et al.* The IceCube Neutrino Observatory Part VI: Ice Properties, Reconstruction and Future Developments. In *Proceedings, 33rd International Cosmic Ray Conference (ICRC2013): Rio de Janeiro, Brazil, July 2-9, 2013* (2013). 1309.7010.

79. Beck, M. The KATRIN Experiment. *J. Phys. Conf. Ser.* **203**, 012097 (2010). 0910.4862.

80. Dell'Oro, S., Marcocci, S., Viel, M. & Vissani, F. Neutrinoless double beta decay: 2015 review. *Adv. High Energy Phys.* **2016**, 2162659 (2016). 1601.07512.

81. Choubey, S. *et al.* International Design Study for the Neutrino Factory, Interim Design Report (2011). 1112.2853.

82. Cao, J. *et al.* Muon-decay medium-baseline neutrino beam facility. *Phys. Rev. ST Accel. Beams* **17**, 090101 (2014). 1401.8125.

83. Abe, K. *et al.* Search for CP Violation in Neutrino and Antineutrino Oscillations by the T2K Experiment with 2.2×10^{21} Protons on Target. *Phys. Rev. Lett.* **121**, 171802 (2018). 1807.07891.

84. Bian, J. Results and Prospects from NOvA (2018). 1812.09585.

85. Nizam, M., Bharti, S., Prakash, S., Rahaman, U. & Uma Sankar, S. Tension between the latest T2K and NOνA data (2018). 1811.01210.

86. Abe, K. *et al.* Neutrino oscillation physics potential of the T2K experiment. *PTEP* **2015**, 043C01 (2015). 1409.7469.

87. Patterson, R. B. The NOvA Experiment: Status and Outlook (2012). [Nucl. Phys. Proc. Suppl.235-236,151(2013)], 1209.0716.

88. Agarwalla, S. K., Prakash, S., Raut, S. K. & Sankar, S. U. Potential of optimized NOvA for large $\theta_(13)$ & combined performance with a LArTPC & T2K. *JHEP* **12**, 075 (2012). 1208.3644.

89. Strait, J. *et al.* Long-Baseline Neutrino Facility (LBNF) and Deep Underground Neutrino Experiment (DUNE) (2016). 1601.05823.

90. Acciarri, R. *et al.* Long-Baseline Neutrino Facility (LBNF) and Deep Underground Neutrino Experiment (DUNE) (2016). 1601.05471.

91. Acciarri, R. *et al.* Long-Baseline Neutrino Facility (LBNF) and Deep Underground Neutrino Experiment (DUNE) (2016). 1601.02984.

92. Alion, T. *et al.* Experiment Simulation Configurations Used in DUNE CDR (2016). 1606.09550.

93. Bilenky, S. M., Hosek, J. & Petcov, S. T. On Oscillations of Neutrinos with Dirac and Majorana Masses. *Phys. Lett.* **94B**, 495–498 (1980).

94. Abada, A., Biggio, C., Bonnet, F., Gavela, M. B. & Hambye, T. Low energy effects of neutrino masses. *JHEP* **12**, 061 (2007). 0707.4058.

95. Malinsky, M., Ohlsson, T. & Zhang, H. Non-Standard Neutrino Interactions from a Triplet Seesaw Model. *Phys. Rev.* **D79**, 011301 (2009). 0811.3346.

96. Gonzalez-Garcia, M. C. *et al.* Atmospheric neutrino observations and flavor changing interactions. *Phys. Rev. Lett.* **82**, 3202–3205 (1999). hep-ph/9809531.

97. Ohlsson, T. Status of non-standard neutrino interactions. *Rept. Prog. Phys.* **76**, 044201 (2013). 1209.2710.

98. Farzan, Y. & Tortola, M. Neutrino oscillations and Non-Standard Interactions. *Front.in Phys.* **6**, 10 (2018). 1710.09360.

99. Falkowski, A., González-Alonso, M. & Tabrizi, Z. Reactor neutrino oscillations as constraints on Effective Field Theory (2019). 1901.04553.

100. Guzzo, M. *et al.* Status of a hybrid three neutrino interpretation of neutrino data. *Nucl. Phys.* **B629**, 479–490 (2002). hep-ph/0112310.

101. Fornengo, N., Maltoni, M., Tomas, R. & Valle, J. W. F. Probing neutrino nonstandard interactions with atmospheric neutrino data. *Phys. Rev.* **D65**, 013010 (2002). hep-ph/0108043.

102. Berezhiani, Z. & Rossi, A. Limits on the nonstandard interactions of neutrinos from e+ e- colliders. *Phys. Lett.* **B535**, 207–218 (2002). hep-ph/0111137.

103. Huber, P., Schwetz, T. & Valle, J. W. F. Confusing nonstandard neutrino interactions with oscillations at a neutrino factory. *Phys. Rev.* **D66**, 013006 (2002). hep-ph/0202048.

104. Barranco, J., Miranda, O. G. & Rashba, T. I. Probing new physics with coherent neutrino scattering off nuclei. *JHEP* **12**, 021 (2005). hep-ph/0508299.

105. Kopp, J., Lindner, M., Ota, T. & Sato, J. Non-standard neutrino interactions in reactor and superbeam experiments. *Phys. Rev.* **D77**, 013007 (2008). 0708.0152.

106. Huitu, K., Karkkainen, T. J., Maalampi, J. & Vihonen, S. Effects of triplet Higgs bosons in long baseline neutrino experiments. *Phys. Rev.* **D97**, 095037 (2018). 1711.02971.

107. Coloma, P. Non-Standard Interactions in propagation at the Deep Underground Neutrino Experiment. *JHEP* **03**, 016 (2016). 1511.06357.

108. Ge, S.-F. & Parke, S. J. Scalar Non-Standard Interactions in Neutrino Oscillation (2018). 1812.08376.

109. Schael, S. *et al.* Precision electroweak measurements on the Z resonance. *Phys. Rept.* **427**, 257–454 (2006). hep-ex/0509008.

110. Mention, G. *et al.* The Reactor Antineutrino Anomaly. *Phys. Rev.* **D83**, 073006 (2011). 1101.2755.

111. Giunti, C. & Laveder, M. Statistical Significance of the Gallium Anomaly. *Phys. Rev.* **C83**, 065504 (2011). 1006.3244.

112. Anselmann, P. *et al.* First results from the Cr-51 neutrino source experiment with the GALLEX detector. *Phys. Lett.* **B342**, 440–450 (1995).

113. Abdurashitov, J. N. *et al.* Measurement of the response of a Ga solar neutrino experiment to neutrinos from an Ar-37 source. *Phys. Rev.* **C73**, 045805 (2006). nucl-ex/0512041.

114. Aguilar-Arevalo, A. *et al.* Evidence for neutrino oscillations from the observation of anti-neutrino(electron) appearance in a anti-neutrino(muon) beam. *Phys. Rev.* **D64**, 112007 (2001). hep-ex/0104049.

115. Dentler, M. *et al.* Updated Global Analysis of Neutrino Oscillations in the Presence of eV-Scale Sterile Neutrinos. *JHEP* **08**, 010 (2018). 1803.10661.

116. Schechter, J. & Valle, J. W. F. Neutrino Masses in SU(2) x U(1) Theories. *Phys. Rev.* **D22**, 2227 (1980).

117. Escrihuela, F. J., Forero, D. V., Miranda, O. G., Tórtola, M. & Valle, J. W. F. Probing CP violation with non-unitary mixing in long-baseline neutrino oscillation experiments: DUNE as a case study. *New J. Phys.* **19**, 093005 (2017). 1612.07377.

118. Blennow, M., Coloma, P., Fernandez-Martinez, E., Hernandez-Garcia, J. & Lopez-Pavon, J. Non-Unitarity, sterile neutrinos, and Non-Standard neutrino Interactions. *JHEP* **04**, 153 (2017). 1609.08637.

119. Fong, C. S., Minakata, H. & Nunokawa, H. Non-unitary evolution of neutrinos in matter and the leptonic unitarity test. *JHEP* **02**, 015 (2019). 1712.02798.

120. Escrihuela, F. J., Forero, D. V., Miranda, O. G., Tortola, M. & Valle, J. W. F. On the description of nonunitary neutrino mixing. *Phys. Rev.* **D92**, 053009 (2015). [Erratum: Phys. Rev.D93,no.11,119905(2016)], 1503.08879.

121. Astier, P. *et al.* Search for nu(mu) —> nu(e) oscillations in the NOMAD experiment. *Phys. Lett.* **B570**, 19–31 (2003). hep-ex/0306037.

122. Ge., S.-F. Nupro: a simulation package for neutrino properties. https://nupro.hepforge.org/.

123. Chikashige, Y., Mohapatra, R. N. & Peccei, R. D. Are There Real Goldstone Bosons Associated with Broken Lepton Number? *Phys. Lett.* **98B**, 265–268 (1981).

124. Higgs, P. W. Broken symmetries, massless particles and gauge fields. *Phys. Lett.* **12**, 132–133 (1964).

125. Nambu, Y. Axial vector current conservation in weak interactions. *Phys. Rev. Lett.* **4**, 380–382 (1960). [,107(1960)].

126. Anderson, P. W. Plasmons, Gauge Invariance, and Mass. *Phys. Rev.* **130**, 439–442 (1963). [,153(1963)].

127. Peccei, R. D. & Quinn, H. R. CP Conservation in the Presence of Instantons. *Phys. Rev. Lett.* **38**, 1440–1443 (1977). [,328(1977)].

128. Peccei, R. D. & Quinn, H. R. Constraints Imposed by CP Conservation in the Presence of Instantons. *Phys. Rev.* **D16**, 1791–1797 (1977).

129. Barger, V. D., Keung, W.-Y. & Pakvasa, S. Majoron Emission by Neutrinos. *Phys.*

Rev. **D25**, 907 (1982).

130. Britton, D. I. *et al.* Measurement of the pi+ —> e+ neutrino branching ratio. *Phys. Rev. Lett.* **68**, 3000–3003 (1992).

131. Cirigliano, V., Ecker, G., Neufeld, H., Pich, A. & Portoles, J. Kaon Decays in the Standard Model. *Rev. Mod. Phys.* **84**, 399 (2012). 1107.6001.

132. Marciano, W. J. & Sirlin, A. Radiative corrections to pi(lepton 2) decays. *Phys. Rev. Lett.* **71**, 3629–3632 (1993).

133. Cirigliano, V. & Rosell, I. pi/K —> e anti-nu(e) branching ratios to O(e**2 p**4) in Chiral Perturbation Theory. *JHEP* **10**, 005 (2007). 0707.4464.

134. Lessa, A. P. & Peres, O. L. G. Revising limits on neutrino-Majoron couplings. *Phys. Rev.* **D75**, 094001 (2007). hep-ph/0701068.

135. Weinberg, S. A New Light Boson? *Phys. Rev. Lett.* **40**, 223–226 (1978).

136. Gu, P.-H., Ma, E. & Sarkar, U. Pseudo-Majoron as Dark Matter. *Phys. Lett.* **B690**, 145–148 (2010). 1004.1919.

137. Shin, M. Light Neutrino Masses and Strong CP Problem. *Phys. Rev. Lett.* **59**, 2515 (1987). [Erratum: Phys. Rev. Lett.60,383(1988)].

138. Dine, M., Fischler, W. & Srednicki, M. A Simple Solution to the Strong CP Problem with a Harmless Axion. *Phys. Lett.* **104B**, 199–202 (1981).

139. Kim, J. E. Weak Interaction Singlet and Strong CP Invariance. *Phys. Rev. Lett.* **43**, 103 (1979).

140. Chikashige, Y., Gelmini, G., Peccei, R. D. & Roncadelli, M. Horizontal Symmetries, Dynamical Symmetry Breaking and Neutrino Masses. *Phys. Lett.* **94B**, 499–504 (1980).

141. Atre, A., Han, T., Pascoli, S. & Zhang, B. The Search for Heavy Majorana Neutrinos.

JHEP **05**, 030 (2009). 0901.3589.

142. Britton, D. I. *et al.* Improved search for massive neutrinos in pi+ —> e+ neutrino decay. *Phys. Rev.* **D46**, R885–R887 (1992).

143. Shrock, R. E. New Tests For, and Bounds On, Neutrino Masses and Lepton Mixing. *Phys. Lett.* **96B**, 159–164 (1980).

144. Bernardi, G. *et al.* FURTHER LIMITS ON HEAVY NEUTRINO COUPLINGS. *Phys. Lett.* **B203**, 332–334 (1988).

145. Albert, J. B. *et al.* Search for Majoron-emitting modes of double-beta decay of ^{136}Xe with EXO-200. *Phys. Rev.* **D90**, 092004 (2014). 1409.6829.

146. Agarwalla, S. K., Prakash, S. & Sankar, S. U. Resolving the octant of theta23 with T2K and NOvA. *JHEP* **07**, 131 (2013). 1301.2574.

147. Agarwalla, S. K., Prakash, S. & Uma Sankar, S. Exploring the three flavor effects with future superbeams using liquid argon detectors. *JHEP* **03**, 087 (2014). 1304.3251.

148. Chatterjee, A., Ghoshal, P., Goswami, S. & Raut, S. K. Octant sensitivity for large theta(13) in atmospheric and long baseline neutrino experiments. *JHEP* **06**, 010 (2013). 1302.1370.

149. Bass, M. *et al.* Baseline Optimization for the Measurement of CP Violation, Mass Hierarchy, and θ_{23} Octant in a Long-Baseline Neutrino Oscillation Experiment. *Phys. Rev.* **D91**, 052015 (2015). 1311.0212.

150. Bora, K., Dutta, D. & Ghoshal, P. Determining the octant of θ_{23} at LBNE in conjunction with reactor experiments. *Mod. Phys. Lett.* **A30**, 1550066 (2015). 1405.7482.

151. Das, C. R., Maalampi, J., Pulido, J. a. & Vihonen, S. Determination of the θ_{23} octant in LBNO. *JHEP* **02**, 048 (2015). 1411.2829.

152. Nath, N., Ghosh, M. & Goswami, S. The physics of antineutrinos in DUNE and determination of octant and δ_{CP}. *Nucl. Phys.* **B913**, 381–404 (2016). 1511.07496.

153. Agarwalla, S. K., Chatterjee, S. S. & Palazzo, A. Degeneracy between θ_{23} octant and neutrino non-standard interactions at DUNE. *Phys. Lett.* **B762**, 64–71 (2016). 1607.01745.

154. Miranda, O. G., Tortola, M. & Valle, J. W. F. New ambiguity in probing CP violation in neutrino oscillations. *Phys. Rev. Lett.* **117**, 061804 (2016). 1604.05690.

155. Dutta, D., Ghoshal, P. & Sehrawat, S. K. Octant of θ_{23} at long baseline neutrino experiments in the light of Non Unitary Leptonic mixing. *Phys. Rev.* **D95**, 095007 (2017). 1610.07203.

156. Agarwalla, S. K., Chatterjee, S. S. & Palazzo, A. Octant of θ_{23} in danger with a light sterile neutrino. *Phys. Rev. Lett.* **118**, 031804 (2017). 1605.04299.

157. Kosmas, T. S., Papoulias, D. K., Tortola, M. & Valle, J. W. F. Probing light sterile neutrino signatures at reactor and Spallation Neutron Source neutrino experiments. *Phys. Rev.* **D96**, 063013 (2017). 1703.00054.

158. Cabrera, A. Double chooz (new multi-detector results), ep seminar. indico.cern.ch/event/548805/attachments/1336343/2017513/DCIVCERN_REF_Anatael_16Sept.pdf.

159. Choi, J. H. *et al.* Observation of Energy and Baseline Dependent Reactor Antineutrino Disappearance in the RENO Experiment. *Phys. Rev. Lett.* **116**, 211801 (2016). 1511.05849.

160. An, F. P. *et al.* Measurement of electron antineutrino oscillation based on 1230 days of operation of the Daya Bay experiment. *Phys. Rev.* **D95**, 072006 (2017). 1610.04802.

161. Akhmedov, E. K., Johansson, R., Lindner, M., Ohlsson, T. & Schwetz, T. Series expansions for three flavor neutrino oscillation probabilities in matter. *JHEP* **04**, 078 (2004). hep-ph/0402175.

162. Szelc, A. M. Developing LAr Scintillation Light Collection Ideas in the Short Baseline Neutrino Detector. *JINST* **11**, C02018 (2016).

163. Majorana, E. Teoria simmetrica dell'elettrone e del positrone. *Nuovo Cim.* **14**, 171–184 (1937).

164. Weinberg, S. Baryon and Lepton Nonconserving Processes. *Phys. Rev. Lett.* **43**, 1566–1570 (1979).

165. Chen, P., Ding, G.-J., Rojas, A. D., Vaquera-Araujo, C. A. & Valle, J. W. F. Warped flavor symmetry predictions for neutrino physics. *JHEP* **01**, 007 (2016). 1509.06683.

166. Cacciapaglia, G., Csaki, C., Marandella, G. & Terning, J. The Gaugephobic Higgs. *JHEP* **02**, 036 (2007). hep-ph/0611358.

167. Huber, P., Lindner, M. & Winter, W. Simulation of long-baseline neutrino oscillation experiments with GLoBES (General Long Baseline Experiment Simulator). *Comput. Phys. Commun.* **167**, 195 (2005). hep-ph/0407333.

168. Babu, K. S., Ma, E. & Valle, J. W. F. Underlying A(4) symmetry for the neutrino mass matrix and the quark mixing matrix. *Phys. Lett.* **B552**, 207–213 (2003). hep-ph/0206292.

169. Morisi, S., Forero, D. V., Romão, J. C. & Valle, J. W. F. Neutrino mixing with revamped A_4 flavor symmetry. *Phys. Rev.* **D88**, 016003 (2013). 1305.6774.

170. Ky, N. A., Quang Van, P. & Hong Van, N. T. A neutrino mixing model based on an $A_4 \times Z_3 \times Z_4$ flavour symmetry. *Phys. Rev.* **D94**, 095009 (2016). 1610.00304.

171. Dinh, D. N., Ky, N. A., Van, P. Q. & Van, N. T. H. A see-saw scenario of an A_4 flavour symmetric standard model (2016). 1602.07437.

172. Li, G.-N. & He, X.-G. CP violation in neutrino mixing with $\delta = -\pi/2$ in A_4 Type-II seesaw model. *Phys. Lett.* **B750**, 620–626 (2015). 1505.01932.

173. Cárcamo Hernéndez, A. E., Kovalenko, S., Valle, J. W. F. & Vaquera-Araujo, C. A.

Predictive Pati-Salam theory of fermion masses and mixing. *JHEP* **07**, 118 (2017). 1705.06320.

174. Chao, W. & Zheng, Y.-j. Relatively Large Theta13 from Modification to the Tri-bimaximal, Bimaximal and Democratic Neutrino Mixing Matrices. *JHEP* **02**, 044 (2013). 1107.0738.

175. Seo, S.-H. Short-baseline reactor neutrino oscillations. *PoS* **NOW2016**, 002 (2017). 1701.06843.

176. Aoki, S. *et al.* Review of lattice results concerning low-energy particle physics. *Eur. Phys. J.* **C74**, 2890 (2014). 1310.8555.

177. Britton, D. I. *et al.* Measurement of the $\pi^+ \to e^+$ neutrino branching ratio. *Phys. Rev.* **D49**, 28–39 (1994).

178. Hardy, J. C. & Towner, I. S. Superallowed beta decay of nuclei with A greater than or equal to 62: The Limiting effect of weak Gamow-Teller branches. *Phys. Rev. Lett.* **88**, 252501 (2002). nucl-th/0308005.

179. Li, H.-B. Recent results on charm physics at BESIII (2012). [Nucl. Phys. Proc. Suppl.233,185(2012)], 1209.3059.

180. Lees, J. P. *et al.* Measurement of the Branching Fraction for $D_s^+ \to \tau^+\nu_\tau$ and Extraction of the Decay Constant f_{D_s} (2010). 1003.3063.

181. White, R. M. Recent charm physics results from BaBar. *J. Phys. Conf. Ser.* **347**, 012026 (2012).

182. Zupanc, A. *et al.* Measurements of branching fractions of leptonic and hadronic D_s^+ meson decays and extraction of the D_s^+ meson decay constant. *JHEP* **09**, 139 (2013). 1307.6240.

183. Adachi, I. *et al.* Evidence for $B^- \to \tau^- \bar{\nu}_\tau$ with a Hadronic Tagging Method Using the Full Data Sample of Belle. *Phys. Rev. Lett.* **110**, 131801 (2013). 1208.4678.

184. Machado, A. C. B., Montaño, J., Pasquini, P. & Pleitez, V. Analytical solution for the Zee mechanism (2017). 1707.06977.

185. Jurkovich, H., Ferreira, C. P. & Pasquini, P. Shadowing Neutrino Mass Hierarchy with Lorentz Invariance Violation (2018). 1806.08752.

186. Machado, A. C. B., Pasquini, P. & Pleitez, V. Zee and Zee-Babu mechanisms in the minimal 331 model (2018). 1810.02817.

Appendix A

Appendix

A.1 Convenient decomposition of Non-Unitary matrix

In this Appendix we will prove the possibility of decomposition in Eq. 4.30, that is, for an $n \times n$ unitary matrix, one can define,

$$U_{n\times n} = \begin{pmatrix} A & W \\ S & T \end{pmatrix} \tag{A.1}$$

where $A = A^{NP}.U_{\text{PMNS}}$, with

$$A^{NP} = \begin{pmatrix} \alpha_{11} & 0 & 0 \\ \alpha_{21} & \alpha_{22} & 0 \\ \alpha_{31} & \alpha_{32} & \alpha_{33} \end{pmatrix}. \tag{A.2}$$

It is well known that a general complex $n \times n$ matrix U has n^2 complex parameters. If we impose an unitary condition, that is $U.U^\dagger = \mathbb{I}$, than the number of parameters drops to n^2 real parameters, those of which, $n(n-1)/2$ are angles and $n(n+1)/2$ are phases*. It is possible to parametrize such a matrix by a product of several rotation matrix around

*Notice that not all phases are physical

an axis. If we define,

$$(\omega_{ij})_{\alpha\beta} = \delta_{\alpha\beta}\sqrt{1-(\delta_{\alpha i}+\delta_{\alpha j})\sin^2\theta_{ij}} + \sin\theta_{ij}e^{-i\phi_{ij}}\delta_{\alpha i}\delta_{\beta j} - \sin\theta_{ij}e^{i\phi_{ij}}\delta_{\alpha j}\delta_{\beta i}. \tag{A.3}$$

Notice that an $\omega_{ij}.\omega_{ij}^{\dagger} = \mathbb{I}$. An $n \times n$ unitary matrix can be written as,

$$U_{n\times n} = \prod_{i<j}^{i,j=n} \omega_{ij}. \tag{A.4}$$

Since not all ω_{ij} commutes between each other, the order of the product is important, in fact, it defines a parametrization of $U_{n\times n}$. If $n = 3$ the PDG [53] uses:

$$U_{\text{PMNS}} = \omega_{23}.\omega_{13}.\omega_{12}, \tag{A.5}$$

where $\delta_{\text{CP}} = -\phi_{12} + \phi_{13} - \phi_{23}$.

If $n > 3$, the $U_{n\times n}$ matrix can be denoted as in Eq. A.1. A is a 3×3 matrix that relates only the S3νO neutrinos and is the only accessible part of the mixing matrix through oscillation experiments, hence, it is the origin of the *non-unitary* effect in the oscillation probability. In [120] it was presented a convenient order of the product in Eq. A.4,

$$U_{n\times n} = \left(\prod_{i,j>3}^{i,j=n} \omega_{ij}\right)\left(\omega_{3n-1}\omega_{2n-1}\omega_{1n-1}\cdots\omega_{34}\omega_{24}\omega_{14}\right).\left(\omega_{23}.\omega_{13}.\omega_{12}\right). \tag{A.6}$$

$\left(\prod_{i,j>3}^{i,j=n}\omega_{ij}\right)$ is a rotation of the heavy states and commutes (and does not change) with the 3×3 part. $(\omega_{23}.\omega_{13}.\omega_{12})$ is the usual definition of the PMNS matrix, it couples only the S3νO neutrinos,

$$\omega_{23}.\omega_{13}.\omega_{12} = \begin{pmatrix} U_{\text{PMNS}} & 0 \\ 0 & \mathbb{I} \end{pmatrix} \tag{A.7}$$

Finaly, the product $(\omega_{3n-1}\omega_{2n-1}\omega_{1n-1}\cdots\omega_{34}\omega_{24}\omega_{14})$ is the non-unitary part and has the triangular form of Eq. 4.31 in its 3×3 part. To see that, we first note that the multiplication of a triangular matrix is still triangular. Then, we notice that the product $\omega_{3j}\omega_{2j}\omega_{1j}$

has a general form,

$$\omega_{3j}\omega_{2j}\omega_{1j} = \begin{pmatrix} \alpha_j & \beta_j \\ \\ \gamma_j & \delta_j \end{pmatrix}. \tag{A.8}$$

where

$$\begin{aligned} (\beta_j)_{ab} =& \delta_{jb} \sum_{i=1}^{3} (\alpha_j)_{aj} \delta_{ia} \\ (\gamma_j)_{ab} =& \delta_{ja} \sum_{i=1}^{3} (\alpha_j)_{jb} \delta_{ib} \\ (\delta_j)_{ab} =& \delta_{ab}\delta_{ja}(\alpha_j)_{jj} \end{aligned} \tag{A.9}$$

and α_j is a lower-triangular matrix. The property,

$$\beta_k . \left(\prod_{j>n1}^{n_2} \delta_j \right) . \gamma_{n_1} = 0$$

with $k > n_2$, shows that

$$(\omega_{3n-1}\omega_{2n-1}\omega_{1n-1} \cdots \omega_{34}\omega_{24}\omega_{14}) = \begin{pmatrix} \prod_{j=4}^{n} \alpha_j & Q_1 \\ \\ Q_2 & Q_3 \end{pmatrix}. \tag{A.10}$$

where Q_i are complecated (but uninteresting) combinations of the matrices $\beta_i, \gamma_i, \delta_i$ and the 3×3 part $(\prod_{j=4}^{n} \alpha_j)$ is lower-triangular. This completes the proof.

A.2 Meson Decay: Prediction versus Measurement

A.2.1 Meson Decay - SM Theoretical Prediction

At tree level, the standard model prediction for the decays are well known and are easily calculated by Eq. (A.11),

$$\Gamma_{l\nu} = \frac{G_F^2 f_P^2 |V_{qq'}|^2 m_p^3}{4\pi} \alpha^2 (1-\alpha)^2 \tag{A.11}$$

where $\alpha = \frac{m_l^2}{m_P^2}$. The fact that $\Gamma_{l\nu} \to 0$ when $\alpha \to 0$ is a reflex of the fact that this reaction is chiral suppressed, ie it can't happen when the lepton is massless due to the fact that it does not conserves chirality. This means that the lower the lepton mass, the lower is the branching fraction, that is why there are no experimental results on electronic branching fraction coming from high mass mesons (one example is the D_s meson which is expected to have the proportion of decays $e : \mu : \tau$ as $10^{-5} : 1 : 10$) and only tauonic on the B mesons case. This difficulty of measuring the decay rates gives rise to big experimental uncertainties (it can reach up to 27% on B decays) and no radiative corrections are needed in almost any case. That is not true for pion and kaon that is very well measured (up to 0.44%) and radiative corrections must be taken into account.

Such corrections were calculated very precisely (up to two loop order) by [132, 39] and are of the form,

$$\begin{aligned} \Gamma\left(P \to l\nu(\gamma)\right) = \Gamma^{(0)} S_{EW} \left[1 + \frac{\alpha_{el}}{\pi} F(\alpha)\right] \\ \times \left\{1 - \frac{\alpha_{el}}{\pi}\left[\frac{3}{2}\log\frac{M_\rho}{M_P} + c_1^{(P)} - \frac{M_P^2}{M_\rho^2}\tilde{c}_2^{(P)}\log\frac{M_\rho^2}{m_l^2} + \right.\right. \\ \left.\left. + \frac{m_l^2}{M_\rho^2}\left(c_2^{(P)}\log\frac{M_\rho^2}{m_l} + c_3^{(P)} + c_4^{(P)}\frac{m_l}{M_P}\right)\right]\right\} \end{aligned} \tag{A.12}$$

where,

$$S_{EW} = \left[1 + \frac{2\alpha_{el}}{\pi}\log\left(\frac{m_z}{m_\rho}\right)\right] \tag{A.13}$$

and is related to the first order correction to the Z boson propagator, also,

$$F(x) = 3\log(x) + \frac{13 - 19x^2}{8(1-x^2)} - \frac{8 - 5x^2}{2(1-x^2)^2}x^2\log(x)$$
$$-2\left(\frac{1+x^2}{1-x^2}\log(x) + 1\right)\log(1-x^2) + 2\frac{1+x^2}{1-x^2}\int_0^x \frac{\log(1-t)}{t}dt \qquad \text{(A.14)}$$

and α_{el} is the electromagnetic constant, this correction is related to the universal long-distance correction for a point-like meson to lepton and neutrinos. The coefficients c_i are structure dependent and are presented on table A.1 taken from reference [131].

	π	Kaon
c_1	-2.4 ± 0.5	-1.9 ± 0.5
$\tilde{c}_2$	0	$(7.84 \pm 0.07) \times 10^{-2}$
c_2	$5.2 \pm 0.4 \pm 0.01$	$4.3 \pm 0.4 \pm 0.01$
c_3	$-10.5 \pm 2.3 \pm 0.53$	$-4.73 \pm 2.3 \pm 0.28$
c_4	1.69 ± 0.07	0.22 ± 0.01

Table A.1 – Values of the $c_i^{(P)}$ constants of the corrections for Pion and Kaon decay rates [131].

The corrections on the curly brackets on Eq. (A.12) comes from short-distance calculations [131, 39] that is connected to long-distance using a somewhat arbitrary [132] mass scale $M_\rho \approx 0.768\text{GeV}$.

An important parameter for the prediction of the decay rate comes from the mesonic form factor f_p. Again the experimental determination of this factors rely on precise knowledge of the CKM matrix, moreover, sometimes those matrix elements are calculated using theoretical predictions from Lattice QCD due to the lack of enough experiments to confront with theory. In this work, we will assume the predictions of lattice QCD to be true within the errors and use it to obtain the CKM matrix elements and limits on the $|g_e|^2$ constants. The data presented on table A.2 summarizes the form factors from the reference [176]

	f_P[MeV]
π	130.2(1.4)
K	156.3(0.9)
D	209(3.3)
D_s	250(7)
B	186(4)

Table A.2 – Form Factors f_p from Lattice QCD.

Using all corrections and the form factors obtained via lattice QCD it is possible to calculate the standard model predictions to each of the decays, the results confronting the experimental and theoretical are presented on table A.3.

	Γ_{exp}[MeV]	Γ_{Theo}[MeV]
$\pi \to e\nu(\gamma)$	$(3.1104 \pm 0.0010) \times 10^{-18}$	$(3.048 \pm 0.066) \times 10^{-18}$
$\pi \to \mu\nu(\gamma)$	$(2.52851 \pm 0.00051) \times 10^{-14}$	$(2.477 \pm 0.053) \times 10^{-14}$
$K \to e\nu(\gamma)$	$(8.4072 \pm 0.045) \times 10^{-19}$	$(8.224 \pm 0.45) \times 10^{-19}$
$K \to \mu\nu(\gamma)$	$(3.3794 \pm 0.0086) \times 10^{-14}$	$(3.391 \pm 0.066) \times 10^{-14}$
$D \to \mu\nu$	$(2.35 \pm 0.13) \times 10^{-13}$	$(2.49 \pm 0.19) \times 10^{-13}$
$D_s \to \mu\nu$	$(6.99 \pm 0.47) \times 10^{-12}$	$(7.12 \pm 0.42) \times 10^{-12}$
$D_s \to \tau\nu$	$(7.5 \pm 0.5) \times 10^{-11}$	$(7.0 \pm 0.4) \times 10^{-11}$
$B \to \tau\nu$	$(3.9 \pm 1.0) \times 10^{-14}$	$(3.0 \pm 0.5) \times 10^{-14}$

Table A.3 – Experimental versus theoretical predictions of the SM.

A.2.2 Meson Decay - Experimental Data

The decay data comes from two different sources, the first is the low mass mesons (π and k) decay data that is obtained from mesonic beans that come from accelerators [177]. Although it has a very good resolution ($\Delta\Gamma/\Gamma_{\text{Tot}} \lesssim 0.44\%$) it can't distinguish the decays $\Gamma(P \to l\nu)$ from $\Gamma(P \to l\nu\gamma)$ very well [53], so both decays are always included in the data and also into the theoretical predictions. The PDG gives the

results [53],

$$\begin{aligned}
\Gamma^{(\mathrm{Exp})}(\pi \to e\nu(\gamma)) &= (3.1104 \pm 0.0010) \times 10^{-18}\mathrm{MeV} \\
\Gamma^{(\mathrm{Exp})}(\pi \to \mu\nu(\gamma)) &= (2.52851 \pm 0.00051) \times 10^{-14}\mathrm{MeV} \\
\Gamma^{(\mathrm{Exp})}(K \to e\nu(\gamma)) &= (8.4072 \pm 0.045) \times 10^{-19}\mathrm{MeV} \\
\Gamma^{(\mathrm{Exp})}(K \to \mu\nu(\gamma)) &= (3.3794 \pm 0.0086) \times 10^{-14}\mathrm{MeV}
\end{aligned} \tag{A.15}$$

There are two CKM matrix elements relevant to these decays, V_{ud} that comes from the super allowed $0^+ \to 0^+$ beta decay [178] $V_{ud} = 0.97425(22)$ and is precisely measured. The other matrix element is not so precisely known, also, the most precise measurement comes exactly from the kaon leptonic or semi-leptonic decay [53] and has a value of $V_{us} = 0.2253(8)$. The main problem with this result is that it is fitted assumed that any possible corrections to the SM are small enough to be ignored. As we shall see, it is not necessarily true at the precision required.

The experimental data that comes from high mass mesons are obtained mostly from accelerator collisions. So that the resulting particles always come with their anti-particle and the energy and momentum of the particle can be measured precisely, allowing what is called tagging[†]. The tagging of the meson allows to constraint the missing energy of the decay to be approximately zero (the neutrino mass). Actually, the energy resolution of the detector allows only to cut missing energy greater than $M^2_{\mathrm{miss}} \gtrsim 0.2\mathrm{GeV}^2$, as can be seen from the picture took from Ref. [16], fig. A.1. In this figure, it can be seen the cut made on the missing energy, denoted by the red arrows.

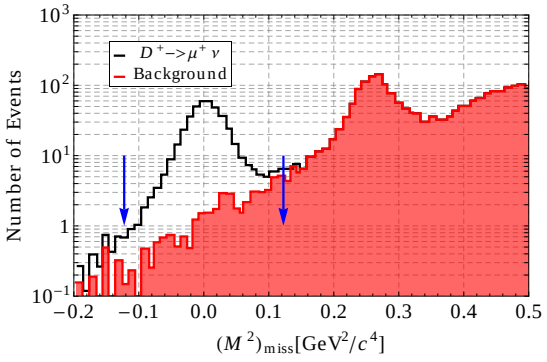

Figure A.1 – The M^2_{miss} distribution for selected single μ^+ candidates, the **Black** histogram is for Monte Carlo simulated signal events of $D^+ \to \mu^+\nu_\mu$ decays, the Red hatched histograms represents the total backgrounds and the Blue Arrows represent the kinematic cut [16].

[†]See for example [16].

This implies that any corrections of possible three body decay mimicking a twobody decay can only be made up to a $M_{\text{miss}} \lesssim 350\text{MeV}$. The experimental data is of the form [179, 180, 181, 182, 183]

$$\begin{aligned}
\Gamma^{(\text{Exp})}(D \to \mu\nu) &= (2.35 \pm 0.13) \times 10^{-13}\text{MeV} \\
\Gamma^{(\text{Exp})}(D_s \to \mu\nu) &= (6.99 \pm 0.47) \times 10^{-12}\text{MeV} \\
\Gamma^{(\text{Exp})}(D_s \to \tau\nu) &= (7.5 \pm 0.5) \times 10^{-11}\text{MeV} \\
\Gamma^{(\text{Exp})}(B \to \tau\nu) &= (3.9 \pm 1.0) \times 10^{-14}\text{MeV}
\end{aligned} \tag{A.16}$$

The three corresponding CKM elements have the same difficulty as the ones from kaon, the measurement are always related to decays, and the uncertainties to the form factors gives rise to theoretical errors as well [53] The PDG values are $|V_{cd}| = 0.225(8)$, $|V_{us}| = 0.986(16)$. In this analysis we will assume unitarity of the CKM matrix and use $|V_{ub}|^2 = 1 - |V_{ud}|^2 - |V_{us}|^2$ so that we will have fewer free parameters.

Appendix B

Attachments

B.1 Scientific Publication

In this attachment, we present a summary of all the scientific production resulted from all the work done during the Ph.D. of the student. We will divide it into three sections, the Published Papers in scientific journals (9). The submitted manuscripts to scientific journals (3) and ongoing works. Notice that this thesis contains a description of works that were already published. In Fig. B.1 we show a fluxogram that organizes the published papers by subject area.

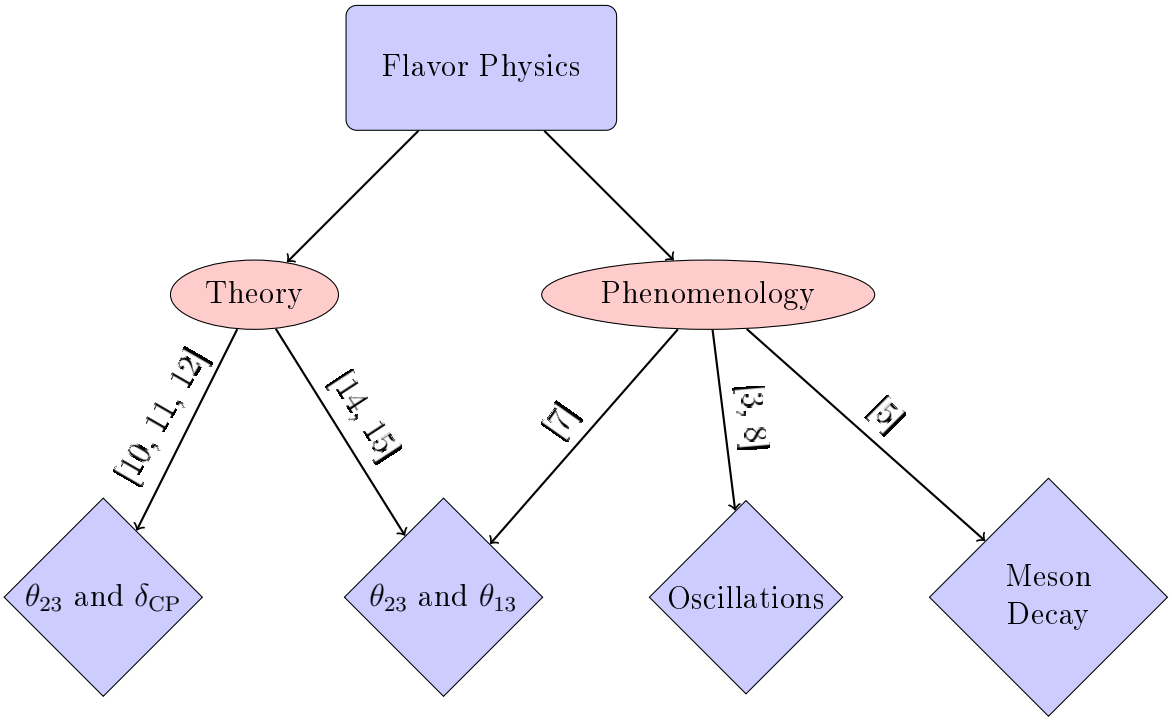

Figure B.1 – Fluxogram representing each of the areas for the published papers as a result of the work done during this thesis.

B.1.1 Published Papers

Below we present in chronological order the published papers in scientific journals and a small description of the content of each one.

1 **Title:** Bounds on Neutrino-Scalar Yukawa Coupling
Authors: Pedro Pasquini and O. L. G. Peres.
Published at Physical Review D [5].
We constrained neutrino-scalar couplings by the use of leptonic decay of mesons and from a heavy neutrino search. Our analysis improves the present limits to $|g_e|^2$ and $|g_\mu|^2$ and includes for the first time the mass of the scalar particle as a variable.
Keywords:
Neutrino Physics,New Interactions,Beyond Standard Model

2 **Title:** Measuring the leptonic CP phase in neutrino oscillations with nonunitary mixing
Authors: Shao-Feng Ge, Pedro Pasquini, M. Tortola, and J. W. F. Valle.

Published at Physical Review D [3].

We take T2K and T2HK as examples to demonstrate a non-unitary mixing matrix contains a complex phase that can spoil the sensitivity of those experiments to the $\delta_{\rm CP}$. We show that this can be fixed by an experimental proposal called TNT2K proposal which supplements T2(H)K with a μDAR source.

Keywords

Neutrino Oscillation,Non-unitarity,CP phase.

3 **Title:** Neutrino oscillations from warped flavor symmetry: predictions for long baseline experiments T2K, NOvA and DUNE.

Authors: Pedro Pasquini, S. C. Chulliá and J. W. F. Valle

Published at Physical Review D [10].

We proposed a novel method for testing high energy models: Using neutrino oscillation and the neutrino mixing parameters measurements. As a case study, we took the Warped Flavor Symmetry Model to show that correlations between the atmospheric angle and the CP phase can be used to probe such theories.

Keywords

Neutrino Oscillation,Flavor Symmetry,CP phase.

4 **Title:** Probing atmospheric mixing and leptonic CP violation in current and future long baseline oscillation experiments *Authors:* Sabya Sachi Chatterjee, Pedro Pasquini, and J. W. F. Valle

Published at Physical Letters B [11].

We took the propose of using long-baseline experiments to constrain high energy models and simulated the DUNE and T2HK experiments in order to show what are the regions of the parameter space that can be used to constrain the WFSM.

Keywords

Neutrino Oscillation,Flavor Symmetry,CP phase.

5 **Title:** Resolving the atmospheric octant by an improved measurement of the reactor angle

Authors: Sabya Sachi Chatterjee, Pedro Pasquini, and J. W. F. Valle

Published as Rapid Communication in Physical Review D [7]. We show that in order to be able to measure the correct octant of θ_{23} it is necessary to know precisely the value of θ_{13}. We quantify the desired level of accuracy for each of the future long-

baseline experiments, T2(H), NOνA and DUNE, that is needed to resolve the octant problem.

Keywords

Neutrino Oscillation,Octant Problem,Neutrino Experiments.

6 **Title:** Cornering the revamped BMV model with neutrino oscillation data.

Authors: Sabya Sachi Chatterjee, Mehedi Masud, Pedro Pasquini, and J. W. F. Valle

Published at Physical Letter B [12].

We took the propose of using long-baseline experiments to constrain high energy models and simulated the DUNE and T2HK experiments in order to show what are the regions of the parameter space that can be used to constrain the revamped BMV model.

Keywords

Neutrino Oscillation,A_4 Symmetry,CP phase.

7 **Title:** Reactor and atmospheric neutrino mixing angles' correlation as a probe for new physics.

Authors: Pedro Pasquini

Published at Physical Review D [14].

We showed that it is possible to use a very special (but general) θ_{23} correlation with θ_{13} that appears in many models too, model independently use the combination of long-baseline experiments and reactor measurements to constraint high energy models of neutrino masses.

Keywords

Neutrino Oscillation,Symmetry Models,Neutrino Experiments.

8 **Title:** Long-Baseline Oscillation Experiments as a Tool to Probe High Energy Flavor Symmetry Models.

Authors: Pedro Pasquini.

Invited Review published at Advances in High Energy Physics [15].

This is an invited review to describe the possibilities of use neutrino physics to probe symmetry based high energy models. It goes through neutrino experiments sensitivity and analyses various models and methods that can be used to constrain new physics.

Keywords

Neutrino Oscillation,Symmetry Models,Long-Baseline Experiments.

9 **Title:** Exploring the Potential of Short-Baseline Physics at Fermilab.

Authors: O. G. Miranda, Pedro Pasquini, M. Tortola, and J. W. F. Valle.

Published in Physical Review D [8].

We explore the physical potential of liquid argon-based near detectors to search for new physics. In special, we analyzed the ability of SBN experiment to probe non-unitarity and Non-standard Interaction as a function of their systematic errors. We also present benchmark designs for the DUNE's near detector to be able to improve such bounds.

Keywords

Neutrino Oscillation,Short-Baseline,Beyond Standard Model.

We would like to thanks the support by the FAPESP-CAPES funding grant 2014/05133-1, 2014/19164-6 and 2015/16809-9. We also Thanks the partial support from FAEPEX funding grant No 2391/17, Fermilab NPC student grant and by the Coordenação de Aperfeiçoamento de Pessoal de Nível Superior - Brasil (CAPES) - Finance Code 001. Which were essential for perform all those works.

B.1.2 Submitted Manuscripts

Below we present in chronological order the papers submitted to scientific journals and a small description of the content of each one.

1 **Title:** Analytical solution for the Zee mechanism.

Authors: A. C. B. Machado, J. Montaño, Pedro Pasquini and V. Pleitez

We took the well known Zee mechanisms and show that it is possible to write down a simple analytical solution of the parameters of the model in terms of the neutrino mixing parameters and masses. We also show that a set of the parameters of the model do not contribute to the final value and can be taken as free parameters [184].

Neutrino Oscillation,Zee Mechanism,Beyond Standard Model.

2 **Title:** Shadowing Neutrino Mass Hierarchy with Lorentz Invariance Violation.

Authors: H. Jurkovich, C. P. Ferreira, and Pedro Pasquini

We show that it is possible to use long-baseline experiments to probe Lorentz invariance violation. We showed the capabilities of DUNE and T2HK to constrain parameters that change the neutrino mass matrix with an energy dependency of the form $a_d E^{d-3}$. Also, we showed that if $d = 4$, the sensitivity to the mass hierarchy is partially lost [185].

Keywords

Neutrino Oscillation,Lorentz Invariance,Beyond Standard Model.

3 **Title:** Zee and Zee-Babu mechanisms in the minimal 331 model.

Authors: A. C. B. Machado, Pedro Pasquini, and V. Pleitez

We studied the possibilities of incorporating neutrino masses in the minimal variant of the well known $SU(3) \times SU(3) \times U(1)$ (m331). The neutrino masses can be incorporated at tree level or via loop diagrams resulting in a Zee mechanism or a Zee-Babu mechanism. We searched for solutions of the neutrino masses and mixings in this context [186].

Keywords

Neutrino Oscillation,331 Model,Beyond Standard Model.